Identification of novel TAM receptor interacting proteins

–

Screening for novel ligands

Dissertation

zur

Erlangung des Doktorgrades (Dr. rer. nat.)

der

Mathematisch-Naturwissenschaftlichen Fakultät

der

Rheinischen Friedrich-Wilhelms-Universität Bonn

vorgelegt von

Simon Görgen

aus

Euskirchen

Bonn, 2018

II

Angefertigt mit Genehmigung der Mathematisch-Naturwissenschaftlichen Fakultät der Rheinischen-Friedrich-Wilhelms-Universität Bonn.

1. Gutachter:	Prof. Dr. med. Eicke Latz
2. Gutachter:	Prof. Dr. med. Joachim L. Schultze
Tag der Promotion:	17.01.2019
Erscheinungsjahr:	2019

Table of Contents

Abstract ..... **V**

1. Introduction **1**
The immune system 1
TAM receptors in health and disease 2
Sortase A mediated transpeptidation 8
Rationale and aims of the study 9

2. Materials and Methods **11**
Instruments 11
Software 12
General chemicals and reagents 12
Tissue Culture 13
Lysis of organs, tissue samples, and tissue culture cells 14
Cloning plasmids 15
Design, nomenclature and production of bait and control proteins 21
Expression and purification of recombinant proteins 22
Immunoprecipitation of proteins 25
Detection of protein-protein interaction 28
Sortase A mediated transpeptidation 30
Cross-Linker activation by UV light 31
SDS-PAGE and protein detection 32
Co-IP of cross-linker activated bait and control proteins from complex samples 36
Protein identification and quantification by LC-MS/MS 37
Protein identification by MALDI-TOF and Ion trap-ESI-LC-MS 39
Statistics 39
Network analysis 41

3. Results **42**
TAM receptor ectodomain bait proteins bind GAS6 and Fibronectin but not Protein S 42
Establishment of optimal SrtA transpeptidation conditions for n-terminal tagging 45
Characterization of Diazirine as cross-linker of bait and control proteins 52
Specificity confirmation of bait and control proteins for label transfer and comparison of enrichment methods 56
Identification of novel TAM receptor interacting proteins in human and mouse tissues 61
Evaluation of putative TAM receptor interacting proteins 71

4. Discussion **75**
Benefits and improvements of the specialized screening method 75
The screening for TAM interacting proteins identifies 83 novel candidates 77
AHSG or Fetuin A may bridge mineral complexes and mineralized vesicles to TAM receptors for phagocytosis 78
A novel function of TAM receptors in the recognition of extracellular vesicles 79
Apoptotic cell associated molecular patters 81
TAM receptor enriched proteins and cancer 82
Conclusion 83

References **85**

Appendix ..... **i**
List of Abbreviations i
List of Figures ii
List of Tables iii
Supplemental data iv

Acknowledgements ..... **xii**

Abstract

The TAM receptors TYRO3, AXL, and MER are well characterized for their roles in cell proliferation and survival, phagocytosis, and inhibition of inflammation. The complexities of these TAM receptor responses imply a level of orchestration beyond binding to the two well-characterized ligands GAS6 and Protein S.

The here presented study was initiated to identify novel TAM receptor interacting proteins to gain novel insight into TAM receptor functions. Previously published studies aimed to identify ligands were insufficiently sensitive to capture weak and transient interactions, yet identified TUBBY, TULP1, and Galectin 3 as TAM activators by screening retinal cDNA libraries. The screen performed for this study was tailored to capture weak and transiently interacting proteins in a wide range of tissues. The attachment of tri-functional Diazirine cross-linker molecules to the n-termini of bait proteins was established via the bacterial transpeptidase Sortase A, as the enzymatic method provides site specificity and product homogeneity superior to chemical linking techniques. The cross-linker tagged bait proteins produced for this study enabled a variety of methods to enrich captured proteins. In total, three methods were compared for their capacity to enrich novel TAM ligand candidates. Applying the optimal enrichment method, several human and mouse tissues were screened for novel TAM receptor interacting proteins. Enriched proteins were identified by mass spectrometry and evaluated by bioinformatic and biochemical methods. A sum of 83 proteins was found to be potential TAM receptor ligands, which were not previously associated with TAM receptors. Beside proteins indicated to interact individually, clusters of proteins were enriched. AHSG (Fetuin A) links TAM receptors to mineralo-organic complexes and calcification of soft tissues such as atherosclerotic plaques, where AHSG inhibits calcification and acts cytoprotective. 19 proteins are characterized as vesicle markers. Recent publications link the release of vesicles by activated immune cells to immunosuppressive TAM receptor signals in cells recognizing these vesicles. In addition, 12 ribosomal proteins were enriched that may be recognized by TAM receptors as an alternative ‘eat me’ signal for phagocytosis, as ribosomal proteins translocate to the outer membrane in apoptotic bodies.

The identification of additional ‘eat-me’ signals and the identified interaction of TAM receptors with vesicles emphasize the question of how TAM receptors differentially recognize vesicles and cells that either do, or do not present Phosphatidylserine. The 83 novel TAM receptor enriched proteins therefore may serve as starting points for the better understanding of TAM receptor mediated regulation of our immune system, maintenance of tissue homeostasis by clearing apoptotic cells and debris, and supporting healthy or causing malignant cell survival and proliferation.

1. Introduction

The immune system

At all time we are confronted with microbes, parasites, and viruses that surround and colonize us. Epithelial surfaces as the skin, the gastrointestinal tract and mucosa as the respiratory tract provide a physical barrier to prevent infection (*1-3*). Microorganisms and other agents passing these barriers and thereby causing harm are referred to as pathogens. As defense against pathogens mammals have developed specialized immune cells separated into the innate and the adaptive immune system.

Specialized immune cells of the innate immune system are Monocytes, Dendritic cells and Macrophages, Mast cells, Neutrophils, Basophils and Eosinophils, all of which are derive from myeloid progenitor cells (*4-7*). These cells recognize molecular patterns characteristic for pathogens and dangers by several receptor families collectively called pattern recognition receptors (PRR) (*8*). Pathogen associated molecular patterns (PAMPs) are for example proteins of bacterial secretion systems and Flagellin, peptidoglycans, lipoglycans and polysaccharides common to pathogen membranes and foreign to host tissues. Further, pathogenic RNA and DNA is recognized due modifications or localization foreign to host tissues and cells. Endogenous stress signals or danger associated molecular patterns (DAMPs) are for example high levels of extracellular ATP as a result of tissue damage and cellular stress (*9*). Pattern recognition receptors of the Toll-like receptor family (TLRs) are best known for the recognition of bacterial lipopolysaccharides by TLR4. Other TLRs recognize proteins, DNA and RNA of bacterial origin. Upon recognition of PAMPs, TLR mediated signaling induces the secretion of cytokines and interferons (IFNs) orchestrating the immune response. Similarly to TLRs, C-Type Lectin receptors induce the secretion of cytokines upon recognition of pathogen characteristic glycoproteins. Further certain C-Type Lectin receptors mediate or regulate the uptake of pathogens (*10*). While TLRs and C-Type Lectin receptors recognize extracellular PAMPs and DAMPs, NOD-like receptors (NLRs) and RIG-I-like receptors (RLRs) recognize intracellular PAMPs and DAMPs. Like TLRs, the activation of RLRs lead to the secretion of cytokines and interferons (IFNs) orchestrating the immune response, while the activation of NLRs like NLRP1, NLRP3, and AIM2 lead to the inflammatory death of the cell called pyroptosis and the secretion of IL1β and IL18 (*11*, *12*).

Additional to immune cells, pathogens can be recognized by proteins complementing the cellular innate immune response, which are therefore summarized as the complement system. Proteins

of the complement system are secreted into the plasma where they either bind to pathogen surfaces directly, to antigen/antibody complexes or to mannose on bacteria. In a cascade of complement protein recruitment and cleavage, immune cells are recruited for phagocytosis and pores are formed in pathogen membranes for direct lysis of the pathogen (*13*).

While the innate immune system recognizes conserved molecular patterns, the adaptive immune system is designed to recognize an infinite variety of foreign molecular patterns. To achieve this variety of receptors the lymphocyte derived B and T cells each have evolved receptors with a variable antigen recognition domain (*14-16*). As the antigen binding domains of B & T-cell receptors potentially bind host antigens, cells are negatively selected for affinities to host antigens (*17*, *18*). Upon recognition of a foreign antigen, B cells begin to secrete Antibodies of the isotypes IgM, IgG, IgA, and IgE. Dependent on cytokines and stimuli by interacting cells, the secretion of the respective isotype is induced or inhibited (*19*). While B-cell receptors and antibodies potentially bind all accessible foreign antigens, the T-cell receptors recognize foreign peptides only when presented by major histocompatibility complex (MHC) molecules (*20*). Functionally, T cells can be separated in helper (CD4+), killer (CD8+) and regulatory T-cells together called effector T-cells. Further subtypes include memory T cells, natural killer T cells and gamma-delta T cells (*21*).

TAM receptors in health and disease

As described, the immune system has a vast array of receptors to identify hostile patterns and to induce an orchestrated inflammatory response. To balance a pro-inflammatory response, to repair damage inflicted during the response, and in order to return to homeostasis a respectively orchestrated anti-inflammatory response is needed. One family of receptors acting as a counter balance to inflammation is the family of the TAM receptors tyrosine kinases TYRO3, AXL, and MER. TAM receptors inhibit pro-inflammatory pathways during inflammation, thereby providing a threshold for a pro-inflammatory response and further limit its intensity (*22*, *23*). During the immune response but also during homeostasis TAM receptors promote phagocytic clearance of apoptotic cells and debris (*24-26*). And finally, TAM receptors restore vascular integrity following an immune response (*27*, *28*).

The main ligands activating the TAM receptors are Protein S and GAS6. Protein S was identified 1995 as a TYRO3 and MER ligand after observing that TYRO3 transfected cells showed an enhanced growth upon treatment with bovine serum. The TYRO3 ectodomain fused to an Immunoglobulin (Ig) Fc domain was used to enrich TYRO3 from serum by affinity chromatography. GAS6 sharing the domains of Protein S was identified in the same study as a

ligand for AXL (*29*). Later studies have identified GAS6 as a ligand for all three TAM receptors (*30*). Additional to the activation of TAM receptors, Protein S is known for its anti-coagulant function (*31*). Although Protein S and GAS6 have a high sequence homology and an identical domain structure of an n-terminal GLA domain, four epidermal growth factor-like domains and two c-terminal Laminin G-like domains, GAS6 affinity is highest to AXL, then TYRO3, and lowest to MER. Protein S binds equally to TYRO3 and MER but not to AXL (*30*, *32*, *33*). As their ligands, also the receptors share a common domain structure. The extracellular n-terminus begins with two Immunoglobulin-like domains followed by two fibronectin type III-like domains essential for receptor dimerization. Within their cytosolic part, TAM receptors posses a tyrosine kinase domain, which auto-phosphorylates and phosphorylate signaling adapter molecules upon activation (*34-36*). Active TAM receptor / ligand complexes have a stoichiometry of 2 receptors and 2 ligands (*37*).

Beside GAS6 and Protein S additional interacting proteins were identified. Retinal pigment epithelial cells were shown to secrete the Mer binding protein Tubby and Tubby like protein 1 (Tulp1), which binds to Tyro3, Axl, and Mer (*38*). Similarly to GAS6 and Protein S, Tubby and Tulp1 bridge the TAM receptors to apoptotic cells in the retina pigment epithelium and Tubby to microglia in the brain (*39*). The same group later identified Galectin-3 released by TLR activated microglia as a fifth MER ligand (*40*, *41*).

TAM receptor dependent immune regulation:

TAM receptors regulate, and are regulated, by many ways during an inflammatory response. Pattern recognition receptors on innate immune cells drive a pro-inflammatory response by the secretion of pro-inflammatory cytokines and chemokines to activate and recruit other innate and adaptive immune cells. Together with this pro-inflammatory response, counter balancing anti-inflammatory factors are produced and activated. IL10 is secreted suppressing T-cell, DC and macrophage functions (*42*). Regulatory and helper T-cells balance the adaptive immune response as well as dampen the innate immune response. In the year 1999 MER was first linked to the inhibition of an immune response when Camenisch and colleagues reported an increased production of TNFα by $Mer^{-/-}$ mice's peritoneal exudates upon LPS challenge (*23*). Dendritic cells up-regulate the expression of TAM receptors after TLR and type I interferon stimulation (*22*, *43*). Additionally AXL up regulation was shown to be due to type-I IFN stimulation in macrophages. The same study demonstrated that TAM receptors stimulated with apoptotic cells, GAS6, or Protein S induced the expression of TWIST1 and TWIST2, which repress NF-κB induced gene transcription and promotes GAS6 expression.(*44*, *45*) A second way TAM receptors inhibit pro-inflammatory responses was observed when dendritic cells were co-stimulated with AXL and IFNα. AXL binds to IFNAR1 and usurps its signaling cascade and leads to STAT1 homo-

dimerization in turn inducing the expression of suppressor of cytokine signaling 1 and 3 (SOCS1 & SOCS3). As the name implies, SOCS1 and SOCS3 inhibit cytokine inducing signaling cascades by the inhibition of adaptor proteins TRAF3, TRAF6 and MAL as well as the NF-κB protein p65, and by the inhibition of the cytokine receptor induced JAK/STAT pathway (*22*, *46-50*). Additional to the stimulation of TAM receptors by free ligands it was shown, that Protein S is transiently exposed on the surface of activated CD4+ and CD8+ T cells (*51*, *52*) and that T cell derived Protein S limits the activation of antigen presenting cells (APC) and the expression of cytokines (*53*). As Phosphatidylserine (PtdSer) was found to be presented on T cells and B cells when activated (*54*), it was proposed that these cells utilize Protein S bound to surface presented PtdSer for the inhibition of TAM receptor presenting innate immune cells (*55*). During an acute phase immune response, Protein S serum levels are increased together with the levels of C4BP blocking Protein S function by binding, and leading to a constant concentration of approximately 126 nM free Protein S (*56*). GAS6 is present in plasma complexed to soluble AXL (*57*). The soluble forms of AXL and MER are generated by shedding the ectodomain of the receptors by the metalloprotease ADAM17, who's expression is up-regulated by TLR stimulation (*58*, *59*). Protein S in serum might therefore serve as a threshold for an inflammatory immune response, as well as to enable a quick removal of apoptotic cells and debris within the vascular system.

TYRO3, AXL and MER as receptors of apoptosis:

Apoptosis of cells is part of the regular cellular turnover during the development of tissues and during homeostasis. During inflammation and cellular stress non-homeostatic factors lead to an increased cell death (*60*). The clearance of apoptotic cells and debris is elemental to maintain homeostasis as deficiencies lead to chronic inflammation and autoimmune disease (*61*). TAM receptors were demonstrated to be major receptors for the sensing of apoptosis and for the subsequent efferocytosis of apoptotic cells and debris. The ability of macrophages to phagocytize apoptotic thymocytes was reduced approximately by half in $Tyro3^{-/-}$, $Axl^{-/-}$ as well as in $Axl^{-/-}$, $Mer^{-/-}$ macrophages, while in other cells types as in bone-marrow derived dendritic cells knock out of $Mer^{-/-}$ did not lead to a significant reduction of efferocytosis efficiency (*24*, *62*). Despite this plasticity of impact TAM receptors have on the efficiency of efferocytosis in individual cell types, the general importance of TAM receptors is demonstrated by the development of a lupus-like disease in $Mer^{-/-}$ mice (*63*). Interestingly it was found that macrophage efferocytosis of apoptotic cells was increased when serum was present, while the efferocytosis of necrotic cells remained unchanged in vitro. Apoptosis is characterized by the exposure of PtdSer on the outer leaflet of the plasma membrane (*64*). The TAM receptor ligands GAS6 and Protein S bind to PtdSer via their γ-carboxylated GLA domain in dependence of

Vitamin K and Ca^{2+}, serving as bridging molecules to the TAM receptors (*65-68*). Further TAM receptor co-expressed PtdSer binding and phagocytosis associated receptors are TIM-4 binding PtdSer directly, and the αvβ5 integrin binding the PtdSer binding MFG-E8 (*69*, *70*). TAM receptors were shown to SRC-dependently phosphorylate the cytosolic protein FAK that in turn phosphorylates and recruits αvβ5 integrin (*71*).

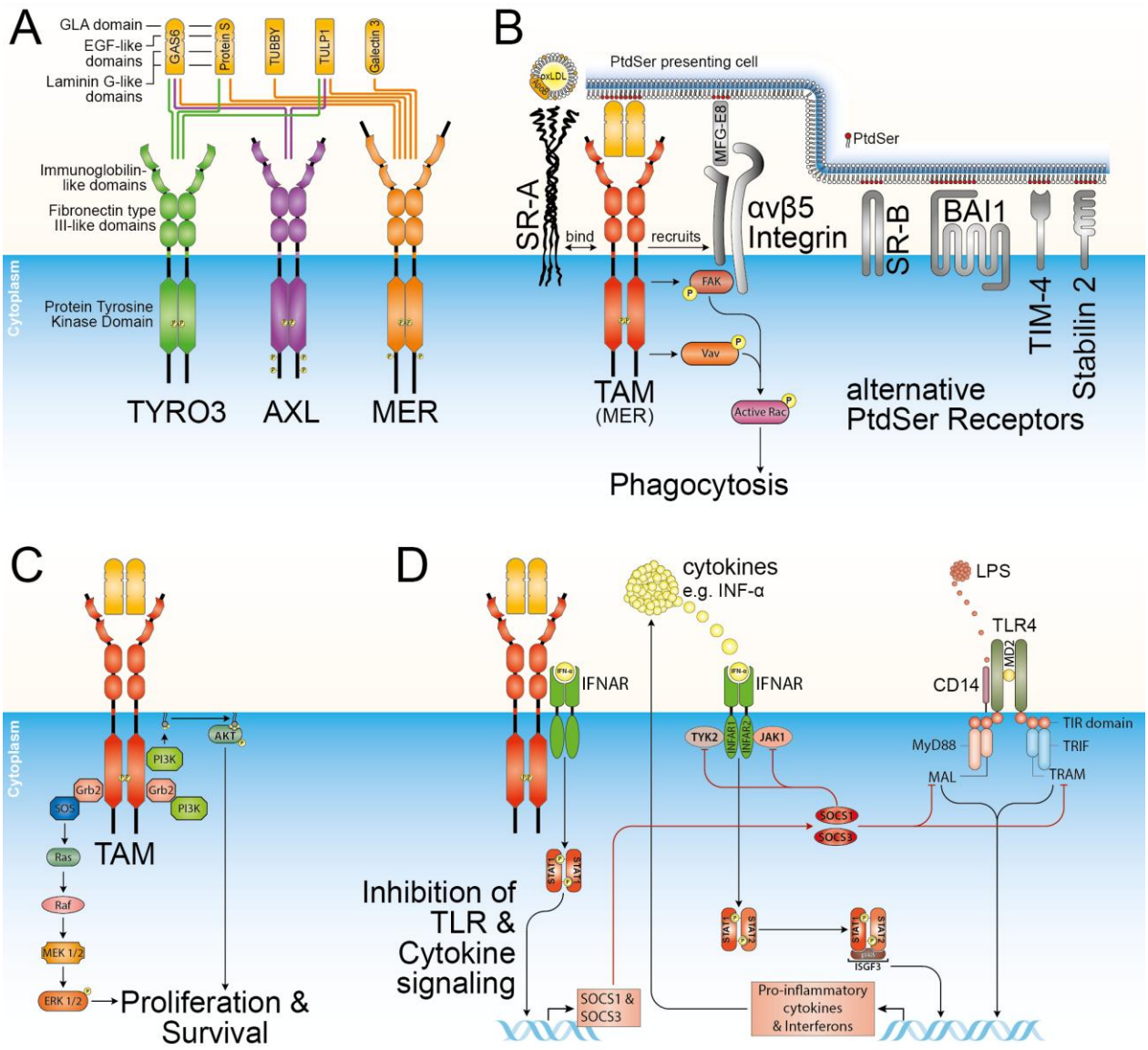

Figure 1. TAM receptors and the regulation of inflammation, phagocytosis and survival.
TAM receptors bind a variety of ligands (A), are regulated on a transcriptional level, by cleavage and ubiquitylation, and are stabilized by heat-shock proteins. TAM receptors sense apoptotic cells by their PtdSer binding ligands and co-operate with certain apoptosis sensing receptors, while no connection of TAM receptors with PtdSer receptors as SCARB1, BAI1, TIM-4, and Stabilin 2 is reported (B). TAM receptors induce proliferation and survival of cells (C). In inflammatory environments, TAM receptors inhibit immune responses by usurping IFNAR signaling and thereby inducing the expression of SOCS1/3 (D).

Additional to the clearance of apoptotic cells by immune cells, TAM receptors are essential for phagocytic processes in other cell types. TAM receptor deficient mice (Tyro3$^{-/-}$, Axl$^{-/-}$, Mer$^{-/-}$ or so-called triple knock out mice (TAM TKO) turn blind after birth due to the retina pigment epithelium's inability to phagocytize and degrade the shed outer segments of photoreceptors (*26*, *33*). Further male TAM TKO mice become infertile due to inefficient clearance of apoptotic spermatogenic cells during spermatogenesis by phagocytosis specialized Sertoli cells (*25*, *26*).

TAM receptors role in vascular integrity:

While drawing blood from TAM TKO mice by tail clipping an increased blood loss was noticed and linked to impaired GAS6 dependent thrombus formation. An inflicted wound in the vasculature activates platelets and increases their $\alpha_{IIB}\beta_3$ integrin's affinity to fibrinogen. Co-stimulation of TAM receptors with GAS6 was shown to be essential for $\alpha_{IIB}\beta_3$ integrin phosphorylation and PI3K and AKT signaling at low levels of platelet activation (*72*, *73*). Further, the TAM receptor AXL is required by VEGF-A to induced neovascularization and migration of epithelial cells. Endothelial cells in the retina showed GAS6 stimulated proliferation, tube formation and migration (*74*). Tyro3 dependent Protein S stimulation prevents the disruption of brain endothelial cell formed barriers, challenged with hypoxia. Protein S stimulates mitosis of vascular smooth muscle cells (*67*, *75*). All together, effects of TAM receptor signaling on the vascular integrity are evident, but complicated to dissect from other effects, as for Protein S a complete knock out is embryonic lethal. Further Protein S is secreted by cells as various as hepatocytes, endothelial cells, and hematopoietic cells where a conditional knock out would only limit one source of Protein S (*27*).

TAM receptors in disease:

TAM receptors are reported to cause or effect diseases like systemic lupus erythematosus (SLE), rheumatoid arthritis, inflammatory bowel disease, and multiple sclerosis, which have a chronic or autoimmune inflammatory character in common. TAM receptors impact cancerogenesis and the infectiousness of several viruses.

TAM receptor triple knock out mice show characteristics of chronic inflammation and SLE beginning 4 weeks after birth and intensifying with age. High levels of antibodies to dsDNA, collagen, and phospholipids as PtdSer, phosphatidylethanolamine, phosphatidylinositol, and cardiolipin were detected. Mice had swollen footpads and joints, lesions in the skin, and especially female mice showed hemorrhages and thrombosis (*76*). Apoptotic cells accumulated in the germinal centers of Mer$^{-/-}$ mice's lymph nodes, which is characteristic for human SLE patients as well (*77*, *78*). Another characteristic found in SLE patients but also in patients suffering from Crohn's disease and ulcerative colitis is a deficiency in Protein S (*79-81*).

TAM receptors were linked to multiple sclerosis investigating the impact of GAS6/AXL signaling on proliferation and survival during toxic demyelination induced by feeding Cuprizone to young mice. $Axl^{-/-}$ mice accumulated more apoptotic oligodendrocytes and myelin debris upon Cuprizone treatment compared to wild type mice and axonal damage and recovery was prolonged (*82*). An effect similarly observed in $GAS6^{-/-}$ mice while exogenous administration of GAS6 into the brain had an opposite effect (*83*, *84*). In humans suffering from multiple sclerosis, polymorphisms in the MER gene were associated with a higher susceptibility to the disease (*85*).
The implications of TAM receptors in cancer are ambiguous. TAM receptors are transforming oncogenes (*34*, *86-88*) leading to several types of cancer further described by Wu and colleagues (*89*). Most prominently acute myeloid leukemia is GAS6/TAM dependent where GAS6 expression levels implicate disease severity (*90*, *91*). TAM receptors were also described to dampen anti-tumor responses (*92*). Contrasting the pro-oncogenic functions described, TAM receptor deficiencies in inflammation induced colon cancers mouse models lead to increased disease susceptibility and reduced survival (*93*, *94*). Another way AXL is involved in the development of cancer is the intramembrane proteolysis by γ-secretase resulting in a cytoplasmic domain with a nuclear localization domain. Translocation of AXL's intracellular domain into the nucleus was reported for various cancer cell lines. NF-κB signaling was partially inhibited by AXL ICD translocation. First experiments indicate an increased chemo-resistance induced by over-expression of an AXL mutant unable to be cleaved by γ-secretase (*95*).
In 2006 Shimojima and colleagues revealed the use of TAM receptors by the *filoviridae* family member Ebola virus to enhance virus entry into TAM receptor expressing cells. Ebola pseudotype virus infection of AXL and MER overexpressing Jurcat cells was highly increased while TYRO3 overexpression only led to a lesser yet significant increase (*96*). The deletion of AXL's Ig-like C2-type 1 domain, the intracellular domains, or preventing ATP binding by introducing a K567M mutation reduced the infection efficiency to levels observed with control cells (*97*). In the following years TAM receptors were found to increase infections with viruses as Vaccinia (*98*), Lassa (*99*), and the *flaviviridae* Dengue (*100*), West-Nile (*101*), and Zika (*102*). Since the causal association between microcephaly and the Zika outbreak in mid 2015 (*103*), many publications focus on investigating this connection. As all of these viruses are enveloped, TAM receptors might not interact with enveloped proteins but indirectly with PtdSer exposed by many viruses for apoptotic mimicry. Indeed many studies revealed a dependency for GAS6 and Protein S to mediate TAM receptor dependent infections (*98*, *100*, *101*). However the major capsid protein of Simian virus SV40 binds directly to TAM receptors and shows structural similarity to the TAM receptor ligands (*104*). Beside the apoptotic mimicry to avoid an extracellular immune reaction, virus infection by TAM receptors caused expression of SOCS1 and SOCS3 and their suppression of PRR signaling and thereby IFN secretion (*101*).

Sortase A mediated transpeptidation

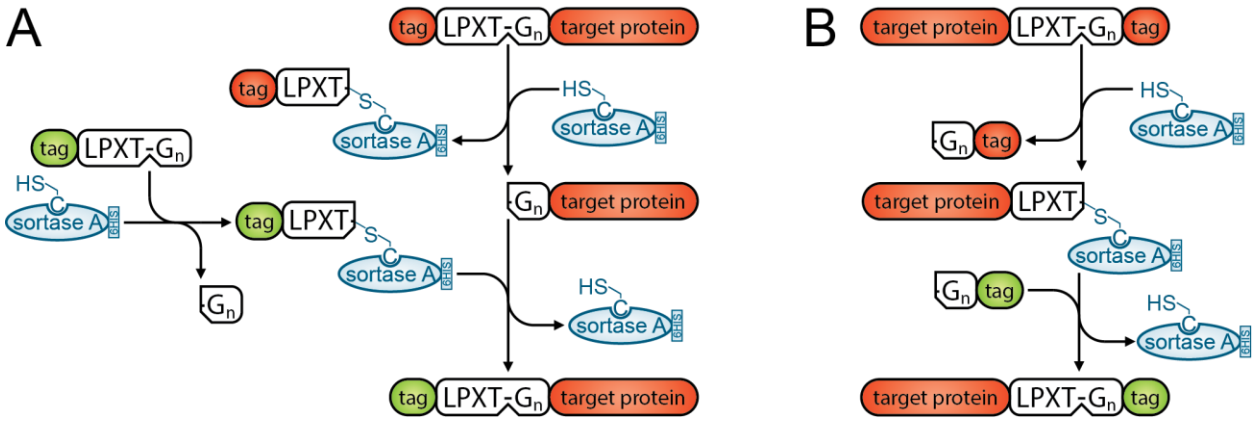

Figure 2. Transpeptidation reaction by sortase A
Schematic description of n-terminal (A) and c-terminal (B) sortase A mediated transpeptidation reactions. The recognition motif LPXTG recognized by *S. aureus* srtA is shown representatively. The enzymes Cysteine marked as C and it's side chains sulfhydryl group marked as HS are shown.

Mazmanian et al., 1999, first characterized the product of the *Staphylococcus aureus* gene *srtA* and named it surface protein sorting A or Sortase A. Sortase A is a membrane-anchored transpeptidase expressed by *S. aureus* and other pathogenic gram-positive bacteria like *Streptococcus pyogenes*. The transpeptidase of *S. aureus* recognizes the peptide motif LPXTG, while *S. pyogenes* srtA recognizes LPXTA/G. After recognition of the motif in proteins secreted, srtA covalently attaches them to the bacterial cell wall by hydrolyzing the peptide bond between Thr and Gly/Ala followed by the ligation to any available n-terminal Gly/Ala (*105*, *106*). Those proteins promote the infection of a host by binding fibrinogen in vascular and endocardial lesions by ClfA and ClfB (*107*), by promoting the interaction with host tissues and invasion of cells via fibronectin binding proteins FnbA and FnbB (*108*, *109*), or by evading the host immune response preventing opsono-phagocytosis binding host antibodies (*110*) and inducing TNFAR1 shedding with Immunoglobulin G-binding protein A (Protein A / spa) (*111*). As expected *S. aureus* $^{srtA-/-}$ was shown to be less virulent compared to wild type *S. aureus* and was therefore suggested as possible antimicrobial drug target (*112*, *113*).

To transform the bacterial enzyme in a biochemical tool, the n-terminal transmembrane domain was removed and replaced by a hexa-His tag for purification (*114*). Since the recognition of sortase as a powerful tool to ligate peptides, mutations in *S. aureus* srtA were characterized improving the enzymatic activity (*115-117*), removing srtA dependency for Ca^{2+} (*118*), and reprogramming the specificities of srtA (*119*). Many studies have shown the use of sortase to link dyes or small molecules to proteins like antibodies (*120*), to label cell surface proteins (*121*), or to link proteins with proteins. One example where sortase ligation of protein to protein is the

development of a papaya mosaic virus (PapMV) coat protein based vaccination platform. As PapMV coat protein stimulates TLR7 (*122*), it serves as an adjuvant expressed with LPETGG as srtA recognition motif. Thérien and colleagues used sortase to tag viral peptides to the PapMV coat proteins and could show that the combinations elicited specific immune responses (*123*). This is just one of many examples where sortase enzymes have been used as a versatile tool of protein engineering.

Rationale and aims of the study

Four years after the discovery of TYRO3, AXL, and MER as an independent family of receptor tyrosine kinases, the major ligands GAS6 and Protein S were identified, followed five years later by TUBBY, TULP1, and Galectin 3. By the extensive research in the past years TAM receptors were uncovered as essential receptors for phagocytosis, the regulation of inflammatory responses and cell proliferation and survival. However, with the ongoing characterization of the known ligands stimulating TAM receptors, more and more situations were discovered where these identified TAM receptor ligands alone could not explain the observed effects. All TAM receptor ligands described induce phagocytosis by recognizing PtdSer, an ‘eat me’ signal recognized by many redundant receptors. Why are TAM receptors so important for efficient phagocytosis that mice lacking them fail to clear apoptotic cells although PtdSer is redundantly recognized? Why are B cells and T cells hyper-activated in mice lacking TAM receptors and why are they spared by TAM expressing antigen-presenting cells when activated and presenting PtdSer? The question how TAM receptors regulate inflammatory responses was partly answered in 2007 by Carla Rothlin and colleagues, where they showed that TAM receptors usurp Interferon-alpha receptor signaling upon co-stimulation and thereby induce the expression of inflammatory signaling inhibitors. But, as all TAM receptor functions described by now are stimulated either by free or Phosphatidylserine bound ligands, the question remains on how TAM receptors discriminate between Phosphatidylserine presenting living and apoptotic cells. Therefore by investigating whether TAM receptors engage additional unidentified proteins or molecules, light can be shed on TAM receptor regulated phagocytic events, immune responses, and homeostatic and malignant cell proliferation and survival.

The specific aims of this project were:

1. To establish a method for the attachment of cross-linker molecules to bait proteins in order to capture weak and transient interacting proteins by:
    a. Optimizing the Sortase A reaction towards the 5M srtA enzyme variant's transpeptidation of small molecules.
    b. Determining at which level of UV irradiation efficient activation of the cross-linker Diazirine is reached comparing two UV light sources, under consideration of time and adverse effects caused by UV irradiation.
    c. Establishing the concept of specific ligand capture and labeling by the bait proteins designed for this study.
2. To select an optimal enrichment method capturing weak and transient interacting proteins by comparing potential enrichment methods possible to be used with regard to the enrichment of weak and transient interacting proteins.
3. To identify novel TAM receptor interacting proteins by screening of multiple TAM receptor expressing tissues, and to characterize the identified interacting proteins by biochemical and bioinformatic methods towards their potential role in regulating TAM receptor functions.

2. Materials and Methods

Instruments

Name	Description	REF number	Supplier
DynaMag™-2 Magnet	For 1.5 ml to 2 ml microcentrifuge tubes	12321D	Thermo Fisher Scientific
gentleMACS Octo Dissociator	Bench-top instrument for the semi-automated and standardized tissue dissociation or homogenization of up to eight samples	130-095-937	Miltenyi Biotec
HOKImag	Free-flow magnetic separation system with a high-gradient 2-Tesla permanent magnetic field. The disposable flow columns do not contain ferromagnetic materials inside, the focusing gradient of the magnetic field is provided from outside the columns by a patented device.	HOKImag	Hoock GmbH Kiel
MACSmix Tube Rotator	Small rack for tubes from 0.5 mL to 2 mL in size, Large rack for tubes from 5 mL to 50 mL in size	130-090-753	Miltenyi Biotec
MINIPULS® 3	Adjustable speed from 0 to 48 rpm by increments of 0.01 rpm up to 9.99 rpm and by 0.1 rpm at above 10 rpm	n.a.	Gilson
Sonopuls HD 2070	Generator GM 2070, ultrasonic transducer UW 2070, diameter probe SH70, micro tip MS 73 with a diameter of 3 mm, the system is set up for volumes of 2 to 50 ml.	n.a.	Bandelin
T Professional TRIO Thermocycler	Multiblock thermocycler with heated lid for DNA amplification.	n.a.	Biometra
T3000 Thermocycler	3 independent 0.2ml blocks with 6x8 wells each	n.a.	Biometra
Neubauer chamber	4 cell counting areas with 1x1x0.1 mm (0.1 mm^3, or 0.1 µl), number of cells in 4 counting areas / 4 * 10,000 = number of cells / ml	n.a.	n.a.
Microplate Washer 405 T5	Automatic removal and washing of 96 well plates	n.a.	BioTek
EPOCH	Microplate spectrophotometer, 200 nm to 999 nm for UV-Vis applications, micro-volume detection with Take3 plate	n.a.	BioTek
SpectraMax i3	Operated with SoftMax Pro software, for 96 or 384 well plates, additional cartridges: Alpha Screen - Alpha 384 STD (0200-7017POS), FP-FLUO (0200-7009POS), HTRF (0200-7011POS), additional equipment: SpectraDrop™ Micro-Volume Microplate,	n.a.	Molecular Devices
OPS-A500	200-500 W DC Arc Lamp Power Supply, Power, Current, and Intensity Control Modes, RS-232/USB control, CE and RoHS compliant, from Oriel Instruments	OPS-A500	Newport Corporation
500W Xe/Hg Arc Lamp	500 Watt Mercury-Xenon Arc Lamp	66142	Newport Corporation
LIK-LMP Light Intensity Controller Kit	A TE cooled Si detector provides light intensity feedback.	71582	Newport Corporation
Liquid Filter	280 to 950 nm light transmission, filters unwanted IR light and resultant heat, hose fittings provided for use with external cooling chamber	6214	Newport Corporation
Beam Turning Mirror Housing	1.5 Inch Series Flange	66245	Newport Corporation
280-400nm dichroic mirror	3 inch series model	66236	Newport Corporation

Lamp Socket Adapter	for 500 W Hg(Xe) Lamp	66159	Newport Corporation
Arc Lamp Housing	For 50-500W, F/0.7, 4 Element FS Aspherab, Collimated, 3 In	66905	Newport Corporation
Electronic Safety Shutter	For 1.5 Inch Series Flange	71445	Newport Corporation
Bio-Link BLX-365	5 x 8 Watt UV lamps, 365 nm, sensor controlled irradiation	n.a.	AG Hornung
X Cell system	XCell SureLock™ Mini-Cell Electrophoresis System	EI0001	Thermo Fisher Scientific
VersaDoc	VersaDoc 4000MP	n.a.	Bio-Rad
28-80mm objective	28-80mm f1/3.5-5.6 AF aspherical	n.a.	Tamron
EPOCH Reader	Microplate Spectrophotometer, monochromator-based optics	n.a.	BioTek Instruments
Take3 Micro-volume plate	2 µL sample volumes for direct DNA, RNA and protein quantification	n.a.	BioTek Instruments

Table 1. List of instruments.

Software

Software	**Supplier**
Gel Scan Quantity One (version 4.6.9)	Bio-Rad
SoftMax Pro (version 6.3)	Molecular Devices
Excel for Mac 2011	Microsoft
Word for Mac 2011	Microsoft
Prism 6	GraphPad Software, Inc.
Prism 7	GraphPad Software, Inc.
Image Studio Lite	LI-COR Biosciences
Image Studio Ver 4.0	LI-COR Biosciences
Geneious	Biomatters Ltd.
Papers 3	Digital Science & Research Solutions Inc.
Gen 5 (version 1.11)	BioTek Instruments
Perseus v1.5.2.11	Prof. Jürgen Cox, PhD, http://www.coxdocs.org
Cytoscape 3.6.0	Open source
ClueGO 2.5.0 & CluePedia 1.5.0, Cytoscape PlugIn	Open source

Table 2. List of software.

General chemicals and reagents

Name	**Formulation**	**REF number**	**Supplier**
Acetic acid	$C_2H_4O_2$, 100%	3738.5	Carl Roth
BSA	Bovine Serum Albumin, heat shock fraction, pH 7, ≥98% purity, CAS # 9048-46-8	A9647	Sigma Aldrich
Calcium chloride	$CaCl_2$	1.06404.5000	VWR
cOmplete™	EDTA-free Protease Inhibitor Cocktail, inhibit a broad spectrum of serine and cysteine proteases	11873580001	Roche
Disodium hydrogen phosphate	Na_2HPO_4, heptahydrated	X987.1	Carl Roth
EDTA, 500 mM	UltraPure™ 0.5M EDTA, pH 8.0	15575020	Thermo Fisher Scientific
EDTA, 500 mM	Ethylenediaminetetraacetic acid solution, pH 8.0, ~0.5 M in H_2O, CAS#: 60-00-4	03690-100ml	Sigma Aldrich
EDTA	Ethylenediaminetetraacetic acid CAS#: 10378-23-1	A1105	PanReac AppliChem
Glycerol	Glycerol BioXtra, ≥99% (GC), CAS#: 56-81-5	G6279	Sigma Aldrich
HCl, 32%	hydrochloric acid, 32% (v/v) CAS#: 7647-01-0	P074	Carl Roth

HEPES	HEPES solution, 1 M, pH 7.0-7.6, sterile-filtered, BioReagent, suitable for cell culture	H0887	Sigma
IPTG	Isopropyl-β-D-thiogalactopyranosid, $C_9H_{18}O_5S$, CAS # 367-93-1	CN08.2	Carl Roth
Isopropanol, analytical	$CH_3CHOHCH_3$, CAS # 67-63-0	131090	PanReac AppliChem
Isopropanol, technical	$CH_3CHOHCH_3$, CAS # 67-63-0	211090	PanReac AppliChem
Methanol	analytical	A0688	PanReac AppliChem
Milk powder	blotting grade, powdered, low fat Milk contains biotin. Not suitable for biotin/streptavidin mediated detection systems.	T145.1	Carl Roth
Sodium hydroxide solution, 1N	NaOH, 1.0N CAS#: 1310-73-2	S2770	Sigma Aldrich
Nonidet P-40	Nonidet® P40 (Substitute) BioChemica	A1694	PanReac AppliChem
Phosphate buffered saline, 10x	1.37M NaCl, 27mM KCl, 100mM Na_2HPO_4, 20 mM KH_2PO_4	P04-53500	PAN Biotech
PhosSTOP	PhosSTOP™, inhibitor tablets for phosphatase	4906845001	Sigma Aldrich
Potassium chloride	KCl	1.04936.1000	Merck
Potassium dihydrogen-phosphate	KH_2PO_4	P018.2	Carl Roth
SDS	Sodium dodecyl sulfate, $CH_3(CH_2)_{11}OSO_3Na$, CAS#: 151-21-3	L5750	Sigma Aldrich
Sodium chloride	NaCl, CAS#: 7647-14-5	1.06404.5000	VWR
Sodium deoxycholate	3, 12-α-Dihydroxy-5β-cholan-24-oic acid, monosodium salt	89905	Thermo Fisher Scientific
Sulfuric acid	Sulfuric acid, 2N	X873.1	Carl Roth
TBS	Tris Buffered Saline	sc-362305	ChemCruz
TRIS, 1M, pH8.0	121.14 g/L (1 M) Tris	A4577	PanReac AppliChem
TRIS base	2-Amino-2-(hydroxymethyl)-propan-1,3-diol CAS#: 77-86-1	A2264	PanReac AppliChem
Triton X-100	Triton® X 100, Alkylphenylpolyethylenglykol, CAS#: 9036-19-5	3051	Carl Roth
Tween-20	TWEEN® 20, Polyethylene glycol sorbitan monolaurate, viscous liquid, CAS # 9005-64-5	P1379	Sigma Aldrich

Table 3. List of general chemicals and reagents.

Tissue Culture

Tissue cultures were grown in a humidified incubator at 37°C with an atmosphere of 95% air and 5% CO_2. Cell lines were passaged using a 0.05% Trypsin-EDTA solution or a solution of 5-25 mM EDTA in PBS to detach the cells from the culture vessel. After detachment of the cells, FBS containing medium was added and the cells were transferred to a falcon. 10 µl of the culture were mixed with 90 µl of trypan blue dilutes 1/10 in PBS. 10 µl of the mixture were pipetted to a Neubauer chamber where the healthy and therefore unstained cells were counted. Based on the healthy cells per milliliter determined, cells were seeded into a culture vessel.

Name	Formulation	REF number	Supplier
293T	(*Homo sapiens* adherent embryonic kidney epithelial cells) Cultured in DMEM, 10% (v/v) FBS, Penicillin 100U/ml, Streptomycin 100µg/ml, Seeded with >10000 cells/cm^2, Grown to <90 confluence	ATCC	CRL-3216
ARPE-19	Cultured in DMEM/F12, 10% (v/v) FBS, L-Glutamine, Seeded to >5000 cells/cm^2, Grown to <90% confluence	Provided by Wen Allen Tseng	n.a.
DMEM	Dulbecco's Modified Eagle Medium, high glucose	41965-039	Gibco
DMEM, supplemented	DMEM supplemented with 10% (v/v) FBS and 100 U/ml PenStrep	n.a.	n.a.
DMEM/F12	Dulbecco's Modified Eagle Medium, with L-glutamine and phenol red, without HEPES	11320074	Thermo Fisher
DMEM/F12, supplemented	DMEM/F12 supplemented with 10% (v/v) FBS and 100 U/ml PenStrep	n.a.	n.a.
FBS	Fetal Bovine Serum, heat inactivated	10270106	Invitrogen/Gibco
PenStrep	Penicillin-Streptomycin (10,000 U/mL)	15140122	Gibco
Phosphate buffered saline	Dulbecco`s Phosphate Buffered Saline, without Ca and Mg, 1x solution, sterile	Gibco	14190-094
Trypsin	Trypsin-EDTA (0.05%), phenol red	Thermo Fisher	25300054

Table 4. List of buffers, solutions, media, and cell lines for tissue culture.

Lysis of organs, tissue samples, and tissue culture cells

Preparation of lysates from mouse organs:

Lungs, hearts, livers, testis, spleens and kidneys were isolated from male and female C57BL/6J mice. The organs were prepared from already sacrificed mice. Before the lysis the organs were washed with PBS to remove remaining blood and then transferred to a M Tube and weighed. 5 ml of N-P40 tissue lysis buffer were added per gram of tissue. The tissues were homogenized using gentleMACS Octo Dissociator with the preset program ‘protein_01_01’. The homogenates were transferred from the M tubes into microcentrifuge tubes and centrifuged with 13200 g at 4°C for 10 minutes. The supernatants were transferred to new microcentrifuge tubes. The protein concentrations were determined for each lysate with the BCA Protein Assay Kit from Pierce™ according to the manufacturers manual before storing the lysates at -80°C.

Preparation of lysates from human tissue samples:

Human brain cortex samples from healthy patients, or patients either diagnosed with Alzheimer or Mild Cognitive Impairment (MCI) were provided as homogenates prepared with a cryogenic grinding method. Two-times concentrated N-P40 tissue lysis buffer was added to a volume ratio of 1/1 to the homogenates and sonicated in 3 cycles of 30 seconds sonication and 30 seconds resting on ice. The lysates were then centrifuged for 10 minutes at 4°C with 13200 g before transferring the supernatants to new microcentrifuge tubes. The protein concentrations were

determined for each lysate with the BCA Protein Assay Kit from Pierce™ according to the manufacturers manual before storing the lysates at -80°C.

Preparation of lysates from tissue culture cells:

To lyse cells grown in tissue culture dishes, the cultures were washed with ice cold PBS. As lysis buffers N-P40, RIPA, or Lysis Buffer 1 from Cisbio were used. Protease or phosphatase inhibitors as cOmplete, PhosStop, and PMSF were added as required. In case of nucleotides forming clots 1/20000 diluted Benzonase was added to the respective lysis buffer. The lysis buffer was incubated on the cells for 10 minutes at 4°C or on ice. Remaining cells were scraped off and the lysates were transferred to microcentrifuge tubes and centrifuged for 10 minutes at 4°C with 13200 g before transferring the supernatants to new microcentrifuge tubes. The protein concentrations were determined for each lysate with the BCA Protein Assay Kit from Pierce™ according to the manufacturers manual before either using the lysates directly or storing the lysates at -80°C.

Name	Formulation	REF number	Supplier
Benzonase® Nuclease	≥250 units/µl, ≥90% (SDS-PAGE), recombinant, expressed in E. coli, buffered aqueous glycerol solution, CAS Number 9025-65-4, Enzyme Commission (EC) Number 3.1.30.2, MDL number MFCD00131010	Sigma Aldrich	E1014-25KU
C57BL/6J mice	Wild type mice	n.a.	Charles River / Janvier Labs
Lysis buffer 1	Part of the cAMP/cGMP kits, contains potassium fluoride and Triton X100	Cisbio	62CL1FDD
M Tubes	gentleMACS™ M Tubes are used in combination with the gentleMACS Dissociator for the fast and convenient automated tissue homogenization, in order to isolate biomolecules like mRNA or total RNA, or to extract proteins.	130-096-335	Miltenyi Biotec
N-P40 lysis buffer	20 mM TRIS base, 150 mM NaCl, 1 mM EDTA, 1% (v/v) Nonidet P-40, 10% (v/v) glycerol, in H_2O, pH7.4	n.a.	n.a.
N-P40 tissue lysis buffer	140 mM NaCl, 2.7 mM KCl, 10mM Na_2HPO_4, 2 mM KH_2PO_4, 1% (v/v) Nonidet P-40, 1x cOmplete™, in H_2O, pH7.4	n.a.	n.a.
PMSF	Used with 1 mM final concentration, stock dissolved in isopropanol and stored at 4°C	n.a.	n.a.
RIPA lysis buffer	1% (v/v) Triton X-100, 0.1% (v/v) SDS, 10% (v/v) glycerol, 20 mM TRIS, 150 mM NaCl, 12 mM sodium deoxycholate, 1 mM EDTA, pH7.4	n.a.	n.a.

Table 5. List of buffers, tissues and mice for preparation of lysis samples.

Cloning plasmids

DNA was quantified using the EPOCH Reader with the Take 3 Micro-volume plate controlled by the Gen 5 software. For DNA quantification a Take 3 Session started selecting ‘Nucleic Acid

Quantification', and dsDNA within Gen 5. The service of GATC Biotech was used to sequence plasmids.

PCR amplification of nucleotide sequences:

Nucleotide sequences were amplified by polymerase chain reaction (PCR). To 12.5 µl of the PFU Ultra II HS 2X Master Mix from Agilent Technologies 5 µg of a template DNA was added together with 0.4 µM per primer and adjusted to 25 µl total volume with water. The program for PCR was as follows:

94°C for 60 s, then 35 cycles of 94°C for 30 s, 50-65°C for 30 s (5°C below Tm of primers), and 72°C for 60 s / 1000 nucleotides before a final 72°C for 10 min.

The products from the PCR were then separated in a 1% (w/v) agarose gel, purified from the gel and ligated into the plasmid pJet1.2 linearized with EcoRV from the CloneJET PCR Cloning Kit from Thermo Fisher Scientific.

Annealing of complementary oligonucleotides to obtain linker sequences:

Short linker sequences were prepared by annealing two complementary oligonucleotides. The oligonucleotides were designed to leave short overhangs that correspond to the restriction sites used to insert the linker into a plasmid. 250 pmol of each oligonucleotide was added to 50 µM NaCl in a total volume of 105 µl. The primer mix was heated to 95°C for 10 minutes and left in the thermo cycler until it reached room temperature to anneal the primers.

Restriction digest of plasmids and DNA fragments:

Restriction digests were performed with <5 µg of DNA in FastDigest Green buffer adding 2 µl per respective FastDigest enzyme adjusting the total volume to 50 µl with water. The digest was performed for 1h at 37°C. The digested fragments were separated in a 1% (w/v) agarose gel and excised and eluted for ligation.

Agarose gel electrophoresis:

1% (w/v) agarose was prepared in TAE buffer and heated until boiling before 0.01% (v/v) of SYBR Green was added and the gel was casted. DNA was loaded in FastDigest Green Buffer and the electrophoresis was performed with 120V.

Purification of DNA from Agarose gels:

DNA fragments needed for further cloning steps were excised from the agarose gel and transferred into a microcentrifuge tube. The extraction of the DNA from excised agarose pieces

was performed with the PureLink Quick Gel Extraction Kit according to the manufactures manual.

Ligation of DNA fragments into a vector:

DNA fragments with matching ends were ligated using the T4 ligase and the 5x ligation buffer from the Rapid DNA Ligation Kit by Thermo Fisher Scientific. Ligations were performed for 20 minutes at 22°C. For ligations of PCR products into linearized pJet1.2, the ligation mix was prepared as follows: 1 µl of T4 ligase, 4 µl of 5x ligation buffer, 1 µl of pJet1.2, 8 µl of gel separated and purified PCR product, and 6 µl water. For ligations of DNA fragments into other plasmids the ligation mix was prepared as follows: 4 µl 5x ligation buffer, 1 µl T4 ligase, and 15 µl of combined DNA fragment to be ligated and the recipient plasmid in a 3 to 1 molar ratio.

Transformation of bacteria with plasmids:

For chemo-competent transformation of DNA into bacteria the following bacterial strains were used: *E. coli* BL21, DH5α, and DH5α-T1R from Thermo Fischer Scientific, and ClearColi® BL21(DE3) from Lucigen.

The chemo-competent bacterial stocks were thawed on ice and 3 µl DNA were added to 10-50 µl bacteria and incubated for 30 minutes on ice. The bacteria were then heat shocked at 42°C for 60 seconds before being incubated for 2 minutes on ice. 200 µl of LB medium were added to the bacteria that were then shaken with 750 rpm at 37°C for 1h before 150 µl were spread on a LB agar plate supplemented with the antibiotic corresponding to the resistance provided by the transformed plasmid. The LB agar dishes were incubated over night at 37°C before colonies were harvested.

Preparation of plasmid DNA from bacteria:

To multiply single copies of plasmids, these plasmids were transformed into bacteria, plated on LB agar dishes and single colonies were used to inoculate 5 ml LB medium per colony. The cultures were shaken over night at 37°C before it was either used for the direct preparation of plasmid DNA or for storage, where 600 µl of the bacterial culture were mixed with 400 µl of 50% (v/v) glycerol in water and stored at -80°C. To inoculate a culture from a glycerol stock, a pipette tip was used to scrape off bacteria and transfer them into 5 ml LB medium for miniprep, or into 120 ml LB medium for a maxiprep. Either way the cultures were then incubated over night at 37°C with constant rotation. The plasmid DNA was isolated from the bacterial cultures using the PureLink Quick Gel Extraction Kit or the PureLink HiPure Plasmid Filter Maxiprep Kit respectively according to the manufacturers manual.

Name	Description	REF number	Supplier
Agarose	LE agarose	840004	Biozym
CloneJET PCR Cloning Kit	Blunt-ended PCR products generated with a proofreading enzyme are ligated directly into the cloning vector.	K1232	Thermo Fisher Scientific
TAE buffer, 50x	2 M Tris, 1 M acetic acid, 50 mM EDTA in H_2O, pH8.5	CL86.2	Carl Roth
SYBR Green	iQ SYBR Green Supermix	170-8884	BioRad
PureLink Quick Gel Extraction Kit	Silica spin column, binding <15 µg DNA, purification of DNA from TAE or TBE based agarose gels	K210012	Thermo Fisher Scientific
PureLink Quick Plasmid Miniprep Kit	Silica Spin Column, plasmid prepared from 2-4 ml bacterial culture	K210011	Thermo Fisher Scientific
Rapid DNA Ligation Kit	The kit contains T4 DNA ligase and a specially-formulated 5X rapid ligation buffer optimized for fast and efficient DNA ligation.	K1422	Thermo Fisher Scientific
DH5α-T1R *E. coli*	MAX Efficiency® DH5α™-T1R Competent Cells	12297016	Thermo Fisher Scientific
DH5α *E. coli*	Subcloning Efficiency™ DH5α™ Competent Cells	18265017	Thermo Fisher Scientific
ClearColi® BL21(DE3)	Genotype: F– ompT hsdSB (rB- mB-) gal dcm lon λ(DE3 [lacI lacUV5-T7 gene 1 ind1 sam7 nin5]) msbA148 ΔgutQΔkdsD ΔlpxLΔlpxMΔpagPΔlpxPΔeptA	60810-1	Lucigen
E. coli BL21	Genotype: E. coli B F– ompT gal dcm lon hsdSB(rB–mB–) [malB+]K-12(λS)	n.a.	n.a.
LB medium	For 1L medium use 25 g	X968.4	Carl Roth
LB agar	For 1L: 10 g SELECT Peptone 140, 5 g SELECT yeast extract, 5 g sodium chloride, 12 g SELECT Agar	22700025	Thermo Fisher Scientific
Glycerol	>99% purity, CAS # 56-81-5	G6279-500ml	Sigma Aldrich
PureLink HiPure Plasmid Filter Maxiprep Kit	For bacterial plasmids <40kb prepared from 100 ml bacterial culture	K210017	Thermo Fisher Scientific

Table 6. List of buffers, reagents, and bacterial strains for plasmid cloning.

Plasmid number	Plasmid description	Protein name	Source
#00506	pRP vector for the integration into a mammalian genome and expression of a recombinant protein. pBR322 origin of replication, *bla* gene for Ampicillin resistance. *Mammalian transcription cassette: CMV promoter, 5'LTR (Moloney murine sarcoma virus AHAH002383S1), packaging signal (FJ756409), pac gene for Puromycin resistance protein (Ref. Seq. M25346.1), SV40 early promoter, SV40 origin of replication, partial SV40 small t-antigen, hEF1 promoter including intron, signal peptide (Ref. seq. EU697460.1 nt: 1-45), hexa-His tag, aa: GAP, $LPETG_5$ tag, Linker: AAA, XA cleavage site (IDGR), aa: AAASG, mouse gamma-2a Ig heavy chain Fc (Ref. Seq. NT96355 Ighg2c, aa 109-340), 3'LTR (Moloney murine sarcoma virus M28247.1)*	6His-LPETG-L2-CTRL-Fc	Simon Görgen
#00834	pRP vector for the integration into a mammalian genome and expression of a recombinant protein. pBR322 origin of replication, *bla* gene for Ampicillin resistance. Mammalian transcription cassette: *CMV promoter, 5'LTR (Moloney murine sarcoma virus AHAH002383S1), packaging signal (FJ756409), pac gene for Puromycin resistance protein (Ref. Seq. M25346.1), SV40 early promoter, SV40 origin of replication, partial SV40 small t-antigen, hEF1 promoter including intron, signal peptide (Ref. seq. EU697460.1 nt: 1-45), hexa-His tag, $LPETG_5$ tag, Linker: APPPFGSLAA, XA cleavage site (IDGR), aa: AAASG, mouse gamma-2a Ig heavy chain Fc (Ref. Seq. NT96355 Ighg2c, aa 109-340), 3'LTR (Moloney murine sarcoma virus M28247.1)*	6His-LPETG-L9-CTRL-Fc	Simon Görgen
#00835	pRP vector for the integration into a mammalian genome and expression of a recombinant protein. pBR322 origin of replication, *bla* gene for Ampicillin resistance. Mammalian transcription cassette: *CMV promoter, 5'LTR (Moloney murine sarcoma virus AHAH002383S1), packaging signal (FJ756409), pac gene for Puromycin resistance protein (Ref. Seq. M25346.1), SV40 early promoter, SV40 origin of replication, partial SV40 small t-antigen, hEF1 promoter including*	6His-LPETG-L19-CTRL-Fc	Simon Görgen

	intron, signal peptide (Ref. seq. EU697460.1 nt: 1-45), hexa-His tag, LPETG$_5$ tag, Linker: APPPRPPDPPRPPPFGSLAA, XA cleavage site (IDGR), aa: AAASG, mouse gamma-2a Ig heavy chain Fc (Ref. Seq. NT96355 Ighg2c, aa 109-340), 3'LTR (Moloney murine sarcoma virus M28247.1)		
#00469	pRP vector for the integration into a mammalian genome and expression of a recombinant protein. pBR322 origin of replication, *bla* gene for Ampicillin resistance. Mammalian transcription cassette: *CMV promoter, 5'LTR (Moloney murine sarcoma virus AHAH002383S1), packaging signal (FJ756409), pac gene for Puromycin resistance protein (Ref. Seq. M25346.1), SV40 early promoter, SV40 origin of replication, partial SV40 small t-antigen, hEF1 promoter including intron, signal peptide (Ref. seq. EU697460.1 nt: 1-45), hexa-His tag, LPETG$_5$ tag, Linker: AP, hTYRO3 aa 42-429 (Ref. seq. NM_006293.3), aa: AAA, XA cleavage site (IDGR), aa: AAASG, mouse gamma-2a Ig heavy chain Fc (Ref. Seq. NT96355 Ighg2c, aa 109-340), 3'LTR (Moloney murine sarcoma virus M28247.1)*	6His-LPETG-L2-hTYRO3-Fc	Simon Görgen
#00792	pRP vector for the integration into a mammalian genome and expression of a recombinant protein. pBR322 origin of replication, *bla* gene for Ampicillin resistance. Mammalian transcription cassette: *CMV promoter, 5'LTR (Moloney murine sarcoma virus AHAH002383S1), packaging signal (FJ756409), pac gene for Puromycin resistance protein (Ref. Seq. M25346.1), SV40 early promoter, SV40 origin of replication, partial SV40 small t-antigen, hEF1 promoter including intron, signal peptide (Ref. seq. EU697460.1 nt: 1-45), hexa-His tag, LPETG$_5$ tag, Linker: APPPFGSAP, hTYRO3 aa 42-429 (Ref. seq. NM_006293.3), aa: AAA, XA cleavage site (IDGR), aa: AAASG, mouse gamma-2a Ig heavy chain Fc (Ref. Seq. NT96355 Ighg2c, aa 109-340), 3'LTR (Moloney murine sarcoma virus M28247.1)*	6His-LPETG-L9-hTYRO3-Fc	Simon Görgen
#00793	pRP vector for the integration into a mammalian genome and expression of a recombinant protein. pBR322 origin of replication, *bla* gene for Ampicillin resistance. Mammalian transcription cassette: *CMV promoter, 5'LTR (Moloney murine sarcoma virus AHAH002383S1), packaging signal (FJ756409), pac gene for Puromycin resistance protein (Ref. Seq. M25346.1), SV40 early promoter, SV40 origin of replication, partial SV40 small t-antigen, hEF1 promoter including intron, signal peptide (Ref. seq. EU697460.1 nt: 1-45), hexa-His tag, LPETG$_5$ tag, Linker: APPPRPPDPPRPP PFGSAP, hTYRO3 aa 42-429 (Ref. seq. NM_006293.3), aa: AAA, XA cleavage site (IDGR), aa: AAASG, mouse gamma-2a Ig heavy chain Fc (Ref. Seq. NT96355 Ighg2c, aa 109-340), 3'LTR (Moloney murine sarcoma virus M28247.1)*	6His-LPETG-L19-hTYRO3-Fc	Simon Görgen
#00470	pRP vector for the integration into a mammalian genome and expression of a recombinant protein. pBR322 origin of replication, *bla* gene for Ampicillin resistance. Mammalian transcription cassette: *CMV promoter, 5'LTR (Moloney murine sarcoma virus AHAH002383S1), packaging signal (FJ756409), pac gene for Puromycin resistance protein (Ref. Seq. M25346.1), SV40 early promoter, SV40 origin of replication, partial SV40 small t-antigen, hEF1 promoter including intron, signal peptide (Ref. seq. EU697460.1 nt: 1-45), hexa-His tag, LPETG$_5$ tag, Linker: AP, hAXL aa 33-451 (Ref. seq. NM_021913), aa: AAA, XA cleavage site (IDGR), aa: AAASG, mouse gamma-2a Ig heavy chain Fc (Ref. Seq. NT96355 Ighg2c, aa 109-340), 3'LTR (Moloney murine sarcoma virus M28247.1)*	6His-LPETG-L2-hAXL-Fc	Simon Görgen
#00794	pRP vector for the integration into a mammalian genome and expression of a recombinant protein. pBR322 origin of replication, *bla* gene for Ampicillin resistance. Mammalian transcription cassette: *CMV promoter, 5'LTR (Moloney murine sarcoma virus AHAH002383S1), packaging signal (FJ756409), pac gene for Puromycin resistance protein (Ref. Seq. M25346.1), SV40 early promoter, SV40 origin of replication, partial SV40 small t-antigen, hEF1 promoter including intron, signal peptide (Ref. seq. EU697460.1 nt: 1-45), hexa-His tag, LPETG$_5$ tag, Linker: APPPFGSAP, hAXL aa 33-451 (Ref. seq. NM_021913), aa: AAA, XA cleavage site (IDGR), aa: AAASG, mouse gamma-2a Ig heavy chain Fc (Ref. Seq. NT96355 Ighg2c, aa 109-340), 3'LTR (Moloney murine sarcoma virus M28247.1)*	6His-LPETG-L9-hAXL-Fc	Simon Görgen
#00795	pRP vector for the integration into a mammalian genome and expression of a recombinant protein. pBR322 origin of replication, *bla* gene for Ampicillin resistance. Mammalian transcription cassette: *CMV promoter, 5'LTR (Moloney murine sarcoma virus AHAH002383S1), packaging signal (FJ756409), pac gene for Puromycin resistance protein (Ref. Seq. M25346.1), SV40 early promoter, SV40 origin of replication, partial SV40 small t-antigen, hEF1 promoter including intron, signal peptide (Ref. seq. EU697460.1 nt: 1-45), hexa-His tag, LPETG$_5$ tag, Linker: APPPRPPDPPRPP PFGSAP, hAXL aa 33-451 (Ref. seq. NM_021913), aa: AAA, XA cleavage site (IDGR), aa: AAASG, mouse gamma-2a Ig heavy chain Fc (Ref. Seq. NT96355 Ighg2c, aa 109-340), 3'LTR (Moloney murine sarcoma*	6His-LPETG-L19-hAXL-Fc	Simon Görgen

	virus M28247.1)		
#00471	pRP vector for the integration into a mammalian genome and expression of a recombinant protein. pBR322 origin of replication, *bla* gene for Ampicillin resistance. Mammalian transcription cassette: *CMV promoter, 5'LTR (Moloney murine sarcoma virus AHAH002383S1), packaging signal (FJ756409), pac gene for Puromycin resistance protein (Ref. Seq. M25346.1), SV40 early promoter, SV40 origin of replication, partial SV40 small t-antigen, hEF1 promoter including intron, signal peptide (Ref. seq. EU697460.1 nt: 1-45), hexa-His tag, LPETG$_5$ tag, Linker: AP, hMER aa 22-505 (Ref. seq. NM_006343 with R466K, I518V, S627S), aa: AAA, XA cleavage site (IDGR), aa: AAASG, mouse gamma-2a Ig heavy chain Fc (Ref. Seq. NT96355 Ighg2c, aa 109-340), 3'LTR (Moloney murine sarcoma virus M28247.1)*	6His-LPETG-L2-MER-Fc	Simon Görgen
#00832	pRP vector for the integration into a mammalian genome and expression of a recombinant protein. pBR322 origin of replication, *bla* gene for Ampicillin resistance. Mammalian transcription cassette: *CMV promoter, 5'LTR (Moloney murine sarcoma virus AHAH002383S1), packaging signal (FJ756409), pac gene for Puromycin resistance protein (Ref. Seq. M25346.1), SV40 early promoter, SV40 origin of replication, partial SV40 small t-antigen, hEF1 promoter including intron, signal peptide (Ref. seq. EU697460.1 nt: 1-45), hexa-His tag, LPETG$_5$ tag, Linker: APPPFGSAP, hMER aa 22-505 (Ref. seq. NM_006343 with R466K, I518V, S627S), aa: AAA, XA cleavage site (IDGR), aa: AAASG, mouse gamma-2a Ig heavy chain Fc (Ref. Seq. NT96355 Ighg2c, aa 109-340), 3'LTR (Moloney murine sarcoma virus M28247.1)*	6His-LPETG-L9-hMER-Fc	Simon Görgen
#00833	pRP vector for the integration into a mammalian genome and expression of a recombinant protein. pBR322 origin of replication, *bla* gene for Ampicillin resistance. Mammalian transcription cassette: *CMV promoter, 5'LTR (Moloney murine sarcoma virus AHAH002383S1), packaging signal (FJ756409), pac gene for Puromycin resistance protein (Ref. Seq. M25346.1), SV40 early promoter, SV40 origin of replication, partial SV40 small t-antigen, hEF1 promoter including intron, signal peptide (Ref. seq. EU697460.1 nt: 1-45), hexa-His tag, LPETG$_5$ tag, Linker: APPPRPPDPPRPP PFGSAP, hMER aa 22-505 (Ref. seq. NM_006343 with R466K, I518V, S627S), aa: AAA, XA cleavage site (IDGR), aa: AAASG, mouse gamma-2a Ig heavy chain Fc (Ref. Seq. NT96355 Ighg2c, aa 109-340), 3'LTR (Moloney murine sarcoma virus M28247.1)*	6His-LPETG-L19-hMER-Fc	Simon Görgen
#00039	pEQ30 vector for the bacterial expression of recombinant proteins. pRB322 origin of replication, *bla* gene for Ampicillin resistance, CmR, rrnBT1 terminator. Bacterial transcription cassette: T5 promoter / lac operator element, MRGS amino acids, hexa-His tag, GS amino acids (BamHI), srtA Δ25 amino acids from n-terminus (Ref. Seq. AP014921.1, 2599644 to 2600264), lambda t0 terminator.	srtAΔ25 (*S. aureus*)	Hidde Ploegh
#00040	pET28a vector for the bacterial expression of recombinant proteins. pRB322 origin of replication, f1 origin of replication, *kanR* gene for Kanamycin resistance, LacI promoter, LacI cds. Bacterial transcription cassette: T7 promoter, lac operator, MRSS amino acids, hexa-His tag, SSGLVPRG amino acids including BamHI site, srtA Δ80 amino acids from n-terminus (Ref. Seq. AP017629.1, 881384 to 882133), T7 terminator.	srtAΔ80 (*S. pyogenes*)	Hidde Ploegh
#00595	pET30b vector for the bacterial expression of recombinant proteins. pRB322 origin of replication, f1 origin of replication, *kanR* gene for Kanamycin resistance, LacI promoter, LacI cds, rop cds. Bacterial transcription cassette: T7 promoter, lac operator, ATG start codon, srtA Δ59 amino acids from n-terminus (Ref. Seq. AP014921.1, 2599644 to 2600264 including the following mutations: P94R, D160N, D165A, G167E, K190E, K196T), LE amino acids (XhoI site), hexa-His tag, TGA stop codon, T7 terminator	5M srtA (*S. aureus*)	Hidde Ploegh
#00636	pET30b vector for the bacterial expression of recombinant proteins. pRB322 origin of replication, f1 origin of replication, *kanR* gene for Kanamycin resistance, LacI promoter, LacI cds, rop cds. Bacterial transcription cassette: T7 promoter, lac operator, ATG start codon, srtA Δ59 amino acids from n-terminus (Ref. Seq. AP014921.1, 2599644 to 2600264 including the following mutations: P94R, E105K, E108Q, D160N, D165A, G167E, K190E, K196T), LE amino acids (XhoI site), hexa-His tag, TGA stop codon, T7 terminator	7M srtA (*S. aureus*)	Hidde Ploegh
#00681	pRP vector for the integration into a mammalian genome and expression of a recombinant protein. pBR322 origin of replication, *bla* gene for Ampicillin resistance. Mammalian transcription cassette: *CMV promoter, 5'LTR (Moloney murine sarcoma virus AHAH002383S1), packaging signal (FJ756409), pac gene for Puromycin resistance protein (Ref. Seq. M25346.1), CMV promoter, signal peptide (Ref. seq. EU697460.1 nt: 1-45), aa: GS, hIGHG1 (Ref. seq. P01857 (Δ1-*	hIGHG1 Fc domain	Rainer Stahl

	98,E236D, M241L, stuffer sequence, 3'LTR (Moloney murine sarcoma virus M28247.1)		
Note that connecting segments of amino acids are marked as 'aa:' followed by the respective amino acid sequence as one letter code.			

Table 7. List and description of plasmids.

Design, nomenclature and production of bait and control proteins

The following experiments were perfomed with bait and control proteins that were designed as follows: Starting from the c-terminus, a mouse IgG2a Fc domain is used for purification and detection. A XA cleavage site was included to separate and potentially cleave the Fc domain from a respective TAM receptor's ectodomain for the bait proteins, and from the n-terminal tags for the control protein. The ectodomain of the TAM receptors without the endogenous signal peptide was fused to the recognition motif of *S. aureus* sortase A separated by one of three linkers. The linkers have a length of 2, 9, or 19 amino acids and are named L2, L9, and L19 respectively. For detection and purification puropses I included a hexa-His tag in front of the srtA motif. At the n-terminus of the bait and control proteins the signal peptide of trypsin leads to the secretion of the proteins. The control proteins contain the same tags as the bait proteins, but do not contain an ectodomain.

The bait and control proteins used in the following experiments were expressed in 293T cells either grown in serum freen DMEM or in 10% FBS containing DMEM and were purified via Protein A alone, or via Protein A followed by a HisTrap purification respectively. The molecular weight, the concentration, and purity of the prepared proteins were determined by comparing a known volume of the preparations to a titration a BSA standard in Coomassie stained SDS-PAGE gels (data not shown).

To distinguish the different versions of the bait and control proteins in the thesis, the proteins only purified and still posessing the unalterd n-terminus with the hexa-His tag will be named hexa-His-L2, -L9, or -L19 bait and control proteins. After the hexa-His-LPET is removed from the n-terminus by a srtA reaction, the proteins will be named L2, L9, or L19 bait and control proteins. The proteins with the diazirine cross-linker sortase tagged to the n-terminus will be named Diazirine-L2, L9, or L19 bait and control proteins.

Expression and purification of recombinant proteins

Expression of recombinant proteins in bacteria:

Transient expression of recombinant protein in bacteria was performed using the strain *E. coli* BL21. For expression of recombinant protein preventing TLR stimulation by LPS the *E. coli* strain ClearColi® BL21(DE3) by Lucigen was used. 50 ng of the expression plasmid were transformed into a 50 µl aliquot of chemo competent bacteria and incubated for 30 minutes on ice before being heat shocked at 42°C for 60 seconds and rested on ice for 2 minutes. 200 µl of LB medium were added to the culture, was incubated for 1 hour at 37°C with constant rotation of 700 rpm, before 150 µl of the culture were spread on a LB dish supplemented with an antibiotic corresponding to the resistance provided by the transformed plasmid. The dish was incubated over night at 37°C. Several colonies were inoculated into 6 ml LB medium supplemented with the antibiotic and incubated at 37°C with constant rotation over night. The cultures were stored as glycerol stocks at -80°C by mixing 600 µl of the bacterial culture with 400 µl of 50% (v/v) glycerol in water. The cultures were then tested for expression levels. From the glycerol stock of the best expressing clone a pre-culture of 24 ml was inoculated and grown at 37°C and constant rotation over night. The optical density at 600 nm was determined and a volume resulting in an OD600 of 0.015 diluted in 1 liter was added to 1 liter LB medium supplemented with the antibiotic to select for the respective expression plasmid. The 1 liter culture was incubated at 37°C and constant rotation until an OD600 of 0.4 was reached. The expression of the protein was induced by the addition IPTG to a concentration of 1 mM in the culture then further incubated for 4 hours. The bacteria were then harvested by centrifugation with 3200 g at 4°C for 15 minutes, washed with 20 ml of PBS and centrifuged again with 3200 g at 4°C for 10 minutes. The bacterial pellet was lysed in 20 ml of bacterial lysis buffer supplemented with 1 mM PMSF, cOmplete^{TM}, and 500 units of Benzonase® Nuclease. The lysate was sonicated with 4 cycles of one-minute sonication with 50% cycles at 100% power and one-minute rest on ice. The lysate was cleared of cellular debris by centrifugation with 12000 g at 4°C for 10 minutes. The supernatant was filtered through a 150ml Vacuum Filter with a pre size of 0.22 µm. The recombinant protein was then purified from the filtrate as described under ‘Protein purification via FPLC’.

Expression of recombinant proteins in mammalian cells:

Transient expression of recombinant protein in mammalian cells was performed using 293T cells. The cells were seeded over night to 40,000 cells per cm^2 a day before the transfection. On the day of transfection DNA and PEI are mixed in OptiMEM using 3 µg PEI per µg DNA. The transfection mix is incubated 20 minutes at room temperature, and then applied to the cells. 30

µg of plasmid was used per 15 cm dish. 4h after the transection the medium is exchanged either to 10% (v/v) DMEM or serum free DMEM.

Protein purification via FPLC:

For purification of proteins by affinity chromatography the ÄKTApurifier ^{TM} 100 from GE was used. TAMecto-Fc and Control-Fc proteins expressed in serum free medium were purified using Protein A columns. TAMecto-Fc and Control-Fc proteins expressed in serum containing medium were purified first using Protein A columns, and then $NiSO_4$ charged HisTrap columns. For all proteins purified, the buffer was exchanged to srtA reaction buffer, and the sample was concentrated using 10k centrifugal filter units according to manufacturers recommendations. Purified proteins were stored at -80°C in LoBind tubes.

Purifying Fc tagged proteins:

Proteins possessing mouse immunoglobulin Fc domains were affinity purified with Protein A columns. For proteins tagged with a photo-activatable cross-linker the procedure was performed in the dark. The pre-packed Protein A columns were used according to manufacturers recommendations. To prevent protein cross over in between preparations, individual columns were used for each type of protein to be purified. The preparations were performed at temperatures between 4 and 10 degree Celsius.

Before loading, the column was washed with 5 times the column volume of water and equilibrated with 5 times the column volume of PBS or TBS. Fc tagged protein-containing medium or lysate was loaded on the column and washed with 5 times the column volume of PBS or TBS. The Fc tagged protein was then eluted during fractionation using the Pierce IgG elution buffer. The protein containing fractions were either used for further purification or to exchange the buffer.

Purifying His tagged proteins:

Proteins possessing multi His tags were affinity purified with HisTrap columns. The columns were charged with $NiSO_4$ and further used according to manufacturers recommendations at temperatures between 4 and 10 degree Celsius.

Before loading, the pre-charged column was washed with 5 times the column volume of water and equilibrated with 5 times the column volume of His binding buffer. His-tagged protein containing solutions were loaded on the column and washed with 5 times the column volume of His wash buffer containing 5 to 20 mM Imidazole. After washing, the protein was eluted with His elution buffer containing 500 mM Imidazole during fractionation. The protein containing fractions were collected and the buffer was exchanged to srtA reaction buffer.

Exchanging buffers using desalting columns:

One 5 ml column or two 5 ml columns aligned consecutively were used according to the manufacturers recommendations. Before loading the sample, the columns were washed with water and equilibrated in the desired buffer. The TAMecto-Fc proteins purified by Protein A or Protein A and His purification were buffered in srtA reaction buffer. The protein sample was loaded with the beginning of sample fractionation. Fractions were pooled from the beginning of protein elution until the original buffer began eluting. The combined fractions were then concentrated using 10k centrifugal filter units according to the manufacturers recommendations.

Name	**Formulation**	**REF number**	**Supplier**
10k centrifugal filter units	Amicon Ultra-2 Centrifugal Filter Unit with Ultracel-10 membrane	UFC201024	Millipore
150mL Vacuum Filter	13.6 cm^2 polyethersulfone membrane with 0.22 µm pore size, 150 ml funnel capacity, 150 ml bottle capacity	431153	Corning
Ampicillin	Ampicillin, ready made solution, 100 mg/mL, 0.2 µm filtered, CAS RN 69-52-3, used at 100 µg/ml	A5354	Sigma Aldrich
Bacterial lysis buffer	50 mM Tris pH8.0, 10% (v/v) glycerol, 0.1% (v/v) Triton X-100, 1 mM PMSF, cOmplete™	n.a.	n.a.
ClearColi® BL21(DE3)	Genotype: F– ompT hsdSB (rB- mB-) gal dcm lon λ(DE3 [lacI lacUV5-T7 gene 1 ind1 sam7 nin5]) msbA148 ΔgutQΔkdsD ΔlpxLΔlpxMΔpagPΔlpxPΔeptA	60810-1	Lucigen
E. coli BL21	Genotype: E. coli B F– ompT gal dcm lon hsdSB(rB–mB–) [malB+]K-12(λS)	n.a.	n.a.
His binding buffer	20 mM sodium phosphate, 500 mM NaCl, pH 7.4	n.a.	n.a.
His elution buffer	20 mM sodium phosphate, 500 mM NaCl, 500 mM Imidazole, pH 7.4	n.a.	n.a.
His wash buffer	20 mM sodium phosphate, 500 mM NaCl, 5-20 mM Imidazole, pH 7.4	n.a.	n.a.
IPTG	Isopropyl-β-D-thiogalactopyranosid, CAS-Nr. [367-93-1]	CN08.3	Carl Roth
Kanamycin	Kanamycin sulfate, used at 100 µg/ml	11815024	Thermo Fisher Scientific
LB medium	25 g/L LB medium (Luria/Miller) in water	X968.4	Carl Roth
LB agar	32 g/L LB Agar, powder (Lennox L agar) in water	22700025	Thermo Fisher Scientific
Pierce™ IgG Elution Buffer	IgG elution buffer, pH2.8	21004	Thermo Fisher Scientific
HiTrap Desalting	Pre-packed with Sephadex G-25 Superfine	17140801	GE
HisTrap FF Crude	Pre-packed with pre-charged Ni Sepharose 6 Fast Flow	11-0004-58	GE
HisTrap HP	Pre-packed with Ni Sepharose High Performance	17-5247-01	GE
HiTrap Protein A HP	Pre-packed Protein A Sepharose High Performance column (1 ml) for preparative purification of antibodies	17-0402-01	GE
HiTrap rProtein A FF	Pre-packed with rProtein A Sepharose Fast Flow for purification and fractionation of IgG subclasses	17-5079-01	GE
1.5 ml LoBind tubes	Protein LoBind Tubes, Protein LoBind, 1.5 mL, PCR clean	0030108116	Eppendorf
2 ml LoBind tubes	Protein LoBind Tubes, Protein LoBind, 2.0 mL, PCR clean	0030108132	Eppendorf
Pierce IgG elution buffer	pH 2.8, amine based	21004	Thermo Fisher Scientific

Table 8. List of buffers, reagents, bacterial strains, and equipment for protein expression and purification.

Immunoprecipitation of proteins

Dynabeads:

Superparamagnetic beads were used to capture, precipitate and wash proteins containing an affinity tag. In case the concentration of protein to be captured in the solution to be purified from was known, beads were used in a volume corresponding to 1.5 times the binding capacity compared to the actual protein concentration. In case the concentration of protein to be precipitated was not known, the effective volume of beads per volume of protein solution was determined empirically.

The general washing procedure for Dynabeads includes 3 steps. First the beads in the sample or in buffer are placed on a DynaMag^{TM}-2 magnet in microcentrifuge tubes for 1 minute. Then the buffer was replaced with 5 times the original bead volume or 1 ml of washing buffer. The microcentrifuge tube was then rotated for 2 minutes on the MACSmix Tube Rotator fitted with the small tube rack. After repeating these steps according to the number of washes, the wash buffer was removed and the beads were resolved according to the follow up procedure.

Washing of Bait-Fc proteins with Protein A Dynabeads:

To wash Bait-Fc proteins in defined solutions, beads with a binding capacity of 1.5 times the concentration of protein to be washed were transferred from the bead stock to a microcentrifuge tube. The beads were once washed with assay buffer before being added to the protein solution. The solution was then incubated with the beads for 30 minutes at room temperature before being washed 3 times with 5 times the volume of the protein solution or maximally 1 ml.

Pre-clearing of lysates from biotinylated proteins via Dynabeads:

An excess amount of twice the volume of Dynabeads M-280 Streptavidin compared to the lysate solution to be cleared was washed. As wash buffer the lysis buffer used during the preparation of the sample to be cleared was used. After washing the beads, the wash buffer was removed and the sample was added to the beads and incubated for 30 minutes at RT. The bead containing lysate was then put on the DynaMag^{TM}-2 magnet for 1 minute, before the cleared lysate was transferred to a new microcentrifuge tube.

Magnetic separation of Microbeads with the HOKImag:

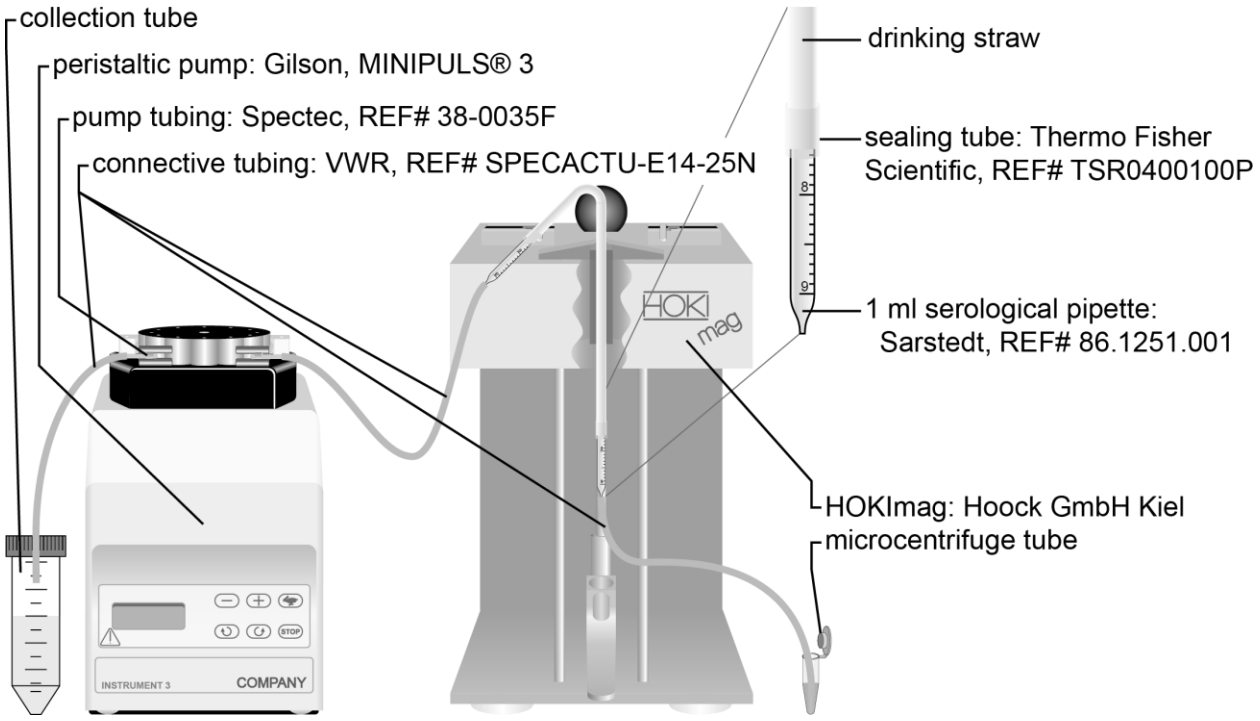

Figure 3. Schematic setup for magnetic separation of microbeads.

To magnetically separate microbeads from the liquid phase a HOKImag with 2-tesla field strength was used. For each separation a column was prepared with a drinking straw as basis. The tips of two 1 ml serological pipettes were cut and one was inserted into each end of the straw. The connections were sealed with 1 cm of a 4 mm silicone tube pushed over the straw and pipette overlapping area. On the long side of the column, a 1.5mm silicone tube was attached to the end of the pipette in order to reach into vessels containing microbead suspensions or buffers. On the short side of the column, a 1.5mm silicone tube was attached to the end of the pipette to connect the column with the pump tubing. The pump tubing was inserted into the MINIPLUS®3 peristaltic pump from Gilson and in turn connected to a 1.5 mm tube reaching into a collection tube.

For the magnetic separation, the HOKImag containing the column was put to a flat angle of 10° to 30° for the liquid to move upwards but to prevent gravitational forces to overcome the suction and the capillary force to cause the liquid column to drip. The liquid containing the microbeads was slowly moved into the column until all the liquid was in the magnetic field. For an efficient magnetic separation the microbeads were kept for 45 minutes in the magnetic field. After the separation the beads were washed slowly with wash buffers.

To remove the magnetic beads from the column, first a plunger from a 1 ml syringe was modified. Therefore a 1000 µl pipette tip was cut where it has about 2 mm of diameter and again

where it has about 5 mm diameter. The 2 to 5 mm diameter part was then used to replace the rubber part of a 1 ml syringe's plunger. Then the part of the column placed in the magnet was emptied from all liquid before being cut above and below the magnet and transferred into a microcentrifuge tube. With the modified plunger the beads were pushed into the tube. With the plunger still stuck though the column the remaining beads were washed from the column wall with the respective suspension buffer. The microcentrifuge tube containing the microbeads in the suspension buffer, the column and the plunger was placed into a 50 ml flacon and centrifuged for 1 minute and 3000 g at RT. Then the column and the plunger were removed from the microcentrifuge tube.

Washing of Bait-Fc proteins with Protein A microbeads:

To wash Bait-Fc proteins in defined solutions, microbeads with a binding capacity of 1.5 times the concentration of protein to be washed were transferred from the bead stock to the protein solution. The solution was then incubated with the microbeads for 30 minutes at room temperature before being loaded into a column inserted into the HOKImag. The microbeads containing protein solution was incubated for 45 minutes in the magnetic field before being washed with 5 ml of wash buffer. The column was then removed and the microbeads were resolved in a desired buffer and eluted into a microcentrifuge tube.

Name	**Description**	**REF number**	**Supplier**
1.5 mm tube	Tubing, silicone, extended life, by Spectrum	SPECACTU-E14-25N	VWR
4 mm tube	Sterilin™ silicone tubing, 4mm inner and 6 mm outer diameter,	TSR0400100P	Thermo Fisher Scientific
Drinking straw	5 mm x 24 cm, transparent, flexible	n.a.	n.a.
Pump tubing	PVC standard – pump tubing with flared end, 2 bridges, 2.565 mm outer, and 0.889 mm inner diameter, color code orange/orange	38-0035F	Spetec
Serological pipette, 1 ml	with cotton plug, polystyrene, sterile, non-pyrogenic/endotoxin-free, non-cytotoxic	86.1251.001	Sarstedt
Dynabeads™ M-280 Streptavidin	Superparamagnetic beads with a uniform size of 2.8 µm, covered with a monolayer of recombinant Streptavidin, blocked with BSA	11205D	Thermo Fisher Scientific
Dynabeads™ Protein A for Immunoprecipitation	Dynabeads™ Protein A are uniform, 2.8 µm superparamagnetic beads with recombinant Protein A covalently coupled to the surface.	10008D	Thermo Fisher Scientific
MicroBeads Protein A	µMACS Protein A MicroBeads	130-071-001	Miltenyi Biotech
Dynabeads™ Anti-Mouse IgG	Dynabeads™ M-280 Sheep Anti-Mouse IgG, 2.8 µm bead size	11201D	Thermo Fisher Scientific

Table 9. List of reagents and material for immunoprecipitation of proteins.

Detection of protein-protein interaction

Detection of protein-protein interaction with recombinant proteins:

To detect binding between a protein of interest and TAM-Fc fusion proteins, a titration of the recombinant protein of interest was prepared and 25 µl from each titration step were added to a half-area 96-well ELISA plate in duplicates and incubated over night at 4°C. After washing to remove unbound protein, the plate was incubated 2h at RT with 50 µl blocking buffer per well. The blocking buffer was removed and 25 µl of TYRO3-Fc, AXL-Fc, MER-Fc, Control-Fc, with the 2L linker version were used with the hexa-His tag removed via srtA tagging with triglycine if not stated elsewise. Proteins were concentrated to 25 µM in blocking buffer was added for 2h at RT if not stated otherwise. Alternatively Antibodies were used in the same volume and concentration. The plate was washed and the remaining Fc tagged proteins were marked with 25 µl per well of HRP labeled rat anti-mouse IgG from Cell Signaling (REF #7076) diluted 1/2000 for 30 minutes in the dark. After washing, 50 µl of ELISA substrate was added until a mid intensive blue color has appeared. The reaction was stopped using 25 µl of 1M sulfuric acid. The absorbance at 450 nm (Lm1) and 570 nm (Lm2) per well were measured with the SpectraMax i3 from Molecular Devices using the SoftMax Pro 6.3 software calculating the combined absorbance of Lm1 – Lm2. 50 µl of 1M TRIS was used to neutralize the solution before discarding it.

Washing of ELISA plates was performed using the BioTek Microplate Washer 405 T5 with 3 cycles of 100 µl ELISA wash buffer or using a multichannel pipette.

Name	Formulation	REF number	Supplier
α-Biotin-Rabbit-Ig	Anti-biotin (D5A7) Rabbit mAb	5597	Cell Signaling
Blocking buffer	5% (w/v) milk powder in PBS	n.a.	n.a.
ELISA plate	High binding, half area, flat bottom, 96-well plate	675061	Greiner Bio-One
ELISA substrate	OptEIA™ TMB Substrate Reagent Set	555214	BD
ELISA wash buffer	0.05% (v/v) Tween-20 in PBS	n.a.	n.a.
OptEIA Substrate A	ELISA substrate for HRP	51-2606KC	BD
OptEIA Substrate B	ELISA substrate for HRP	51-2607KC	BD
Wash buffer	0.1% (v/v) Tween-20 in TBS	n.a.	n.a.
hAHSG / hFETUA	Human fetuin-A (His tag), Met1-Val367 with a C-terminal poly-His tag, Ref seq. NP_001613.2, Expression host: human cells	10318-H08H	Sino Biological
bAlb	Pierce Bovine Serum Albumin Protein Assay Standard, buffered in 0.9% saline solution with 0.05% sodium azide, formulated at 2.00 +/-0.03 mg/mL	23209	Thermo Scientific
hC6	Human recombinant C6 protein, His tagged, expressed in HEK293 Cells, Purity > 90% as determined by SDS-PAGE	12426-H08H-100	Sino Biological
hCNDP2 / hCPGL	Recombinant human cytosol nonspecific dipeptidase, *Spodoptera frugiperda* (Sf 21, baculovirus) derived, Met1-Asp475, with a C-terminal 10-His tag	3560-ZN	R&D
hENO1	Human ENO1 / Enolase 1 / alpha-enolase protein (His tag), Ref Seq P06733-1, Met1-Lys434 with poly His tag at N-	11554-H07E	Sino Biological

	terminus, expression host: *E. coli*		
hFINC / hFN1	Human plasma-derived Fibronectin protein, Purity > 90% confirmed by SDS-PAGE	1918-FN-02M	Sino Biological
hGAS6	Recombinant human Gas6 protein Ala49-Ala678, with a c-terminal 6-His tag, reconstituted in water, expressed in Mouse myeloma cell line NS0, Purity >90% confirmed by SDS-PAGE	885-GS-050	R&D
hGNB2L1 / hRACK1	Human GNB2L1 (P63244), Met1-Arg317, with an N-terminal poly-His and MBP tag, expression host: *E. coli*	12498-H10E	Sino Biological
hMPO	Recombinant human Myeloperoxidase/MPO protein Ala49-Ser745, with a C-terminal 10-His tag, expressed in Mouse myeloma cell line NS0, Purity >90% confirmed by SDS-PAGE	3174-MP	R&D
mMPO	Recombinant mouse Myeloperoxidase/MPO protein Met16-Thr718, with a C-terminal 10-His tag, expressed in Mouse myeloma cell line NS0, Purity >90% confirmed by SDS-PAGE	3667-MP-250	R&D
hNPEPPS	Recombinant human Puromycin-sensitive aminopeptidase / NPEPPS, *Spodoptera frugiperda* (Sf 21, baculovirus) derived, Pro46-Val919, with an N-terminal Met and a C-terminal 10-His tag, Accession # P55786	6410-ZN-010	R&D
hPKM2	Recombinant human PKM2, E. coli derived, Ser2-Pro531, with N-terminal Met and 6His tag	7244-PK-020	R&D
hPRDX5	Human peroxiredoxin 5 (His tag), Met53-Leu214, with a poly-His tag at N-terminus, Ref seq. P30044-2, expression host: *E. coli*	11263-H07E	Sino Biological
hRAB14	Buffered in 50mM Tris HCl, 2mM beta-mercaptoethanol, 100mM Sodium chloride, 10mM Magnesium chloride, 0.01mM GDP, pH 8.0	ab90105	Abcam
hRAN	Recombinant protein with a His-tag corresponding to amino acids 1 to 216 of human RAN, Source is *E. coli*, Buffered in 20 mM Tris-HCl (pH8.0) containing 1 mM DTT, 10% (v/v) glycerol, >90% purity confirmed by SDS-PAGE	NBP1-45255-0.05mg	Novus Biologicals
hRPS3	Recombinant protein with a His-tag corresponding to amino acids 1 to 243 of human RPS3, Source is *E. coli*, Buffered in 20 mM Tris-HCl (pH8.0) containing 1 mM DTT, 10% (v/v) glycerol, 0.1 M NaCl, >90% purity confirmed by SDS-PAGE	NBP1-72495-50ug	Novus Biologicals
hS100A6	Recombinant human S100A6 with 6His tag, Source is Baculovirus-Insect Cells, lyophilized from 50mM Tris, 100mM NaCl, 0.5mM PMSF, 1mM TCEP, pH 8.0, additionally 5% - 8% trehalose, mannitol and 0.01% Tween80, Purity > 96% determined by SDS-PAGE	10939-H08B-20	Sino Biologicals
hS100A8/A9 chimera	E. coli-derived human S100A8/ S100A9 non-covalently-linked heterodimer protein Met1-Glu93 (S100A8) & Thr2-Pro114 (S100A9), reconstituted in PBS, Purity >95% confirmed by SDS-PAGE	8226-S8-050	R&D
hSPR	Recombinant protein with a His-tag corresponding to SPR, Source is *E. coli*, Buffered in 20 mM Tris-HCl (pH8.0), 10% (v/v) glycerol, >95% purity confirmed by SDS-PAGE	NBC1-21657	Novus Biologicals
hSR-B1-Fc	Recombinant human SR-BI Fc protein chimera, Pro33-Tyr443 (hSR-BI) + IEGRMD + Pro100-Lys330 (hIgG1), expressed in HEK293 cells, Purity >90% confirmed by SDS-PAGE	8114-SR-050	R&D
mThy1-Fc	Recombinant Mouse CD90/Thy1 Fc Chimera Protein, Mouse Thy (Gln20-Lys130) + IEGRMDP + mouse IgG2A (Glu98-Lys330), Source is mouse myeloma cell line NS0, reconstituted in PBS, purity confirmed >95% by SDS-PAGE with silver staining	7335-CD-050	R&D

Table 10. List of buffers and reagents for the detection of protein-protein interaction.

Sortase A mediated transpeptidation

The enzymes used for Sortase A mediated transpeptidation was the 5M srtA (Plasmid #00595) from *S. aureus*. The enzyme was expressed and purified as described under 'Expression of recombinant proteins in bacteria' and stored as aliquots at -80°C. Bait-Fc proteins used for transpeptidation contained an n-terminal $LPETG_5$ tag recognized by the enzyme. Small molecules used for transpeptidation by sortase A contained a c-terminal LPETGG peptide. N-terminal Sortase transpeptidation was performed in two steps.

For the first step the protein to be sortase tagged was added together with 5M srtA and triglycine into the reaction buffer. The reaction was performed at 37°C with 6 µM 5M srtA and 1-2 mM triglycine if not stated elsewise. The protein was then washed utilizing affinity based magnetic separation methods like Dynabeads described under 'Washing of Bait-Fc proteins with Protein A Dynabeads', Microbeads described under 'Washing of Bait-Fc proteins with Protein A microbeads' or affinity matrices in FPLC columns described under 'Purifying Fc tagged proteins' binding the Fc tag of the Bait-Fc proteins. As wash buffers PBS, TBS, or the reaction buffer without any additives were used.

For the second step the Bait-Fc proteins from the first Sortase tagging step were added to the reaction buffer together with a small molecule linked to a LPETGG peptide and the respective sortase. If not stated elsewise the reaction was performed using 6 µM 5M srtA and the small molecule with 40 times the concentration of Bait-Fc protein for 30 minutes at 37°C. The reaction was stopped by the addition of 20 mM EDTA. After the reaction was completed, the Bait-Fc proteins were washed as described before.

To calculate the free Ca^{2+} concentrations in srtA reaction buffer titrating EDTA, EGTA, or BAPTA as chelator, the online tool WEBMAXC STANDARD (7/3/2009) was used available at (http://maxchelator.stanford.edu/webmaxc/webmaxcS.htm).

Name	Formulation	REF number	Supplier
Diazirine-LPET*GG	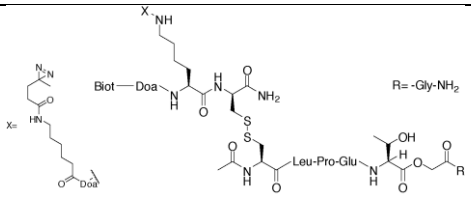 1702.79 Da, 97.5% purity by RP-HPLC, 2.5 mg, lyophilized as trifluoroacetic acid salt resolved in 10% (v/v) DMSO in water to 4000 µM, aliquots stored at –80°C protected from light	n.a. (Lot 13106/HS_ Fragment AB_F25-28Pool)	Intavis
TAMRA-LPET*GG	TAMRA-GGLPET*GG (* = depsi peptide)	67225	Peptide 2.0 Inc.
Triglycine (Gly-Gly-Gly)	50 mM stock prepared in water, aliquots stored at -80°C	G1377-1G	Sigma
srtA reaction buffer	20 mM HEPES, 150 mM NaCl, 10 mM $CaCl_2$ in H_2O, pH7.4	n.a.	n.a.

Table 11. List of buffers and reagents used for sortase tagging.

Cross-Linker activation by UV light

Cross-linker activation by BLX-365:

For UV irradiation with the BLX-365 samples in 1.5 ml microcentrifuge tubes were placed into a rack with the lid open. The microcentrifuge tubes were placed centrally below a light tube. To illuminate the sample with a defined dose of UV light, the machine was set to ‘UV Energy exposure‘. For experiments with UV doses above 9 Joule the microcentrifuge tubes were placed into a rack where the lower part of the tube reached into an ice water bath.

Cross-linker activation with the 500W arc lamp:

The arc lamp was controlled and powered by the OPS-A500 from Oriel Instruments. The arc lamp used was a 500W Hg/Xe arc lamp set up together with the Lamp Socket Adapter in the Arc Lamp Housing. LIK-LMP Light Intensity Controller Kit was connected to the housing to control the light intensity. To limit infra red light a liquid filter was connected to the focusing mount of the Arc Lamp Housing and filled with deionized water. To limit the exposure of a sample, an electronic safety shutter was connected to the liquid filter followed by the Beam Turning Mirror Housing equipped with a 280-400nm dichroic mirror defining the wavelength applied to the sample. The light path was initially adjusted by the technical support of Newport. The light path was focused into 1.5 ml microcentrifuge tubes containing the samples. The electronic safety shutter automatically controlled the time of illumination.

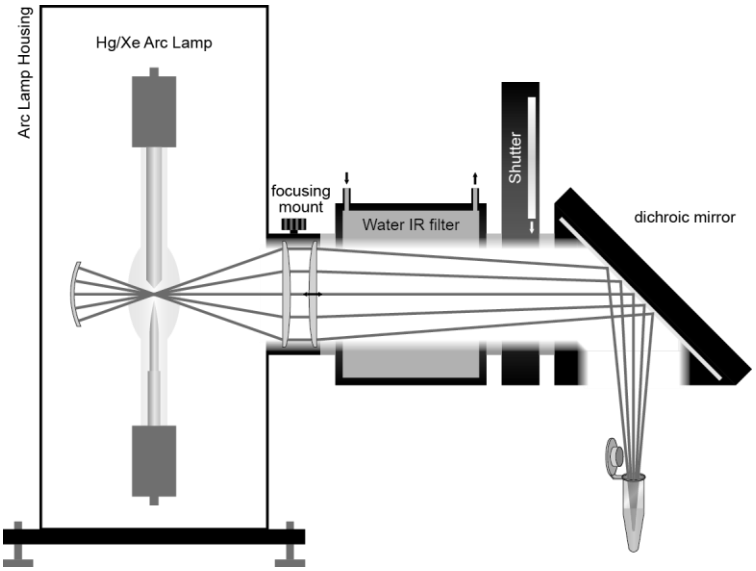

Figure 4. Schematic setup of the Hg/Xe Arc Lamp.
The Hg/Xe 500W arc-lamp was combined with a focusing mount to enable a site specific application of UV irradiation, a water filter to remove the irradiated IR spectrum, a dichroic mirror to further reduce the irradiated spectrum, and a shutter to limit the irradiation time.

SDS-PAGE and protein detection

For SDS-PAGE, samples were prepared with LDS Sample Buffer and if not stated elsewise, with Sample Reducing Agent. Both were used diluted to 1 times concentration in the samples that were then boiled at 85°C to 95°C for 10 minutes before being loaded on pre-cast 4-12% Bis-Tris gels. The gels were run in either MOPS or MES buffer using the X Cell system. The electrophoresis was performed under cooling conditions with 100 to 200 Volts as limiting factor, while Amperage and Watts were adjusted to the respective conditions based on the voltage set. Proteins were then detected either by western blotting, silver staining, Coomassie R250 staining, fluorescent detection, or by a combination of those. Proteins were either quantified in coomassie stained SDS-PAGE gels as described below, or with the BCA Protein Assay Kit according to the manufacturer's manual.

Protein detection via western blot:

For the transfer of proteins from a SDS-PAGE gel to a PVDF membrane (Merck Millipore, Immobilon FL, REF #IPFL0010) the Thermo Fisher X Cell II Blot Module (REF #E19051) was used in combination with the X Cell system used for the SDS-PAGE according to the manufacturers protocol using 15% (v/v) methanol in Tris-Glycine buffer prepared from (Thermo Fisher, Pierce™ 10X Tris-Glycine Buffer, REF #28363). The PVDF membrane was activated with methanol before usage. After the transfer of proteins, the membrane was incubated for 1h at RT or over night at 4°C with blocking buffer in a 50 ml falcon. The proteins of interest were marked with specific primary Antibodies (see Table 13) and unspecific bound antibodies were removed with 3 washes of 10 ml of wash buffer. The primary antibodies or Fc tagged proteins were then marked with secondary antibodies fluorescently labeled with IRDye680 or IRDye800 purchased from LI-COR. After removing unspecific bound antibodies with 2 washes of 10 ml wash buffer and one wash of 10 ml of TBS, the blots were scanned with the LiCor Odyssey and analyzed with the Image Studio Ver 4.0 software. The Channels were adjusted to a linear relation between signal input and output. The lower signal cut off was set to the minimal signal intensity measured on the blot. The higher signal cut off was set to the maximal signal intensity measured on the blot excluding the marker bands if not stated else wise. Images were exported as .png files.

Protein detection via Coomassie:

To stain proteins in SDS-PAGE gels with Coomassie R250, the gels were incubated for 15 minutes in 50 ml of Coomassie staining buffer on a rotary shaker at RT. The staining buffer was removed and the gel was washed with water before 50 ml of Coomassie destaining buffer was

added. The destaining was performed over night on a rotary shaker at RT. The destaining buffer was once replaced in the evening and, in case the destaining was insufficient, in the morning. The gel was destained until most of the Coomassie was removed from the gel parts not containing any protein. Coomassie stained SDS-PAGE gels were imaged with the VersaDoc system and the setup suggested by the software. Gels were illuminated for 0.2-0.4 seconds depending on the remaining background staining. Illuminations were adjusted within the dynamic range of the system.

Protein quantification in coomassie stained SDS-PAGE gels:

To quantify a protein, a defined volume was loaded on a SDS-PAGE gel as well as known amounts of BSA (taken from the BCA kit). At least 0.5, 0.75, 1.0, and 1.5 µg of BSA were used. After the separation, proteins were detected via coomassie as described before. The gel was then imaged with the VersaDoc and the image was imported into the software 'Image Studio Lite', or 'Image Studio Ver 4.0'. Shapes were placed around the protein to be quantified and around the BCA standards. The quantification values were imported into excel. A graph for the BSA standards was created with the known amounts on the y-axis and the quantification intensities on the x-axis. A trend line including x=y=0 was calculated. The amount of protein loaded in the sample wells was calculated by inserting the sample's color intensity value into the trend line formula. The amount of protein calculated to be loaded onto the gel, divided by the volume of sample loaded, gives the concentration of protein within the sample.

Protein detection via Silver Stain:

To stain proteins in SDS-PAGE gels by silver staining the Pierce™ Silver Stain for Mass Spectrometry kit was used according to the manual. Silver stained SDS-PAGE gels were documented with the VersaDoc system with the setup suggested by the software. Illumination times were chosen within the dynamic range of the system.

Protein detection via fluorescence:

Proteins labeled with fluorescent molecules were visualized in the VersaDoc gel documentation chamber equipped with a Tamron 28-80mm f1/3.5-5.6 AF aspherical objective. The setup of the chamber was prepared according to the instructions provided by the software. Illumination times were chosen within the dynamic range of the system.

Name	Formulation	REF number	Supplier
BCA Protein Assay Kit	Two-component, high-precision, detergent-compatible assay reagent set to measure total protein concentration compared to a protein standard.	23225	Pierce™
Bis-Tris gel, 4-12%, 1.0 mm X 10 well	1D well format, separation range: 15 to 260 kDa (MOPS buffer), 3.5 to 160 kDa (MES buffer)	NP0321BOX	Thermo Fisher Scientific
Bis-Tris gel, 4-12%, 1.5 mm X 10 well	1D well format, separation range: 15 to 260 kDa (MOPS buffer), 3.5 to 160 kDa (MES buffer)	NP0335BOX	Thermo Fisher Scientific
Bis-Tris gel, 4-12%, 1.0 mm X 15 well	1D well format, separation range: 15 to 260 kDa (MOPS buffer), 3.5 to 160 kDa (MES buffer)	NP0323BOX	Thermo Fisher Scientific
Bis-Tris gel, 4-12%, 1.5 mm X 15 well	1D well format, separation range: 15 to 260 kDa (MOPS buffer), 3.5 to 160 kDa (MES buffer)	NP0336BOX	Thermo Fisher Scientific
Immobilon® FL	Immobilon-FL PVDF, 0,45 µm, 26,5 cm x 3,75 m, needs to be treated with methanol before use.	IPFL00010	Merck Millipore
PageRuler™ Plus	Prestained Protein Ladder from 10 to 250 kDa	26619	Thermo Fisher Scientific
Transfer buffer	15% (v/v) methanol in 1xTris Glycine buffer	n.a.	n.a.
Tris Glycine buffer, 10x	Diluted to 1x: 25 mM Tris, 192 mM glycine, pH8.5	28363	Thermo Fisher Scientific
α-hTYRO3 mouse IgG	Detects human Tyro3 in ELISAs and Western blots. Monoclonal Mouse IgG1, Protein A or G purified from hybridoma culture supernatant The Immunogen is S. frugiperda insect ovarian cell line Sf 21-derived recombinant human Tyro3/Dtk (Ala41-Ser428 (predicted), Accession # Q06418)	MAB859	R&D Systems
α-hAXL rabbit Ig (Ectodomain)	Detects human and monkey AXL in western blots, polyclonal antibodies of rabbits immunized with a synthetic peptide around Leu283 of the human Axl extracellular domain.	#3269	Cell Signaling
α-hAXL rabbit Ig (Kinase domain)	Detects human AXL in western blots, polyclonal antibodies of rabbit synthetic peptide corresponding to sequences surrounding amino acid residue 740 of human Axl.	#4977	Cell Signaling
α-phospho Tyr702 hAXL rabbit Ig	Phospho-Axl (Tyr702) (D12B2) Rabbit monoclonal Antibody for western blot, may cross-react with related tyrosine-phosphorylated tyrosine kinases, such as EGFR.	#5724	Cell Signaling
α-hAXL goat IgG	Detects human Axl in direct ELISAs and Western blots. In direct ELISAs, less than 25% cross-reactivity with recombinant mouse Axl is observed. Polyclonal Goat IgG, Immunogen was Mouse myeloma cell line NS0-derived recombinant human Axl (Glu33-Pro440, Accession # AAA61243)	AF154	R&D Systems
α-hAXL mouse IgG	Detects human Axl in direct ELISAs. In direct ELISAs, this antibody shows no cross-reactivity with recombinant mouse Axl, recombinant human (rh) TYRO3 or rhMER. Monoclonal Mouse IgG1, Immunogen was Mouse myeloma cell line NS0-derived recombinant human Axl (Met1-Pro440, Accession # AAA61243)	MAB154	R&D Systems
α-hMER mouse IgG (Ectodomain)	Detects endogenous levels of human MER in western blots, does not show cross-reactivity, monoclonal mouse IgG1 of animals immunized with human MER ectodomain.	# 9178S	Cell Signaling
α-hMER mouse IgG (Ectodomain)	Detects human Mer in direct ELISAs and Western blots. In Western blots, does not cross-react with recombinant human (rh) Axl, rhTYRO3, or rmMER, Monoclonal Mouse IgG2B, Immunogen was cell line Sf 21-derived recombinant human MER (Ala21-Ala499, Accession # Q12866.2)	MAB8911	R&D Systems
α-hGAS6 goat IgG	Detects human Gas6 in ELISAs and Western blots. Cross-reaction is expected, Polyclonal Goat IgG, Immunogen was Mouse myeloma cell line NS0-derived recombinant human Gas6 (Asp118-Ala678, Accession # NP_000811)	AB885	R&D Systems

α-hGAS6 goat IgG (biotinylated)	Detects human Gas6 in Western blots. In Western blots, approximately 15% cross-reactivity with recombinant mouse Gas6 is observed. Polyclonal Goat IgG, Immunogen was Mouse myeloma cell line NS0-derived recombinant human Gas6 (Asp118-Ala678, Accession # NP_000811)	BAF885	R&D Systems
α-hGAS6 mouse IgG	Detects human Gas6 in direct ELISAs and Western blots. In direct ELISAs and Western blots, this antibody shows approximately 5% cross-reactivity with recombinant mouse Gas6. Monoclonal Mouse IgG2A, Immunogen was Mouse myeloma cell line NS0-derived recombinant human Gas6 (Asp118-Ala678, Accession # NP_000811)	MAB885	R&D Systems
α-hGAS6 rat IgG	Detects mouse Gas6 in direct ELISAs and Western blots. In direct ELISAs and Western blots, this antibody does not cross-react with recombinant human Gas6. Monoclonal Rat IgG2A, Immunogen was Mouse myeloma cell line NS0-derived recombinant mouse Gas6 (Asp115-Pro674 (Del Pro530), Accession # Q61592.2)	MAB986	R&D Systems
α-hGAS6 mouse IgG	Detects human GSA6 in western blots, polyclonal mouse Ig from animals immunized with GAS6 (NP_000811.1, 1 a.a. ~ 678 a.a)	SAB1410502	Sigma Aldrich
α-hProtein S mouse IgG	Detects human Protein S in direct ELISAs and Western blots. In direct ELISAs and Western blots, does not cross-react with recombinant mouse Protein S. Monoclonal Mouse IgG1, Immunogen was Mouse myeloma cell line NS0-derived recombinant human Protein S (Ala42-Trp670, Accession # P07225)	MAB4036	R&D Systems
α-Mouse-IRDye680	IRDye® 680RD Donkey anti-Mouse IgG (H + L), 0.5 mg	926-68072	LI-COR
α-Mouse-IRDye800	IRDye® 800CW Donkey anti-Mouse IgG (H + L), 0.5 mg	926-32212	LI-COR
α-Rabbit-IRDye680	IRDye® 680RD Donkey anti-Rabbit IgG (H + L), 0.5 mg	926-68073	LI-COR
α-Rabbit-IRDye800	IRDye® 800CW Donkey anti-Rabbit IgG (H + L), 0.5 mg	926-32213	LI-COR
α-Goat-IRDye800	IRDye® 800CW Donkey anti-Goat IgG (H + L), 0.5 mg	926-32214	LI-COR
Strept-IRDye680	IRDye® 680RD Streptavidin, 0.5 mg	926-68079	LI-COR
Strept-IRDye800	IRDye® 800CW Streptavidin, 0.5 mg	926-32230	LI-COR
LDS Sample Buffer, 4x	NuPAGE® LDS Sample Buffer, lithiumdodecylsulfate, glycerol, pH8.4	NP0008	Thermo Fisher Scientific
Sample Reducing Agent, 10x	NuPAGE® Sample Reducing Agent, 500 mM Dithiothreitol	NP0009	Thermo Fisher Scientific
MOPS buffer, 20x	At 1x concentration: 50 mM MOPS, 50 mM Tris Base, 0.1% (w/v) SDS, 1 mM EDTA, pH 7.7	NP0001-02	Thermo Fisher Scientific
MES buffer, 20x	At 1x concentration: 50 mM MES, 50 mM Tris Base, 0.1% (w/v) SDS, 1 mM EDTA, pH 7.3	NP0002-02	Thermo Fisher Scientific
Coomassie Brilliant Blue R-250	Binds primarily to basic amino acids in acidic conditions, the coomassie dye on a protein is approximately proportional to positive charges on the protein, absorption maximum 595 nm	20278	Thermo Fisher Scientific
Coomassie staining buffer	For 1L: 3 g Coomassie R-250, 450 ml methanol, 100 ml acetic acid, in water, dissolved for 1 day, filtered	n.a.	n.a.
Coomassie destaining buffer	15% (v/v) isopropanol, 10% (v/v) acetic acid, in water	n.a.	n.a.
Silver Staining Kit	Pierce™ Silver Stain for Mass Spectrometry containing Silver Stain Sensitizer, Silver Stain Enhancer, Silver Stain Developer, Silver Stain, Silver Destain Reagent A, Silver Destain Reagent B	24600	Pierce

Table 12. List of buffers, reagents, and kits for immunoblots.

Co-IP of cross-linker activated bait and control proteins from complex samples

Preparation of bait proteins in complex samples:

The proteins used as bait, TYRO3-Fc, AXL-Fc, and MER-Fc and the control protein CTRL-Fc were tagged with the photo-activatable cross-linker Diazirine. The complex samples used were human plasma, lysates from C57BL/6J wild type mice's adipose tissue, brain, spleen, and testis, and human brain lysates from healthy patients, and patients either diagnosed with mild cognitive impairment (MCI) or Alzheimer's disease (AD). Prof. Dr. Michael T. Heneka provided the human brain samples. Lysates and plasma from 3 individuals were used per bait protein.

The samples were prepared on ice and in subdued light. Whenever possible the samples were protected from light until the activation of the photosensitive cross-linker. For each sample 13 pmol of bait protein were added to 1 mg of lysate or 100 µl of human plasma in a 1.5 ml microcentrifuge tube. The volumes of bait proteins were adjusted to 29.74 µl with TRIS neutralized Pierce IgG elution buffer. The volumes of lysates and plasma were adjusted to 125.1 µl with N-P40 tissue lysis buffer. The samples were incubated at 37°C for 30 minutes protected from light.

Photo-activation of cross-linker:

If not specified otherwise, the Diazirine cross-linker was activated with 9 Joules in the BLX-365 UV box as described under 'Cross-linker activation by BLX-365'.

Co-immunoprecipitation of bait proteins:

Following the UV activation of Diazirine, the bait proteins were immunoprecipitated with anti-Mouse IgG Dynabeads. 61 µl beads per sample were washed two times in PBS, added to the samples and incubated 30 minutes at RT with constant rotation in a MACSmix Tube Rotator on maximal speed. The sample containing microcentrifuge tubes were placed in a DynaMag™-2 magnet for 2 minutes. The supernatant was discarded and 200 µl RIPA buffer was added before the beads were resuspended and washed by >2 minutes of rotation. The RIPA wash step was repeated 4 times. The supernatant was discarded and 200 µl PBS was added before the beads were resuspended and washed by >2 minutes of rotation. The PBS wash step was repeated 2 times. The supernatant was discarded and the beads were stored and shipped at -80°C.

Name	Description	REF number	Supplier
Neutralized Pierce IgG elution buffer	For 280 µl: 250 µl Pierce IgG elution buffer (pH2.8), 30 µl 1M TRIS (pH8.0)	n.a.	n.a.

Table 13. List of Buffers and Solutions for Co-IP of cross-linked bait and control proteins.

Protein identification and quantification by LC-MS/MS

The following procedures for ‘peptide identification and quantification by LC/MS’ were conducted and reported by Annika Frauenstein at the Max Planck Institute in Munich, supervised by Dr. Felix Meissner. Data of proteins identified and quantified comparing methods were provided log2 transformed and filtered. Data of proteins identified and quantified screening for novel TAM interacting proteins were provided already transformed and filtered including meta-data.

Preparation of samples on beads for LC/MS:
The samples of baits and control proteins cross-linked to putative interacting proteins and molecules immunoprecipitated by anti-Mouse IgG Dynabeads were resolved in 50 µl 8M Urea in 10 mM HEPES and sonicated for 10 minutes. 1 µl DTT was added before a 30-minute incubation at RT, followed by the addition of 10 µl IAA and 20 minute incubation at RT in the dark. Then 11 µl Thiourea and 2 µl LysC were added before a 1-hour incubation at RT, followed by the addition of 200 µl ABC and 2 µl Trypsin. The samples were then incubated over night before 27 µl of the stop solution was added.

Preparation of lysates and plasma for LC-MS/MS:
Aliquots of the lysates and of the plasma used for the co-immunoprecipitation of cross-linker activated bait and control proteins from complex samples were used as controls for the LC/MS analysis.

LC-MS/MS:
The peptides prepared were separated on an EASY-nLC 1000 HPLC coupled to the Q Exactive HF mass spectrometer via a nanoelectrospray source. For the separation, the peptides were run in buffer A through a column packed with 1.9 µm C18 particles and eluted with a nonlinear 180 min gradient of 5-60% buffer B at a flow rate of 0.25 µl/min and a column temperature of 55°C. The column had an inner diameter of 75 µm and a length of 50 cm. The Q Exactive HF was data dependently operated with a survey scan range of 300-1,650 m/z and a resolution of 60,000 to 120,000 at m/z 200. Up to 10 of the most abundant Isotype patterns having a charge above 1 were isolated with a 1.8 Thomson window and administered to fragmentation by higher-energy collisional dissociation at normalized collision energy of 26. The fragmentation spectra acquired had a resolution of 15,000 at m/z 200. Sequenced peptides were dynamically excluded after 30 seconds in order to reduce repeated sequencing. The thresholds used for ion injection time were

set to 20 ms and 3E6, and the thresholds for ion target values were set to 55 ms and 1E5 for the MS/MS scans. The Xcalibur software was used to acquire the data.

LC-MS/MS protein identification and filtration:

MS Raw files were analyzed with the MaxQuant software. Peptide sequences were compared to the UniProtKB FASTA files from human or mouse respectively (Version July 2015). Common contaminants were identified by a second database.

In Perseus, the data of proteins identified and quantified were analyzed separately for mouse tissue samples, human brain samples and human plasma samples. The samples were grouped according to bait or control and tissue. The LFQ intensity values were log2 transformed and proteins marked 'reverse', 'only identified by site' or 'potential contaminant' were excluded from the matrix. The matrix was then reduced to proteins having 3 valid values in at least one group. Missing values were replaced by imputation with a width of 0.3 and a downshift of 1.8.

Name	Description	REF number	Supplier
Octadecyl (C18) Solid Phase Extractions Disks	Empore™, provides up to 90% solvent reduction, contamination-free extractions	n.a.	n.a.
Bioruptor Plus	Sonication device	n.a.	Diagenode
Concentrator plus	Vacuum concentrator	n.a.	Eppendorf
ReproSil-Pure C18-AQ column	20-50 cm, 75 µm inner diameter, 1.9 µm resin	n.a.	Dr. Maisch GmbH
UHPLC	Ultra-high pressure liquid chromatography, e.g. EASY-nLC 1000 ultra-high pressure system	n.a.	Thermo Fisher Scientific
Mass spectrometer	High resolution mass spectrometer, e.g. Q Exactive or Q Exactive HF	n.a.	Thermo Fisher Scientific
Column oven	n.a.	n.a.	Sonation
MaxQuant	Software available at http://www.coxdocs.org/doku.php?id=maxquant:common:download_and_installation	n.a.	n.a.
Perseus	Software for MS data analysis (www.coxdocs.org/doku.php?id=perseus:common:download_and_installation	n.a.	n.a.
SprayQC	Software	n.a.	n.a.

Table 14. List of equipment and software for LC & MS analysis.

Name	Description	REF number	Supplier
1 M HEPES, pH8.0	For 50 ml: 11.9 g HEPES in water, pH adjusted with NaOH, 0.22 µm sterile filtered	n.a.	n.a.
1 M ABC	For 50 ml: 4 g NH_4HCO_3 in water, 0.22 µm sterile filtered	n.a.	n.a.
Digestion buffer, 4x	8M urea, 40 mM HEPES pH8.0, 0.22 µm sterile filtered	n.a.	n.a.
1 M DTT	1M Dithiothreitol (DTT), 50 mM ABC, 0.22 µm sterile filtered	n.a.	n.a.
0.55 M IAA	0.55 M Iodoacetamide (IAA), 50 mM ABC, 0.22 µm sterile filtered	n.a.	n.a.
1M Thiourea	1M Thiourea, 50 mM ABC, 0.22 µm sterile filtered	n.a.	n.a.
1 mM HCl	For 50 ml of 1 mM hydrochloric acid (HCl): 4 µl (v/v) to 50 ml water	n.a.	n.a.
Trypsin	Used at 0.5 µg/µl trypsin in 1 mM HCl	n.a.	Sigma
LysC	Used at 0.5 µg/µl Lysyl endopeptidase (LysC) in 50 mM ABC	n.a.	Wako
Stop solution	6% (v/v) Trifluoroacetic acid (TFA), 60% (v/v) acetonitrile	n.a.	n.a.

Buffer A	0.5% (v/v) acetic acid in water	n.a.	n.a.
Buffer A*	0.5% (v/v) acetic acid, 0.1% (v/v) TFA, 2% (v/v) acetonitrile in water	n.a.	n.a.
Buffer B	0.5% (v/v) acetic acid, 80% (v/v) acetonitrile in water	n.a.	n.a.
Running buffer B	0.1% (v/v) formic acid, 80% (v/v) acetonitrile, in water	n.a.	n.a.

Table 15. List of buffers and reagents for LC & MS analysis.

Protein identification by MALDI-TOF and Ion trap-ESI-LC-MS

Proteins contained in gel slices from silver stained SDS-PAGE gels were identified by the mass spectrometry core facility of the University of Bonn by MALDI-TOF and Ion trap-ESI-LC-MS instruments. The exact protocols of protein isolation and digestion as well as for the protein identification were not specified.

Statistics

Nomenclature for statistics:

x	= data point	p	= probability value
x_i	= each of the data points	q	= corrected probability value
$\bar{x}$	= mean of data points	*	= p or q < 0.05
n	= number of data point	**	= p or q < 0.01
σ	= standard deviation	***	= p or q < 0.001
Σ	= sum of	◡	= exponential curve fit
$\surd$	= square root	∫	= sigmoidal curve fit
H_0	= null hypothesis	Q	= threshold p-Value in %
H_A	= alternative hypothesis	S0	= artificial within groups variance

Mean:

The mean of data points was either calculated automatically by Prism6 or Prism7, by the function '=MITTELWERT(x_i)' in Excel, or manually by the following formula:

$$\bar{x} = \frac{x_1 + x_2 + \cdots x_n}{n}$$

Sample standard deviation (SD):

The sample standard deviation of data points was either calculated automatically by Prism6 or Prism7, by the function '=STABW.S(x_i)' in Excel, or manually by the following formula:

$$\sigma_{n-1} = \sqrt{\frac{\sum_{i=1}^{n}(x_i - \bar{x})^2}{n-1}}$$

Standard error of the mean (SEM):

The sample standard deviation of data points was calculated automatically by Prism6 or Prism7, by the function '=STABW.S(x_i)/WURZEL(ANZAHL2(x_i))' in Excel, or manually by the following formula:

$$SE_{\sigma_{n-1}} = \frac{\sigma_{n-1}}{\sqrt{n}}$$

Analysis of protein enrichment by bait proteins in MS screen and method comparison:

General differences or similarities of samples were analyzed by Perseus' clustering according to the Spearman correlation (hierarchical cluster of row and tree by Spearman correlation of distances, and 300 clusters processing with k-means), by Spearman rank correlation of samples (Row correlation, Spearman rank correlation), and by principle component analyses (PCA without category enrichment). For each tissue two-sided and unpaired Student's T.Tests with an alpha of 5% assuming same variance were performed comparing either TYRO3 or AXL to the control testing proteins with at least 3 valid values for the bait protein. Probabilities were corrected for multiple testing using Perseus' permutation based FDR of 5% (two-sided Student's t-test with S0=0, including rows with 3 valid values in the bait group, corrected by permutation-based FDR, FDR=0.05 and 250 randomizations without preserving the grouping). Proteins were sorted for FDR discoveries or for significant enrichment in at least 3 conditions.

Probability calculation of a certain number of significant events or more for a certain number of tests to be random:

A two-sided t-test with a cut-off of 0.05 accepts 5% of events being considered as significant in a random and normally distributed system. As the test is two-sided 2.5% of all tests enriched towards the control and 2.5% of all hits enriched towards the bait result together in the total of 5% accepted as significant. To calculate the probability of a certain number of 'significant' events enriched by bait protein in a random and normally distributed system, the probabilities of the events have to be multiplied with each other and with the number of possible combinations leading to the specific number of significant and non-significant events. The probability of a certain number of significant events or more is the sum of those probabilities.

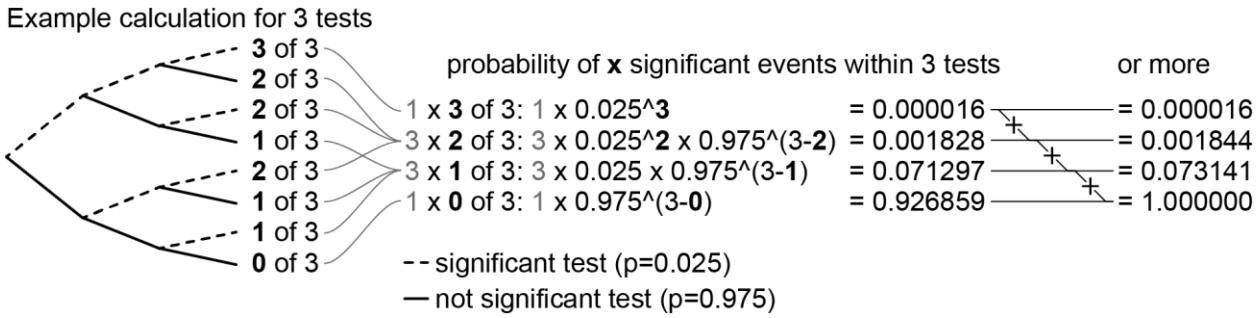

Non-linear regression and multiple t-test for protein-protein binding in 96 well data:

Using the program Prism7 it was tested whether the binding curves of different bait proteins to a recombinant protein share a common curve for all data sets as H_0 or if they have different curves for each dataset as H_A. First, using nonlinear regression testing 'sigmoidal, 4PL, X is log(concentration)' it was determined if one curve adequately fits all the other data sets using the extra sum-of-squares F-test, where the simpler model is selected unless the P value is less than 0.05. In case a sigmoidal curve fit could not be calculated for the data, the data were tested for a 'second order polynomial (quadratic)' curve fit using the same test parameter as for the sigmoidal curve fit. The null hypothesis was rejected when the p value was smaller than 0.05.

In case the null hypothesis was rejected, multiple t-tests were performed comparing the bait proteins to the control. Discoveries were determined using the Two-stage linear step-up procedure of Benjamini, Krieger and Yekutieli with Q=5%. Each row was analyzed individually, without assuming a consistent SD.

Network analysis

The online database STRING10 (date: 10.04.2018) was used to search for published associations between proteins. Gene ontology enrichments were performed with the Cytoscape tools ClueGO & CluePedia. Protein localization was based on associated 'Cellular Component' GO terms. These GO terms were provided by the online databases 'Gene ALaCart' (date: 16.04.2018; LifeMap Sciences and Weizmann Institute of Science) and QuickGO (16.04.2018; EMBL-EBI).

3. Results

Since the discovery and characterization of the tyrosine receptor kinases TYRO3, TYRO7 known as AXL and TYRO12 known as MER 1991 (*87*, *124*) Protein S and GAS6 were discovered as the main functional ligands 1995 by evaluating conditioned media for their ability to activate TYRO3 (*29*). Examples of further interacting proteins are the proteins TUBBY and TULP1 identified as 'eat me' signals in a phage display assay and subsequently identified to bind MER in retinal pigment epithelial cells after testing various receptors in co-IP experiments (*38*). LGALS3 was identified in a functional phagocytosis and receptor binding enriched phage-display screen (*41*) by the same group, which additionally reconfirmed the interaction of MER with TULP1 (*125*). An example of interacting receptors is IFNAR1, discovered by investigating how TAM receptor stimulation leads to the inhibition of inflammation (*22*).

The goal of this study is the identification of novel TAM receptor interacting proteins focusing on interactions with the ectodomain of the receptors in a broader variety of tissues reported to express TAM receptors. To achieve this aim, first a method needed to be designed to enrich also weak and transient interacting proteins from a variety of tissues. The method of choice was based on co-immunoprecipitation of TAM receptor ectodomains by a c-terminally attached mouse IgG Fc domain. To allow the formation of dimers the hinge region of the Fc domain was included. An n-terminal srtA recognition motif (LPETG) enabled the site-specific attachment of molecules like cross-linkers or fluorescent dyes. For the cross-linker used, the addition of a biotin molecule and a disulfide bond connecting the biotin/Diazirine moiety to the LPETG motif enabled multiple ways of usage. Amongst others, it allows the cross-linker to be used either for the fixation of weak and transient interacting proteins to the bait and thereby for their enrichment via co-IP, or for labeling such proteins with biotin and enrichment of biotin labeled proteins. The cross-linker chosen was photo-activatable to control the time of activation. Avoiding the cross-linker moiety being linked to a possible site of interaction on the bait protein, site-specific transpeptidation by the bacterial enzyme sortase A was chosen to link maximally one cross-linker per bait protein specifically to its n-terminus. Following the conceptual design of the method all components were tested and optimized to ensure optimal functionality.

TAM receptor ectodomain bait proteins bind GAS6 and Fibronectin but not Protein S

TAM receptor ectodomains fused c-terminally to mouse IgG Fc domains were used succesfully in many studies for co-IP experiments and to prevent TAM receptor signalling by sequestering GAS6 and Protein S from the stimulating medium (*29*, *126*, *127*). GAS6 is reported to bind all

three TAM receptors with varrying affinities (*1*), while Protein S is reported to only show very weak affinity to TYRO3 and MER but not to AXL (*126*). Chen and colleagues determined the affinity of human TAM receptor ectodomain-Fc proteins to GAS6 by Surface Plasmon Resonance spectroscopy resulting in equilibrium dissociation constants (K_d) of 1.6±0.3 nM for hAXL-Fc, 3.6±1.3 nM for hTYRO3-Fc, and 9.7±1.8 nM for hMER-Fc (*30*). As the bait and control proteins used in the following experiments differ from previously published versions, especially in their n-terminally added hexa-His-linker peptide sequence, I reconfirmed the affinities of the used bait and control proteins to recombinant human GAS6 and Protein S (Figure 5). The 19L linker versions of the three TAM receptors bait proteins showed significantly higher affinities to GAS6 compared to the control-Fc protein. In compliance with literature (*32*), no TAM ectodomain Fc bait protein showed a distuingishable affinity to Protein S compared to Control-Fc protein (Figure 5 C). Bait and control protein binding detected for 81 nM immobilized Protein S were significantly higher as Control-Fc binding to a comparable concentration of GAS6. Together this indicates an affinity of the bait and control protein's Fc domain to Protein S. In accordance with previous publications detection of TAM receptor-Fc protein binding to Protein S in ELISA or Co-IP assays is not expected (*32*). However Protein S activation of TAM receptors could be detected by kinase receptor activation assays (*126*). Together, TAM receptor bait proteins show affinities to GAS6 significantly higher as the Control protein and affinities to Protein S as expected and are therefore valid to be used as bait for affinity enrichment experiments.

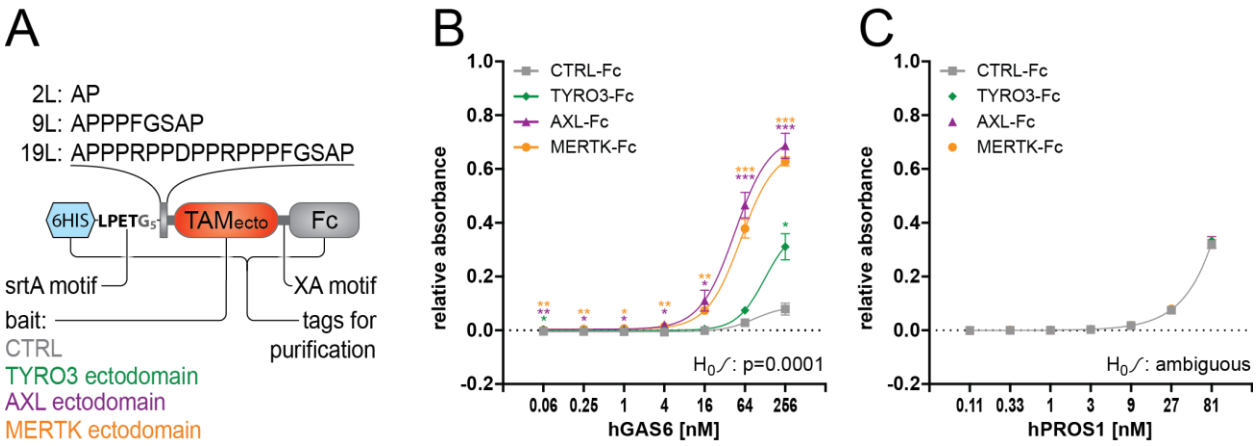

Figure 5. Affinity of TAM receptor bait proteins to hGAS6 and hProtein S.

The affinity of TAM receptor ectodomain bait proteins, schematically described under A, were tested for their affinity to hGAS6 (B) and hProtein S (C) in an ELISA assay and compared to control proteins including a spacer instead of a TAM ectodomain. Bait and control proteins with the 19L linker version lacking the n-terminal hexa-His tag were used to detect protein interaction. Wells without protein served as negative control (Neg). α-GAS6 IgG (MAB885) and α-PROS1-IgG (MAB4036) as detection antibodies binding to the maximal concentrated GAS6 and Protein S respectively served as positive control (Pos).

The MEAN values minus the negative control relative to the positive control are shown with the SEM of 3 technical repeats with technical duplicates each. The probability of a common sigmoidal curve fit (H_0) is shown and significant differences of respective bait to control in FDR corrected T-Tests are indicated as follows: * q<0.05, ** q<0.01, *** q<0.001

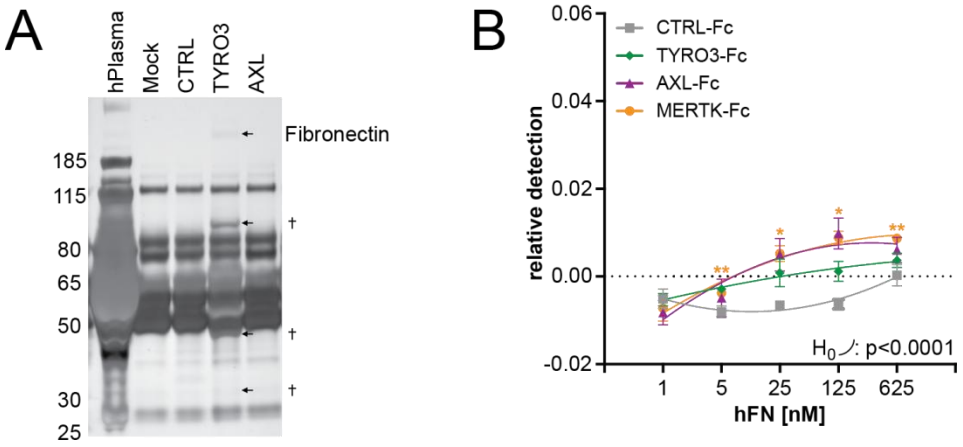

Figure 6. Co-IP enriching FN1 as TAM receptor interacting protein in human plasma.
Proteins, co-immunoprecipitated from human plasma with hexa-His-L2 bait or control proteins were separated via SDS-PAGE and silver stained. Differentially enriched proteins, marked with an arrow, were excised and identified via mass spectrometry. Protein bands with known contaminants as major protein identified are marked with a cross, otherwise the most abundant protein identified is named (A). Human Fibronectin was tested for TAM receptor interaction in an ELISA assay (B), utilizing L2 bait and control proteins as detection proteins. Wells without protein served as negative control (Neg) and AXL-Fc binding to 50 nM GAS6 served as positive control (Pos).
The MEAN values minus the negative control relative to the positive control are shown with the SEM of 3 technical repeats with technical duplicates each. The probability of a common exponential curve fit (H_0) is shown and significant differences of respective bait to control in FDR corrected T-Tests are indicated as follows: * q<0.05, ** q<0.01, *** q<0.001

Although TAM receptor ectodomains fused to IgG Fc domains are commonly used for TAM receptor ligand studies and to neutralize ligands (*29*, *127*), I tested whether the designed bait and control proteins can be used to isolate proteins binding specifically to TAM ectodomains via co-immunoprecipitation from a complex sample as an organ lysate or body fluid. Comparing proteins enriched by hexa-His L2 versions of CTRL-Fc, TYRO3-Fc, and AXL-Fc from human plasma, 4 protein bands were uniquely detected in the hexa-His L2 TYRO3-Fc immunoprecipitation (Figure 6 A). These unique protein bands were excised handed to the Mass Spectrometry Core Facility of the University of Bonn for identification of contained proteins. LC-MS analysis identified Fibronectin as the major Protein from the first band, while no proteins were identified in the other excised bands exceeding Keratin, a known contaminant (data not shown). Recombinant human Fibronectin was then tested for direct interaction with TAM receptor ectodomains (Figure 6 B). Fibronectin showed a higher affinity to the ectodomains of TAM receptors compared to the control protein and the difference in binding of the MER bait protein compared to the control protein reached statistical significance, however bait proteins were detected with below 2% compared to the signal of AXL bait binding 50 nM hGAS6.
With the functionality of the bait and control proteins confirmed, Fibronectin was successfully enriched from human plasma in a co-IP without cross-linking and detection by silver staining. However the assay was not sensitive enough to enrich TAM receptor ligands as GAS6 or Protein S.

Establishment of optimal SrtA transpeptidation conditions for n-terminal tagging

In order to attach a single cross-linker molecule site specifically to the n-terminus of the bait and control proteins, transpeptidation mediated by the bacterial enzyme sortase A was the method of choice. As the products obtained by srtA transpeptidation of photo-activatable cross-linker to proteins were about to be used as bait and control in co-immunoprecipitation and label transfer experiments the products had to meet the following requirements: The bait and control proteins had to be in solution to ensure optimal distribution within the prey matrix. The proteins had to be separated from materials like beads, excess cross-linker molecules and enzyme used during transpeptidation. All steps including the photo-activatable cross-linker needed to be performed in conditions protecting from UV light to prevent premature cross-linker activation. Comparable amounts of cross-linker needed to be tagged to bait and control proteins.

The protocol published for srtA transpeptidation used as reference needed to be optimized for the 5M srtA version used in this study, small molecules as peptides for n-terminal tagging, and to lower protein concentrations obtained by mammalian in contrast to bacterial protein expression. The following experiments determine optimal concentrations and conditions for srtA transpeptidation of small LPETGG peptide linked molecules to the n-terminus of mammalian expressed and purified bait and control proteins.

To prepare a protein for n-terminal srtA transpeptidation with a payload, first a glycine needs to be exposed at the protein's n-terminus. For this purpose the bait and control proteins were designed with an n-terminal hexa-His tag followed by an LPETG motif. SrtA was used to hydrolyze the bond between threonine and glycine in the LPETG motif leaving a glycine at the n-terminus of the protein. To prevent re-ligation of the hexa-His-LPET peptide to the available free glycine of the protein, an excess amount of triglycine was added to the reaction. The concentration of enzyme needed to achieve maximal reaction efficiency at 30 minutes reaction time was determined for the control and the three bait proteins and for each linker version L2, L9, and L19 by titrating the srtA enzyme (Figure 7 A). For all control and bait protein versions, the minimal concentration of srtA necessary to achieve a complete exposal of a glycine at the n-terminus characterized by the removal of hexa-His-LPET was 6 µM (Figure 7 B to E).

For the transpeptidation of a payload to the exposed n-terminal glycine of control or bait proteins having completed the first tagging step, several conditions were compared in order to reach optimal efficiencies. TAMRA-LPET*GG was titrated with L19 AXL-Fc at a srtA concentration of 6 µM, 30 minutes reaction time at 37°C. The titration resulted in a sigmoidal increase of TAMRA tagged to the protein. At 20 µM TAMRA-LPET*GG concentration, approximately 80% of the maximal efficiency was reached (Figure 8).

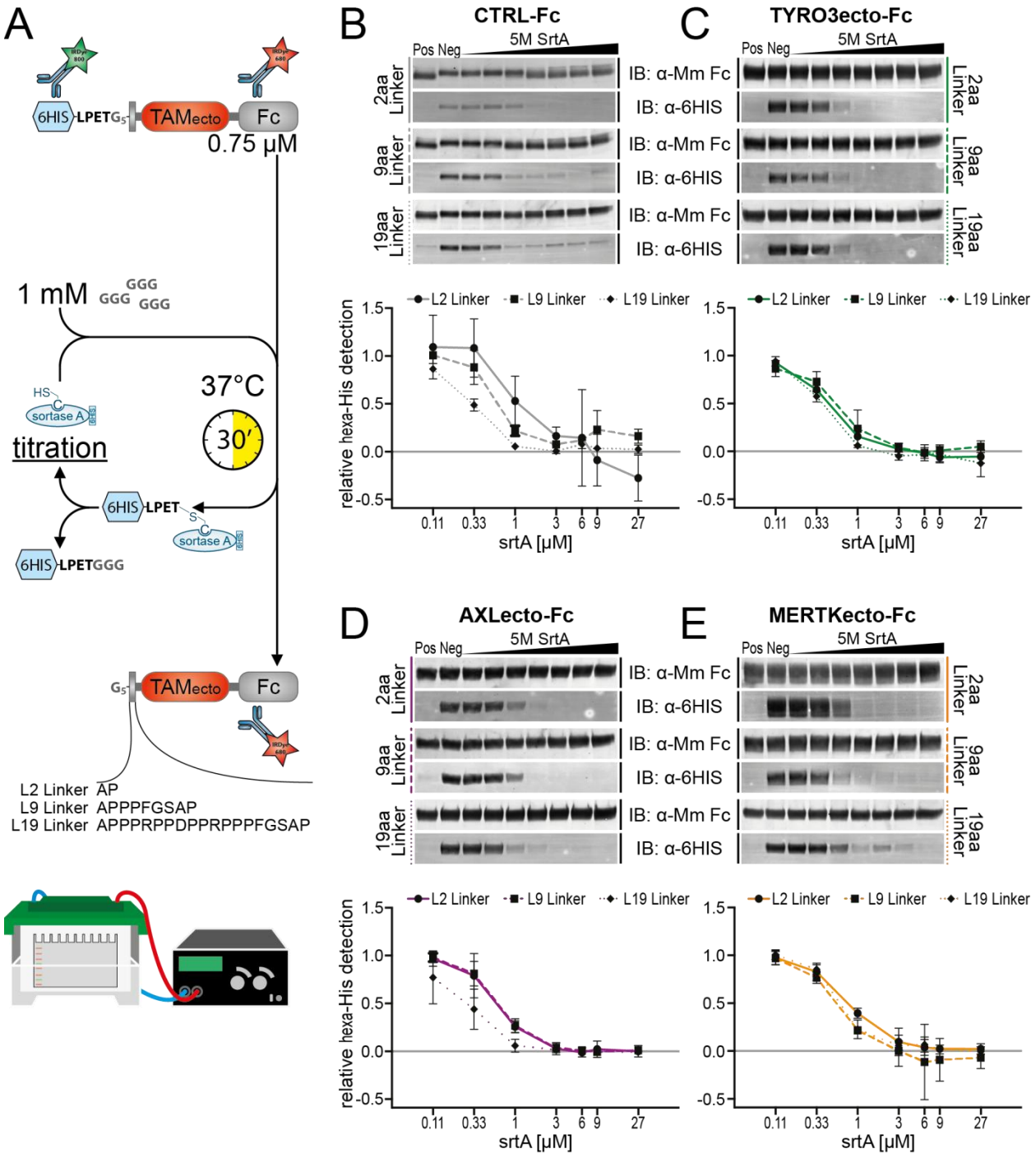

Figure 7. SrtA titration for the first tagging step.

Titrations of srtA in reactions with 1000 µM tri-glycine and 0.75 µM bait or control proteins were tested for each linker version (A). The reaction efficiencies were accessed by detecting and quantifying hexa-His-LPET remaining on the respective protein after the srtA reaction via Western Blot. The efficiencies were compared to reactions performed with 4 µM srtA serving as a positive control (Pos) and reactions without srtA serving as the negative control (Neg). Signals of detected His tag were divided by the signal of detected Fc tag, subtracted by the positive control and divided by the negative control (B to E).

The MEAN and SD of three technical replicates is shown.

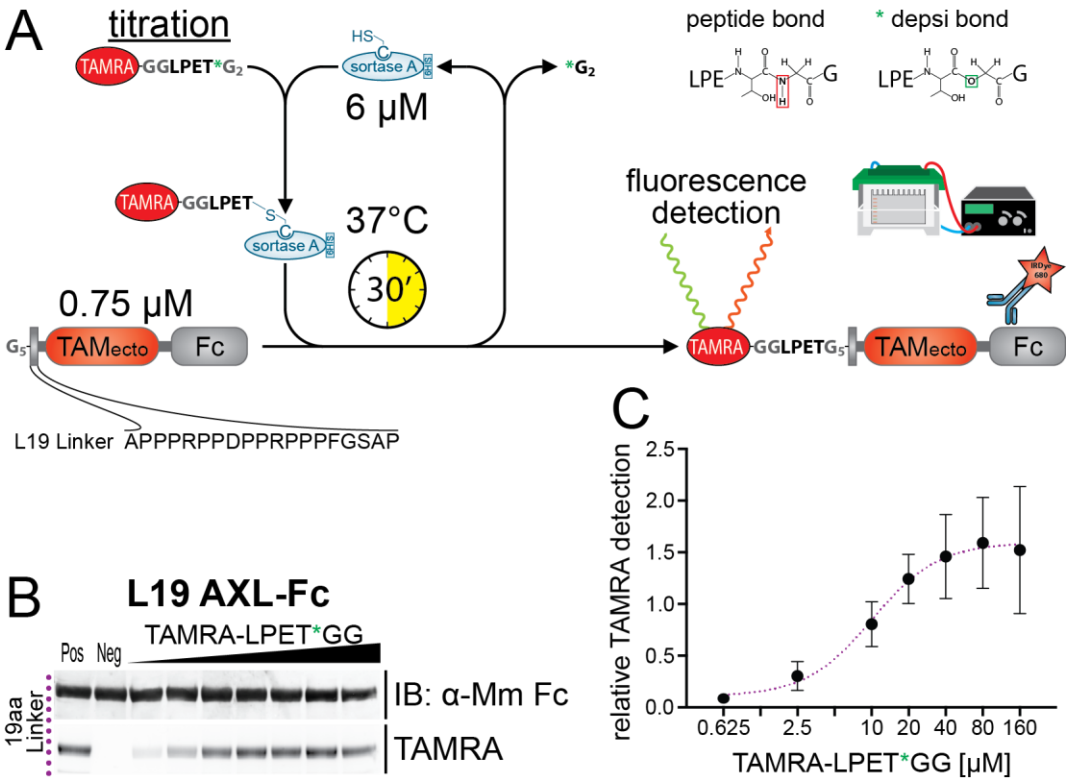

Figure 8. Titration of TAMRA-LPET*GG in srtA reactions.
TAMRA-LPET*GG was titrated in reactions with 0.75 µM L19 AXL-Fc and 6 µM srtA. The reaction was stopped with 20 mM EDTA after 30 minutes incubation at 37°C. TAMRA linked to L19 AXL-Fc was quantified by detecting the fluorescence intensity of AXL-Fc proteins separated from free TAMRA-LPET*GG via SDS-PAGE. L19 AXL-Fc protein was quantified after Western Blot detection of its Fc tag. Reactions without TAMRA-LPET*GG served as negative control (Neg) and samples with 40 µM TAMRA-LPET*GG served as positive control (Pos). The relative TAMRA detection was calculated by subtracting the negative control from the TAMRA signal relative to the positive control. The MEAN and SD of three technical replicates is shown with a sigmoidal curve fit.

To determine the effect of srtA concentration in reactions with 0.75 µM protein, 30 µM TAMRA-LPET*GG and 30 minute reaction time at 37°C, titrations of srtA were tested for the bait and control proteins and each of their linker variants. The efficiencies determined shown in Figure 9 do not vary depending on the linker separating the site of tagging from the protein, except for L2 MER-Fc. For the MER-Fc linker version L2 the efficiency was lower compared to the L9 and L19 linker versions at srtA concentrations below 3 µM. The efficiency curves from all protein variants rise from low srtA concentrations to reach a maximum between 3 and 9 µM sortase A. At 27 µM srtA, close to the concentration of TAMRA-LPET*GG, the tagging efficiency dropped.

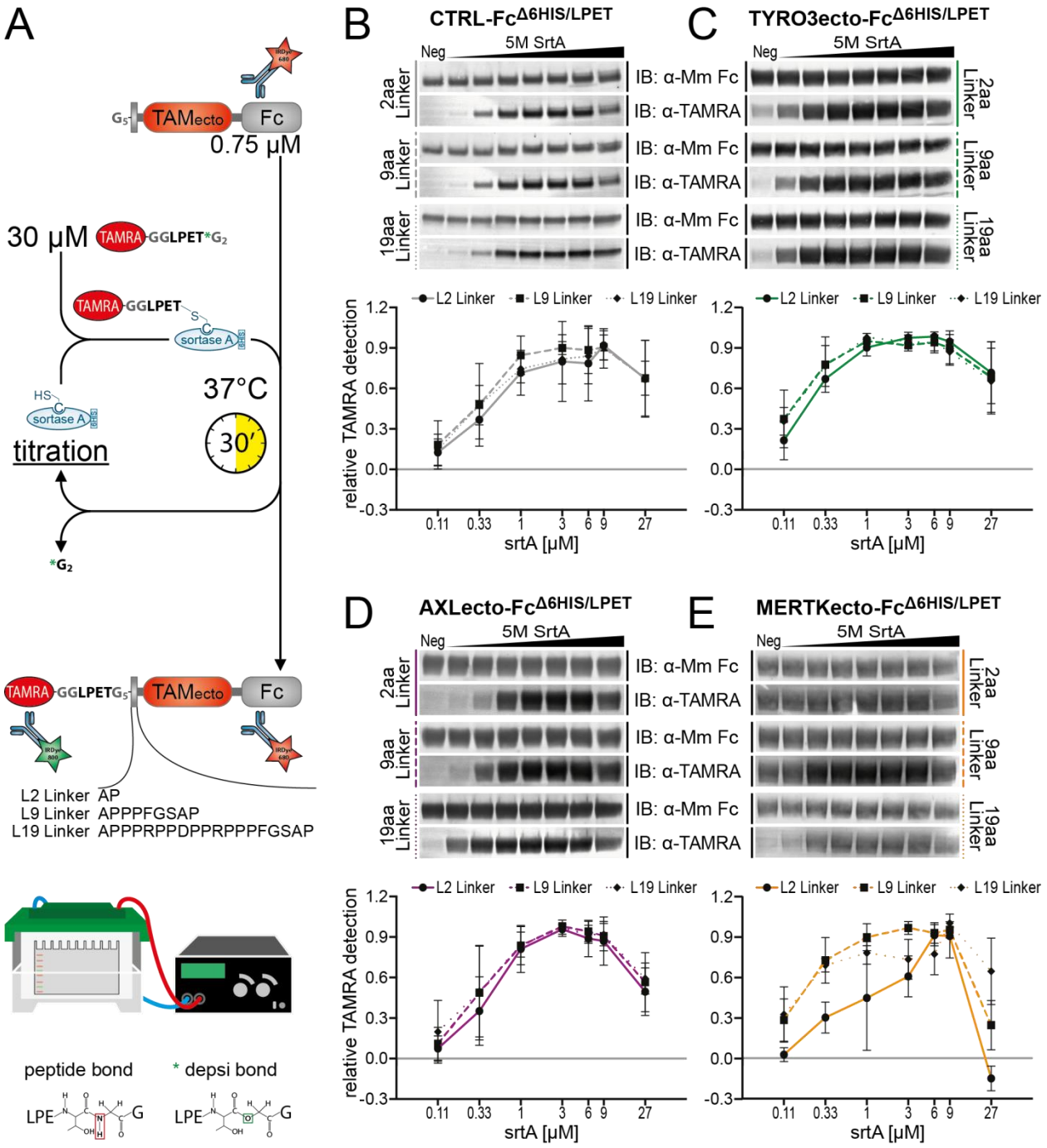

Figure 9. SrtA titration for second tagging step.
The efficiency of ligating TAMRA to the n-terminally free glycine of L2, L9, and L19 linker versions of control and bait proteins was tested for srtA titrations. Reactions without srtA served as negative control (Neg). TAMRA tagged to bait and control proteins was quantified via western blot (B to E). The relative TAMRA detection was calculated by dividing the TAMRA signal by the signal of Fc tag detected, followed by subtracting the negative control. The MEAN and SD of three technical replicates is shown.

Optimal reaction times for srtA tagging TAMRA-LPET*GG to control and bait proteins were determined in a time course performed exemplarily for L19 control and bait proteins. One minute of reaction yielded at least 70% of maximal efficiency for each protein. Maximal reaction

efficiencies were reached between 4 to 16 minutes. Within 4 to 32 minutes the mean intensity of TAMRA detected on the respective proteins was stably above 95% of the mean maximal intensity. At reaction times longer than 32 minutes less TAMRA was detected being linked to the proteins tested.

A reduction of peptide tagged to proteins after reaching the equilibrium is unreported. Without further data only speculative explanations such as chemical bleaching of TAMRA, or stable linkage of srtA to Threonine of TAMRA-LPET peptide can be offered. As TAMRA-LPET ligation to bait and control proteins was efficient up to reaction times of 32 minutes, incubations of the second step of srtA tagging were performed at 30 minutes. However this observation emphasized the necessity to tightly control the reaction time of the srtA enzyme.

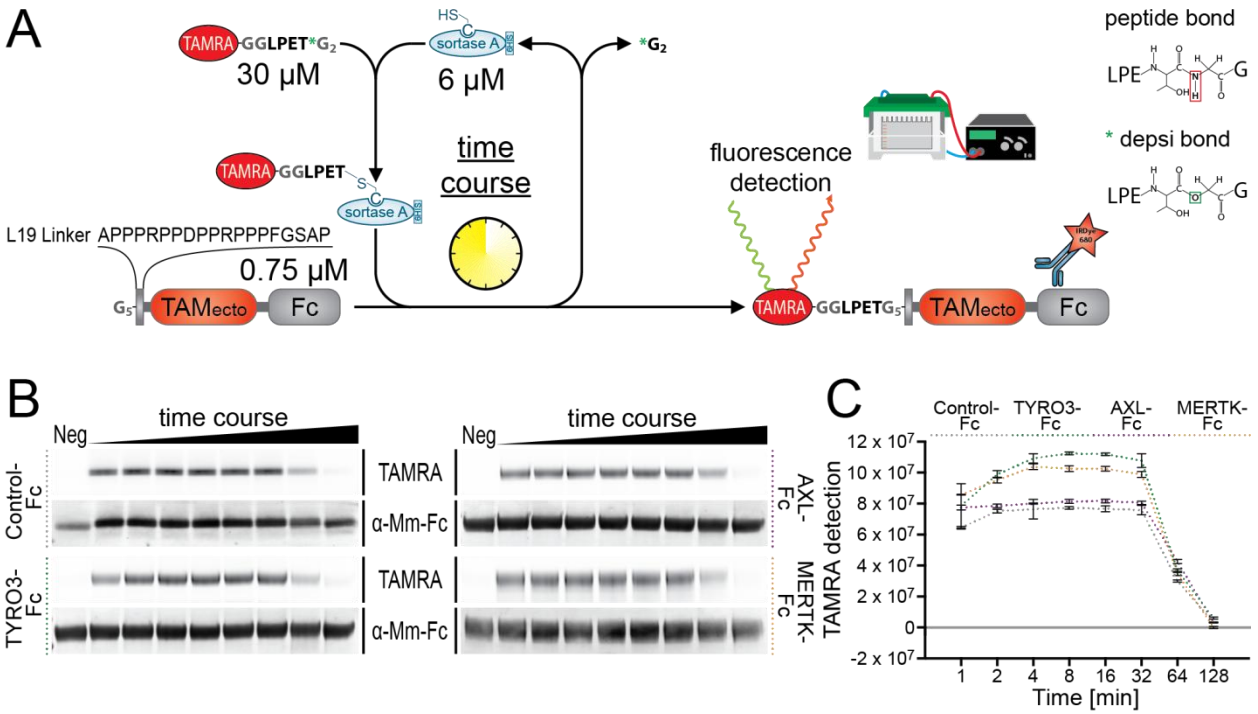

Figure 10. Time course for second srtA tagging reaction.

Time courses were performed for srtA (6µM) mediated reactions of L19 linker variant control or bait proteins at 0.75 µM with 30 µM TAMRA-LPET*GG. The fluorescence intensity of TAMRA linked to control or bait protein was detected via fluorescent imaging following SDS-PAGE separation. Control and bait proteins were detected via Western Blot (B). A reaction without srtA served as negative control (Neg). The quantified signals of TAMRA were divided by the signal of detected Fc tag, subtracted by the negative control. TAMRA intensities are represented relative to those at 32 minutes reaction time. The MEAN and SD of three technical replicates is presented.

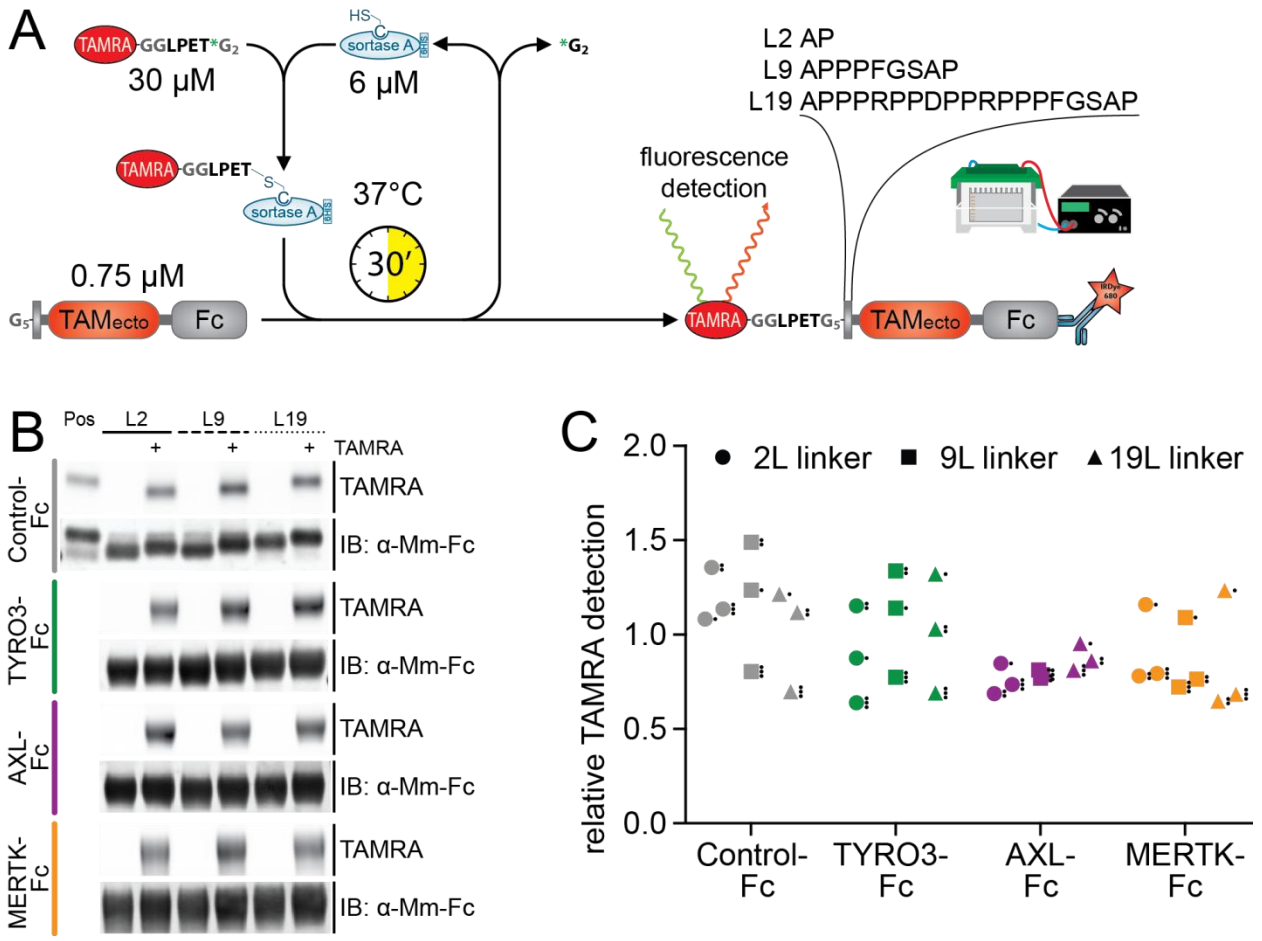

Figure 11. Comparison of control and bait proteins linker variants.
Three independent SrtA (6µM) reactions were performed with 0.75 µM of control and bait proteins for each linker variant with 30 µM TAMRA-LPET*GG for 30 minutes at 37°C. The reaction efficiency was observed by the determination of fluorescence of TAMRA linked to control or bait protein. Fc tags of control and bait proteins were detected via Western Blot (B). One aliquoted sample of TAMRA L19 Control-Fc (7.6 µM) served as a common positive control (Pos) for all reactions. For reactions including TAMRA-LPET*GG, TAMRA signals were divided by the detected Fc intensities before being divided by the positive control (C). MEAN and SD of three independent reactions is shown. Reactions are labeled with one to three dots for the respective replicate. Reactions of Control-Fc and TYRO3-Fc, and reactions of AXL-Fc and MER-Fc were performed simultaneously.

Three linker variants were used to separate the LPETG motif from the TAM receptor ectodomains of bait proteins, and from the Fc domain of control proteins respectively. To compare srtA reaction efficiency for the bait and control proteins for each linker version, these 12 proteins were srtA tagged with TAMRA-LPET*GG. All samples were compared to a previously prepared batch of TAMRA L19 Control-Fc and equal amounts were added to each SDS-PAGE gel. While the AXL-Fc reactions yielded very reproducible efficiencies within the technical replicates for each linker variant, there was more variation within the technical replicates of the CTRL-Fc, TYRO3-Fc and MER-Fc reactions. In mean, the bait and control protein variants resulted in over all comparable efficiencies.

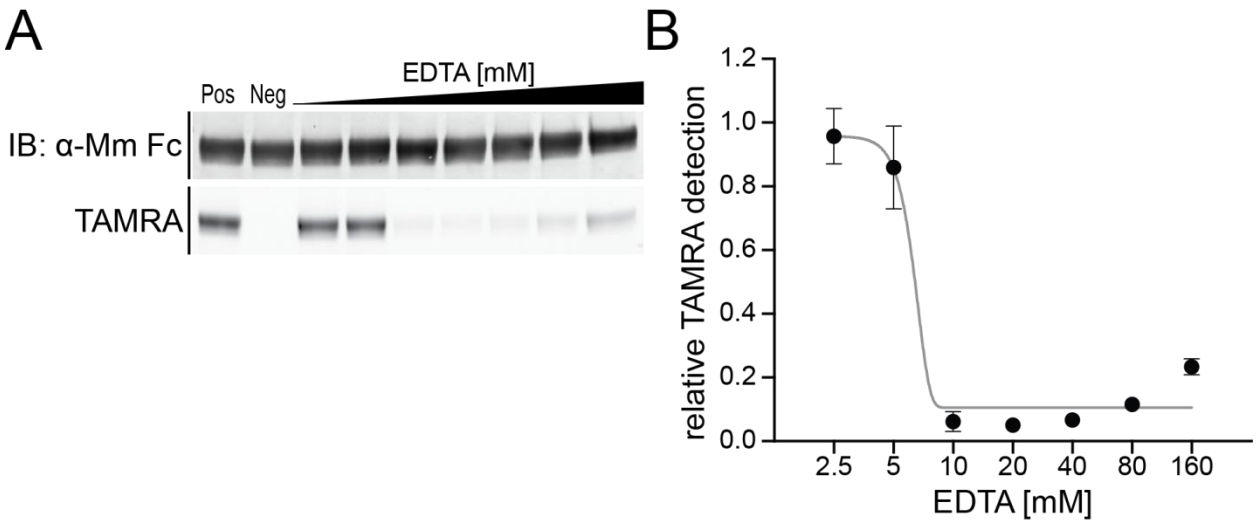

Figure 12. Inhibition of srtA by chelation of Calcium ions.
In reactions with 6 µM srtA, 30 µM TAMRA-LPET*GG, and 0.75 µM L2 AXL-Fc in srtA reaction buffer containing 10 mM $CaCl_2$, EDTA was log2 titrated from 2.5 mM to 160 mM to determine the effect of calcium chelation on the transpeptidation efficiency of srtA. Reactions without addition of EDTA were used as positive control (Pos) and reactions without srtA were used as negative control (Neg). Proteins were separated via SDS-PAGE and TAMRA linked to L2 AXL-Fc was detected by fluorescent imaging. The Fc tag was detected via Western Blot (B). Images of a representative experiment are shown (A). The MEAN minus Neg relative to Pos for three technical replicates and the CI 95% is shown with an asymmetric sigmoidal curve fit (B).

To predict the concentration of EDTA, EGTA or BAPTA to chelate free Ca2+ ions in the srtA reaction buffer the online tool by MAXCHELATOR by Chris Patton was used to predict the concentration of free Calcium ions in the presence of different chelating molecules (Figure App 4). At concentrations of 10 mM and higher of EDTA, EGTA, or BAPTA the predicted concentration of free Ca^{2+} ions started to decrease rapidly to below 1 nM at 16 mM chelator concentration. Free Ca^{2+} concentrations at EDTA concentrations of 16 mM and above were predicted to be 2.8 or 8.3 fold lower compared to corresponding concentrations of EGTA or BAPTA respectively.

The efficiency of srtA transpeptidation was determined for a log2 titration of EDTA added to the reaction buffer (Figure 12). The reactions were performed with 0.75 µM L2 AXL-Fc, 30 µM TAMRA-LPET*GG, and 6 µM srtA for 30 minutes at 37°C. Compared to the positive control where no EDTA was applied to the reaction, 10 mM EDTA efficiently inhibited srtA transpeptidation. Inhibition reached a minimum at 20 mM EDTA where approximately 5% of the TAMRA signal was detected compared to a reaction without EDTA. At EDTA concentrations of 80 mM and 160 mM, the inhibition of srtA decreases and 11.6% and 23.4% of relative TAMRA signal was detected.

As the first tagging step of a LPETG motif containing protein via srtA is not limited by the availability of peptide, the desired reaction time was defined as 30 minutes and 6 µM srtA was

found to remove the hexa-His-LPET from the n-terminus of bait and control proteins efficiently. Also for the second tagging step, 6 µM sortase A was found to be the concentration where linkage of payloads to the three bait proteins, or the control protein was either optimal or close to optimal. For this step as well optimal reaction times were observed to range between 5 to 32 minutes. The reaction time was controlled with the addition of EDTA inhibiting srtA maximally at 20 mM concentration. The establishment of optimal conditions for the enzymatic reaction achieved high efficiency of payload linking to the variants of bait and control proteins and product homogeneity.

Characterization of Diazirine as cross-linker of bait and control proteins

The influence of hexa-His (hexa-His) or Diazirine cross-linker molecule (Diazirine), or nothing (-/-) attached to the n-terminus of L19 bait and control proteins on their affinity to recombinant human GAS6 was examined by an indirect ELISA with the bait and control proteins replacing the primary antibody and GAS6 serving as the antigen at a defined concentration (Figure 13 A). The ELISA was performed with 25 µl of 15 nM GAS6 immobilized by the high protein binding dish, blocking with 5% milk in PBS, and a 2h incubation at room temperature with the protein variants concentrated to 0.1 µM in blocking buffer, before detecting the bound proteins with an HRP linked anti-Mouse IgG and quantifying its conversion of TMB reagent to substrate (Figure 13 B). The experiment was performed under a yellow light source with a known spectrum avoiding UV light to prevent cross-linker activation.

Hexa-His L19 Control-Fc shows hardly detectable binding to GAS6. Detection of hexa-His variants of MER-Fc and TYRO3 bound to GAS6 is at about 8 and 17 percent respectively compared to binding of hexa-His L19 AXL-Fc, which shows the highest affinity to GAS6 amongst the tested proteins in this experiment. The versions of Control-Fc, TYRO3-Fc, and AXL-Fc with a free n-terminus (-/-) show comparable affinities as the hexa-His versions, while the affinity of L19 MER-Fc to GAS6 is increased 2.5 fold compared to hexa-His-L19 MER-Fc. Again TYRO3-Fc and AXL-Fc do not vary notably with the Diazirine cross-linker at their n-terminus compared to the other versions, while Diazirine-L19 Control-Fc and Diazirine-L19 MER-Fc show a significantly increased affinity to GAS6 compared to the other respective protein versions.

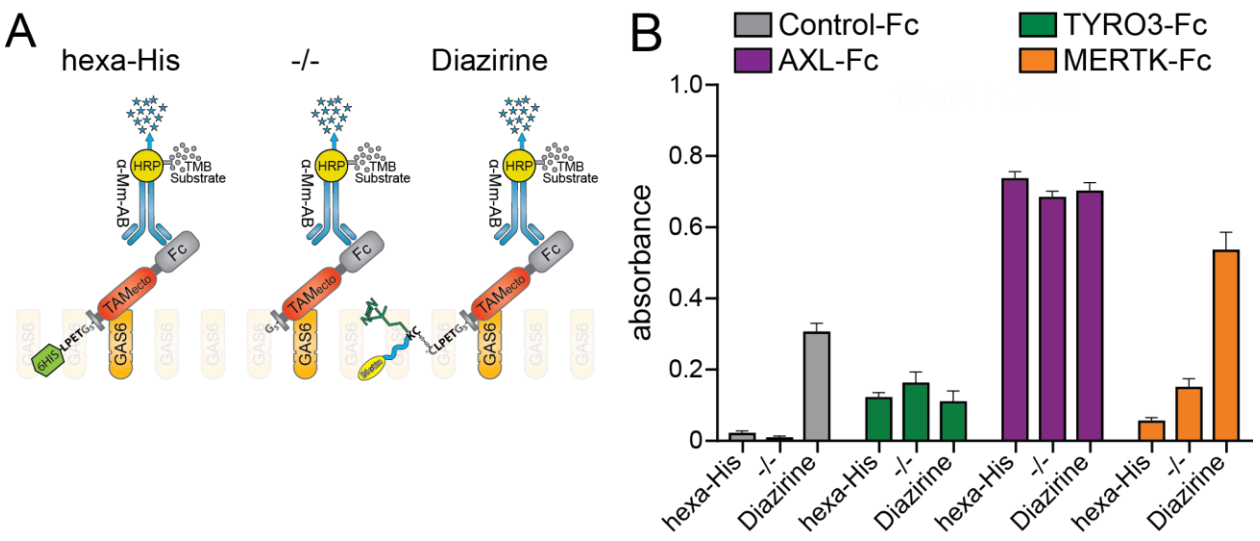

Figure 13. Effect of n-terminal modification of bait and control proteins on GAS6 binding.
The effect of n-terminal tags on the affinity of bait and control proteins was tested for their affinity to GAS6 via ELISA assays. L19 bait and control proteins in versions with an either unmodified n-terminal hexa-His-LPET peptide (hexa-His), without the peptide (-/-), or with the peptide replaced by the Diazirine cross-linker molecule (Diazirine) were used at 0.1 µM in 25 µl to bind to 25 µl of 15 nM GAS6 immobilized per well. Wells without GAS6 served as negative control. The MEAN subtracted by the negative control and SEM of four technical replicates with technical duplicates each is shown (B).

The Diazirine cross-linker molecule was designed with the photo-activatable cross-linker Diazirine linked to a Biotin molecule, and both together linked via a disulfide bond to a LPET*GG peptide to be sortase tagged to the n-terminus of bait and control proteins. The star marking a depsi bond linking the threonine and the first glycine. In the following experiments the UV activation of Diazirine by two light sources is compared as well as the efficiencies of Diazirine L19 AXL-Fc to Diazirine L19 Control-Fc labeling GAS6 with the biotin moiety in an increasingly complex solution.

To activate the photosensitive cross-linker Diazirine, two UV light sources were available (Figure 14 B). The Bio-Link BLX-365 emits light from five 8W UV lamps installed above the UV chamber. The BLX-365 allows the application of light limited by time of exposure, or by Joules of energy exposed per square centimeter. The second available light source was a 500W Hg/Xe arc lamp emitting light down to a wavelength of 200 nm. The emitted light was focused with a 4 element Aspherab® condenser to produce large, collimated beams or small, bright, and focused spots. Finally, a dichroic mirror limited the emitted wavelength spectrum from 280nm to 400nm, and a digitally operated shutter limited the time of exposure.

The activation of Diazirine dependent on UV doses of the two light sources was examined in solutions with low complexity. 10 µM SrtA and 20 µM Diazirine cross-linker molecule were combined in reaction buffer and incubated for 10 minutes at 37°C to allow the sortase to covalently link to the Threonine of the cross-linker molecule's LPET*GG peptide. After the

incubation, Diazirine was activated by UV irradiation at different doses. To ensure optimal irradiation, the tubes were placed either centrally in the BLX-365 UV box or under the focused light beam of the arc lamp. The irradiation intensities compared for the BLX-365 UV box ranged between 1 J/cm^2 to 15 J/cm^2. Noteworthy, the time necessary to expose a sample with 12 J/cm^2 was approximately 45 minutes. Comparing the activation of Diazirine by the arc lamp, samples were exposed with maximal energy for 1 to 60 seconds. Following the activation, 20 mM DTT was added to reduce the disulfide bond and therefore releasing the Diazirine/Biotin group from the cross-linker molecule (Figure 14 A). The efficiency of Diazirine activation was characterized by quantifying Biotin cross-linked to srtA by Western Blot (Figure 14 C and D). Biotin detected relative the sortase A before UV irradiation or DTT release of the cross-linker molecule was used as positive control. Samples without UV irradiation but with DTT release of the cross-linker molecule served as negative control.

The maximal cross-linking efficiency reached by UV irradiation with the UV box is estimated to be reached with 56% biotin detection relative to the positive control based on one-phase association non-linear curve fit. Approximately 79% of the maximal activation is reached with 12 J/cm^2 after 45 minutes. After approximately 3 minutes and 45 seconds or 1 J/cm^2 only approximately 10% of the maximal activation is reached (Figure 14 C). With the higher energy of the arc lamp, after 5 seconds of exposure an efficiency of activation comparable to 12 J/cm^2 applied by the UV box was achieved. Arc lamp irradiations longer than 5 seconds lead to the degradation of srtA and the formation of complexes (Figure App 6). To avoid UV induced protein degradation and prolonged incubation times favor stronger interactions and lead to increased background (*128*), the 5-second Arc-lamp activation was favored as soon as it was available.

The dose dependent hydrolysation of the disulfide bond connecting the Diazirine/Biotin group to the LPET*GG peptide of the cross-linker molecule was characterized for a batch of Diazirine L19 AXL-Fc treated with a titration of DTT. Biotin bound to the AXL-Fc protein was quantified in relation to total AXL-Fc via Western Blot following a non-reducing SDS-PAGE (Figure App 5). L19 AXL-Fc without Diazirine cross-linker molecule tagged to its n-terminus served as positive control, while Diazirine L19 AXL-Fc without DTT treatment served as negative control. Diazirine L19 AXL-Fc diluted to 1.5 µM lost approximately 85% of its Biotin signal after treatment with 16 mM DTT for 10 minutes at room temperature. Treatment with 64 µM DTT reduced the Biotin signal below 2% compared to the untreated sample.

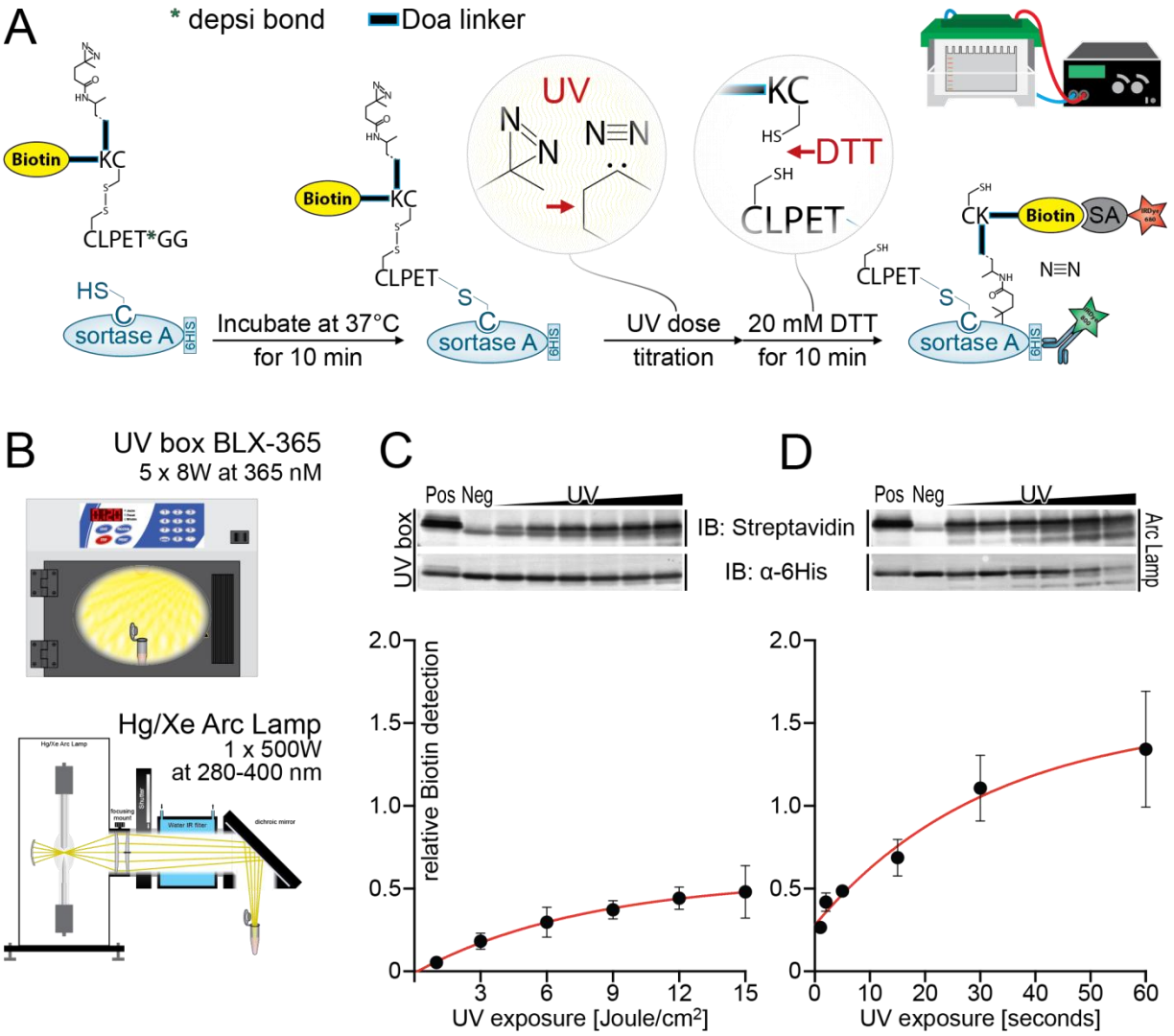

Figure 14. Photo-activation of Diazirine via a UV box and an Arc lamp.
Two UV light sources were tested for their Diazirine activation performance (B). SrtA was incubated with the Diazirine cross-linker molecule and incubated for 10 min at 37°C before the cross-linker was activated by either of the two lamps with increasing UV exposures. Following the activation, the disulfide bond linking the Diazirine/Biotin part to the LPET*GG peptide of the cross-linker molecule was reduced with DTT (A). Biotin linked to srtA and total srtA were detected and quantified via Western Blot for each light source (C&D). Samples without UV activation or DTT treatment were used as positive control (Pos). Samples without UV activation but with DTT treatment were used as negative control (Neg). Curves were fitted according to one-phase association. The MEAN minus Neg relative to Pos is shown with SD of three technical replicates.

As the recovery of bait and control proteins in a co-immunoprecipitation is of crucial importance, various beads were compared for their recovery of Fc tagged proteins from complex solutions and for the purity of each preparation. Using Protein A microbeads and anti-Mouse IgG agarose slurry the highest recovery rates of 41% were achieved based on quantifications in Coomassie R250 stained SDS-PAGE gels. However the protein A Microbead purification showed a significant amount of unspecific purified proteins. The anti-Mouse IgG agarose even purified mostly unspecific proteins compared to Fc-tagged protein. Anti-Mouse IgG Dynabeads resulted

in the third highest recovery rate of 37.2% but, beside the heavy and light chain of the anti-Mouse IgG, no undesired proteins could be detected via Coomassie staining. The experiment was performed once and the results are shown in the Appendix (Figure App3).
As the previous described experiments have shown, the addition of a hexa-His tag to the n-terminus of bait and control proteins only lead to a decrease in affinity to GAS6 by MER-Fc. More importantly, the addition of the cross-linker molecule lead to an increased affinity to GAS6 by Control-Fc and MER-Fc while the affinities of TYRO3-Fc and AXL-Fc remained unchanged. The altered affinities of bait and control proteins compared to endogenous TAM receptors may lead to false positive or negative detection of interactions, which has to be taken into consideration analyzing the interactions of the following screen.

Specificity confirmation of bait and control proteins for label transfer and comparison of enrichment methods

With the components of the bait and control proteins individually tested for their functionality, the combinatorial functionality of all components remained to be confirmed. In tissue lysates Biotin is found due to its function as coenzyme, and the Fc domain of an IgG used as tag potentially gets recognized by Glycan and Fc-receptors (*129*, *130*). Therefore the ability to label proteins known to interact with the ectodomain of TAM receptors separating bait proteins from the control protein needed to be confirmed in a complex matrix. Therefore Diazirine-AXL-Fc and Diazirine-Control-Fc were compared for their specificity to transfer the Biotin label to recombinant GAS6 in increasingly complex matrices. Further 3 methods were compared for their performance in enriching AXL ectodomain interacting proteins from mouse spleen lysates.
As shown in Figure 13, Diazirine tagged L19 Control-Fc shows an increased affinity to the TAM receptor ligand GAS6 even when 5% milk in PBS is used to block unspecific protein-protein interaction. To determine the difference in specificity of label transferred to GAS6 by Diazirine-L19 Control-Fc compared to Diazirine-L19 AXL-Fc in matrices with increasing complexity, 0.3 µM bait or control protein was added to 0.3 µM recombinant human GAS6 in 20 µl of either PBS, or 1, 3, or 9 µg mouse spleen lysate added to the PBS (Figure 15 A). Following 30 minutes of incubation at 37°C, the cross-linker was activated with 5 second exposures with the Hg/Xe arc lamp. The Diazirine/Biotin part of the cross-linker molecule was released during a 10 minute incubation with 50 mM DTT before the proteins were separated via SDS-PAGE. Via Western Blot GAS6 and Biotin were detected.
Biotin was linked to GAS6 by the Diazirine-L19 AXL-Fc bait protein, as well as by the control protein when the label transfer was performed in a simple matrix as PBS (Figure 15 B). In more

complex matrices Biotin cross-linked to GAS6 by Diazirine-L19 Control-Fc was reduced to 20% compared to the label-transfer performed in the simple matrix. The decreasing effect of lysate applied to the label-transfer matrix is not dose dependent in the case of Diazirine-L19 Control-Fc.

By the addition of lysate to the Diazirine tagged AXL-Fc and Control-Fc proteins the efficiencies to biotinylate GAS6 were decreased for both proteins. With the addition of lysate, the sample turbidity increased having a negative effect in UV transmission. However for Diazirine-L19 AXL-Fc, cross-linking of GAS6 was only reduced to 62% in the presence of 1 µg lysate in PBS compared to PBS alone, while for Diazirine Control-Fc GAS6 cross-linking was reduced to 20%. The effect of lysate proteins reducing the cross-linking efficiency to GAS6 by Diazirine-L19 AXL-Fc was observed to be dose dependent. The efficiency in presence of 9 µg lysate was reduced to 40%, again possibly due to decreased UV transmission in the samples. With the labeling of GAS6 by control protein dropping to a level significantly lower than the labeling by AXL bait protein, and independent on the complexity of the matrix, the interaction of Control-Fc protein with GAS6 was shown to be unspecific. Therefore the control protein was confirmed for its use to separate proteins interacting specifically with the ectodomain of a bait protein from proteins interacting with any other part of the bait protein.

The enrichment of proteins interacting with the bait proteins was compared for three methods (Figure 16 A). For all three methods Diazirine-L19 AXL-Fc and Diazirine-L19 Control-Fc were used. The bait and control proteins were incubated in mouse spleen lysate for 30 minutes preventing cross-linker activation. The first method was performed enriching the bait and control proteins with anti-mouse IgG coated magnetic beads. In the second and third method, Diazirine was activated for 5 seconds with the UV arc lamp and incubated for 10 minutes. The bait and control proteins were then enriched by either anti-mouse IgG coated or streptavidin coated magnetic beads. Enriched proteins were identified and quantified via mass spectrometry.

According to Spearman rank correlation, the samples did not show a clear correlation by method (Figure 16 B). Rather samples clustered by bait and control in two groups (Figure 16 C). The groups are not separated by the enrichment method, neither by the batch. The grouping is also reflected in the first component of a PCA representing 48.7% of variation, where those samples that formed both groups when spearman clustered, associate either positively or negatively. AXL-Fc samples trend to associate slightly more positively with the first component compared to Control-Fc samples for the anti-mouse IgG coated magnetic beads enrichments with or without UV activation. Samples of streptavidin-coated enrichments do not separate by bait and control. The same trend can be observed more clearly in the second component representing 7.7% of variance, while in the third component representing 5.2% of variance only the AXL-Fc samples

of the anti-mouse IgG methods vary in their association for the component from positive to negative and the other samples show uniformly low association with the component.

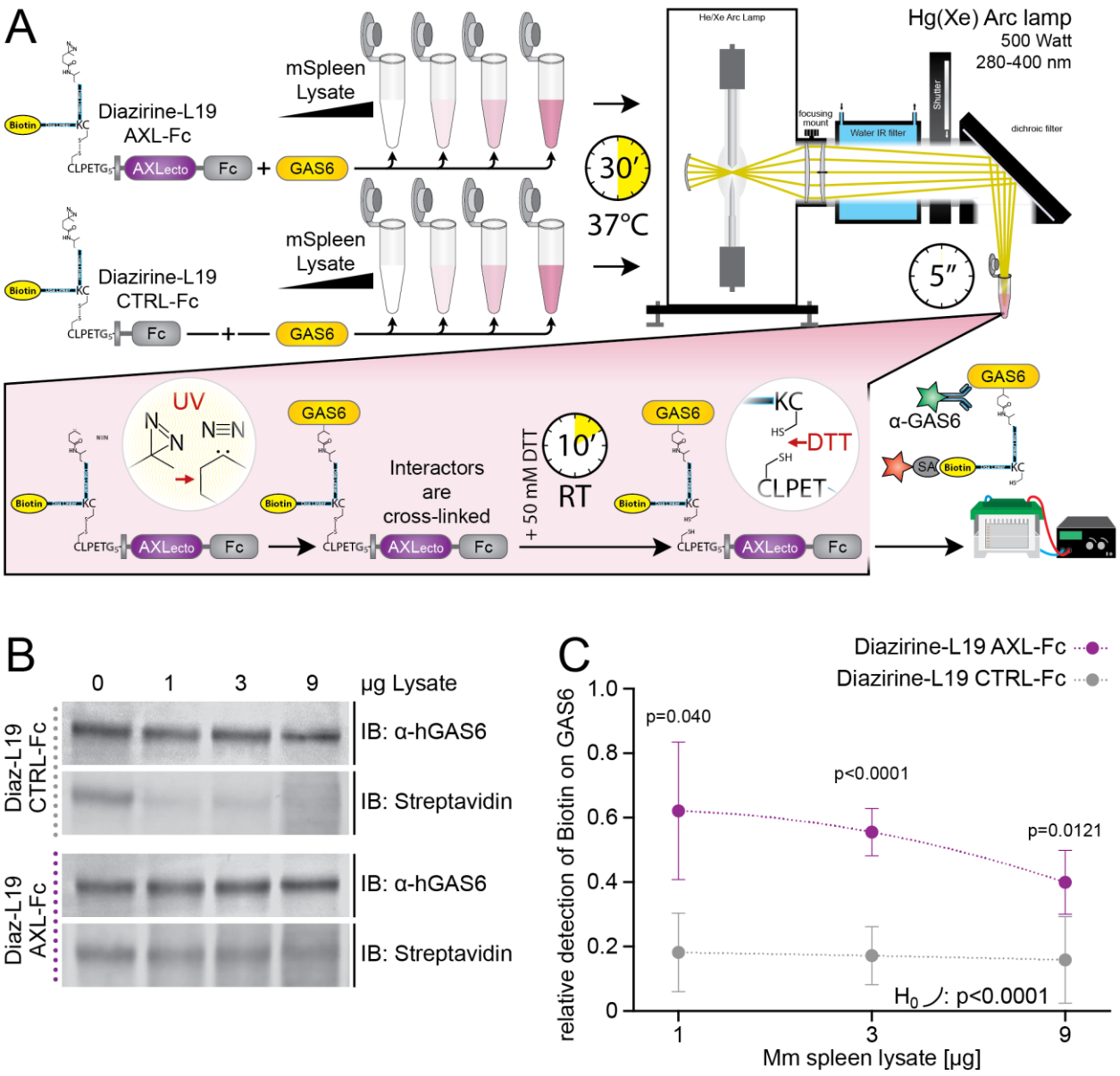

Figure 15. Specificity of label transferred by Diazirine-L19 AXL-Fc compared to Diazirine-L19 Control-Fc.

The specificity of Diazirine-L19 AXL-Fc and Diazirine-L19 Control-Fc cross-linking to human GAS6 was determined in media with increasing complexity (A). 0.3 µM Diazirine-L19 AXL-Fc or Diazirine-L19 Control-Fc were incubated for 30 minutes at 37°C together with 0.3 µM recombinant human GAS6 either in PBS, 1, 3, or 9 µg mouse spleen lysate in a total volume of 20 µl. Following the incubation, the cross-linker was UV activated with 5 seconds exposure by a 500W Hg/Xe arc lamp. The disulfide bond of the cross-linker molecule was reduced with 50 mM DTT before Biotin linked to GAS6 was detected and quantified via Western Blot (B & C). The MEAN, relative to 0 µg lysate, and SD of five technical replicates is shown. The test, whether both exponential curves share a common fit resulted in p<0.0001. Further the data sets of bait proteins were compared to the control within the individual conditions with a 2-step up method of Benjamini, Krieger and Yekutieli FDR corrected multiple T-Test. Discoveries with q<0.05 are labeled with the respective p value.

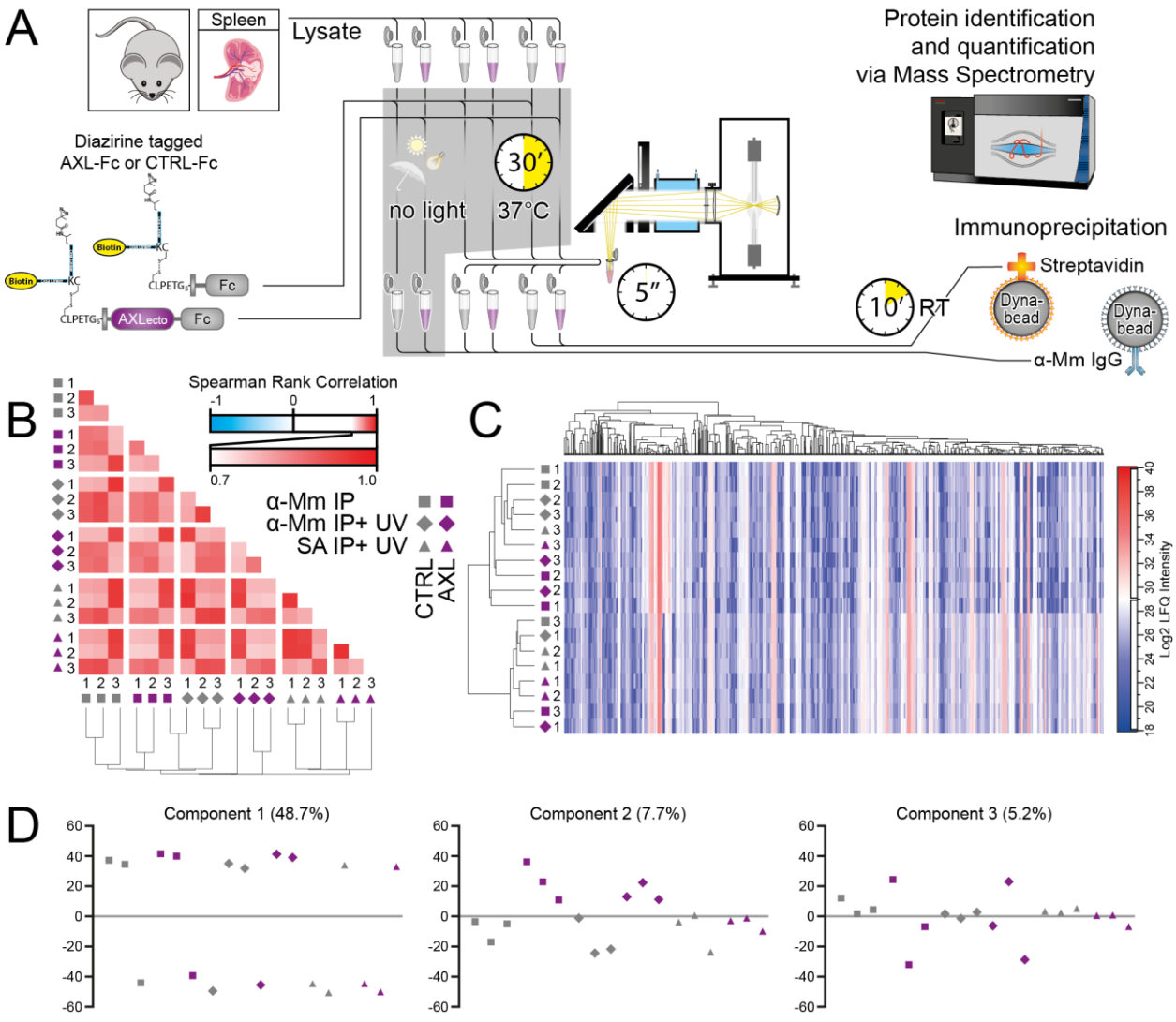

Figure 16. Comparison of enrichment methods.

For the comparison of enrichment methods, aliquots of mouse spleen lysate were combined with either Diazirine-L19 Control-Fc or Diazirine-L19 AXL-Fc (A). One set was protected from UV light, while for two sets Diazirine was activated via 5 second UV irradiation with the UV arc lamp. Control and bait proteins were isolated using anti-Mouse IgG Dynabeads from the UV protected, as well as from one set of UV treated samples. Biotinylated proteins were isolated from the second UV treated set of samples with Streptavidin Dynabeads. Enriched proteins were identified and quantified via mass spectrometry. Spearman Rank Correlation of samples (B), clustering of samples and proteins according to Spearman (C), and principle component analysis (D), were performed to describe the relations of samples. The enrichment of proteins within each condition visualized as volcano plots with the difference of means of log2 transformed LFQ intensities on the x-axis, and the negative log2 of p Values of unpaired two-sided T.Tests on the y-axis (E). Tests were controlled for multiple testing using the permutation based FDR by Perseus with 250 randomizations. Proteins with multiplicity adjusted q values below 0.05 were marked with darker circles. The mean fold change and p Values of Control and AXL enriched proteins within the different conditions were compared (F).

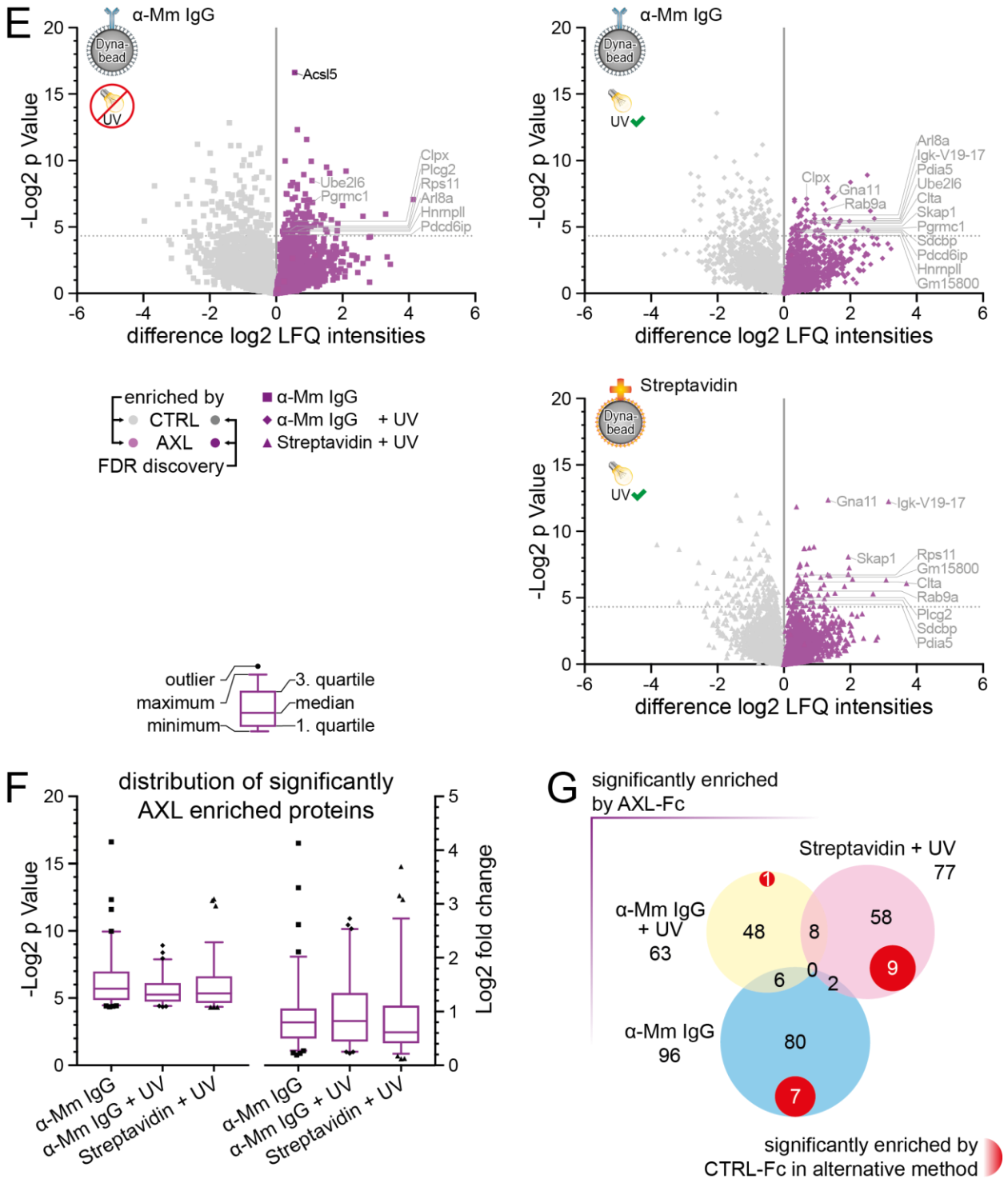

When testing the difference of enrichment by AXL-Fc and Control-Fc with a two-sided t-test and an alpha of 5%, the highest number with 96 proteins ‘significantly’ enriched by AXL-Fc is observed for anti-mouse IgG coated magnetic beads enrichments without UV activation (Figure 16 G). 1 protein is discovered significant after permutation based false discovery rate correction

of 5% for multiple tests in the anti-mouse IgG bead enriched samples. Anti-mouse IgG coated magnetic bead enrichment with UV activation of Diazirine lead to the significant enrichment of 63 proteins, and enrichment after UV activation with streptavidin to 77 significantly AXL-Fc enriched proteins (Figure 16 F). Comparing the proteins significantly enriched by AXL-Fc of the two anti-mouse IgG based enrichment methods, those enriched without UV show a higher confidence of the enrichments not being random by having the lower p values, while those enriched with UV activation are enriched stronger compared to those without UV activation. The enrichment methods based on anti-mouse IgG and streptavidin, both UV activated, have 8 out of 140 significantly AXL-Fc enriched proteins in common. Again the UV activated anti-mouse IgG enrichment method resulted in a higher enrichment of significant AXL-Fc enriched proteins, although the enrichments with the UV activated streptavidin based method resulted in enrichments tested less likely to be random. Another positive observation of anti-mouse IgG enriched proteins with UV activation is, that only one of the 63 significantly AXL-Fc enriched proteins was found significantly enriched by Control-Fc in one of the other methods. In contrast 7 and 9 proteins significantly AXL-Fc enriched respectively by the methods without UV activation using anti-mouse IgG beads, and with UV activation using streptavidin beads, were found significantly enriched by Control-Fc in an alternative method.

The comparison of enrichment and labeling methods has shown that enrichment of bait and control proteins after UV activation of cross-linker lead to a stronger enrichment of AXL-Fc interacting proteins. Together with the lowest number of AXL-Fc interacting proteins identified as significantly Control enriched by the alternative methods, Fc enrichment after UV activation turned out to be the most promising method for the identification of weak and transient TAM receptor interacting proteins.

Identification of novel TAM receptor interacting proteins in human and mouse tissues

The central aim of this study is the identification of novel TAM receptor interacting proteins. To decide where to search for novel TAM receptor ligands and interacting proteins, the expression of TAM receptors and their ligands GAS6 and Protein S was compared for a variety of tissues (Figure 17 B). According to mRNA expression data published by the online database BioGPS, TYRO3 is highly expressed in brain and kidney tissues, AXL in adipose tissues, muscular tissues like arteries, kidney and certain glandular tissues, and MER mostly correlating with AXL expression. The TAM receptor ligand GAS6 is highly expressed in muscular tissues like arteries, the heart, and the diaphragm, glandular tissues like the seminal vesicle and the prostate gland as examples, and female sex organs like the uterus, vagina and the umbilical cord. Focusing on

the TAM receptor's function as regulators of immune responses, human blood plasma and mouse spleen lysates were included amongst the tissues to be screened, while mouse testis lysate was included due to its constant and TAM receptor dependent phagocytosis of debris by Sertoli cells (*26*). Adipose tissue was included due to its high expression of AXL. Brain tissue was especially interesting as the TAM receptor TYRO3 is highly expressed while the ligands GAS6 and Protein S show a relatively low expression indicating a putative role of alternative ligands. Special thanks go to Prof. Dr. med. Michael Heneka for providing brain samples from healthy human patients, and patients either diagnosed with mild cognitive impairment or Alzheimer's disease. Additionally mouse brain lysates were included amongst the screened tissues as by the example of GAS6, human TAM receptors have shown a higher affinity to the rodent version compared to endogenous version of the ligand.

Homogenates were prepared from the described tissues and proteins that interacted with Diazirine tagged and L19 linked Control-Fc, TYRO3-Fc, and AXL-Fc were cross-linked by UV activation of Diazirine, and enriched by immunoprecipitation using anti-Mouse IgG Dynabeads. The enriched proteins were identified and quantified via mass spectrometry by Annika Frauenstein and Felix Meissner at the Max Planck Institute of Biochemistry who deserve thanks also for their advice concerning the data analysis.

To obtain an overview on proteins enriched by the different baits and control proteins in the tissues used, samples were clustered according to Spearman (Figure 18, A, C, D). As the mouse tissue samples were processed again separate from the human tissue samples, where plasma samples were processed separately from the brain samples during the mass spectrometry measurements and data processing, the three sample groups were clustered individually. Within the mouse samples, clusters formed according to the respective tissue with the exception of the control, the TYRO3, and the AXL sample of Adipose tissue lysate 1, which clustered closer to the spleen samples. The control and bait samples clustering appears mostly random except for the spleen samples, where the control samples are clearly separated from the samples of both baits. For the human plasma samples clustering identified the control in plasma 1 having a differential enrichment pattern compared to the other plasma samples where enrichments did not lead to clusters defined by baits or the individual plasma. For the human brain samples, AXL bait enrichment showed a clearly separated pattern compared to enrichments with TYRO3 bait or the control protein. Within the TYRO3 bait and the control samples two clusters were identified with one TYRO3 sample dominated cluster and one Control sample dominated cluster, leaving 3 samples out of both. No clustering based on healthy, MCI, or Alzheimer's disease samples was observed. The clustering pattern of samples can be as well observed in component 1 of the principal component analysis performed separately for mouse

samples, human plasma, and human brain samples. Within the second and third component, differences between Control-, TYRO3-, and AXL-Fc enriched samples were less pronounced.

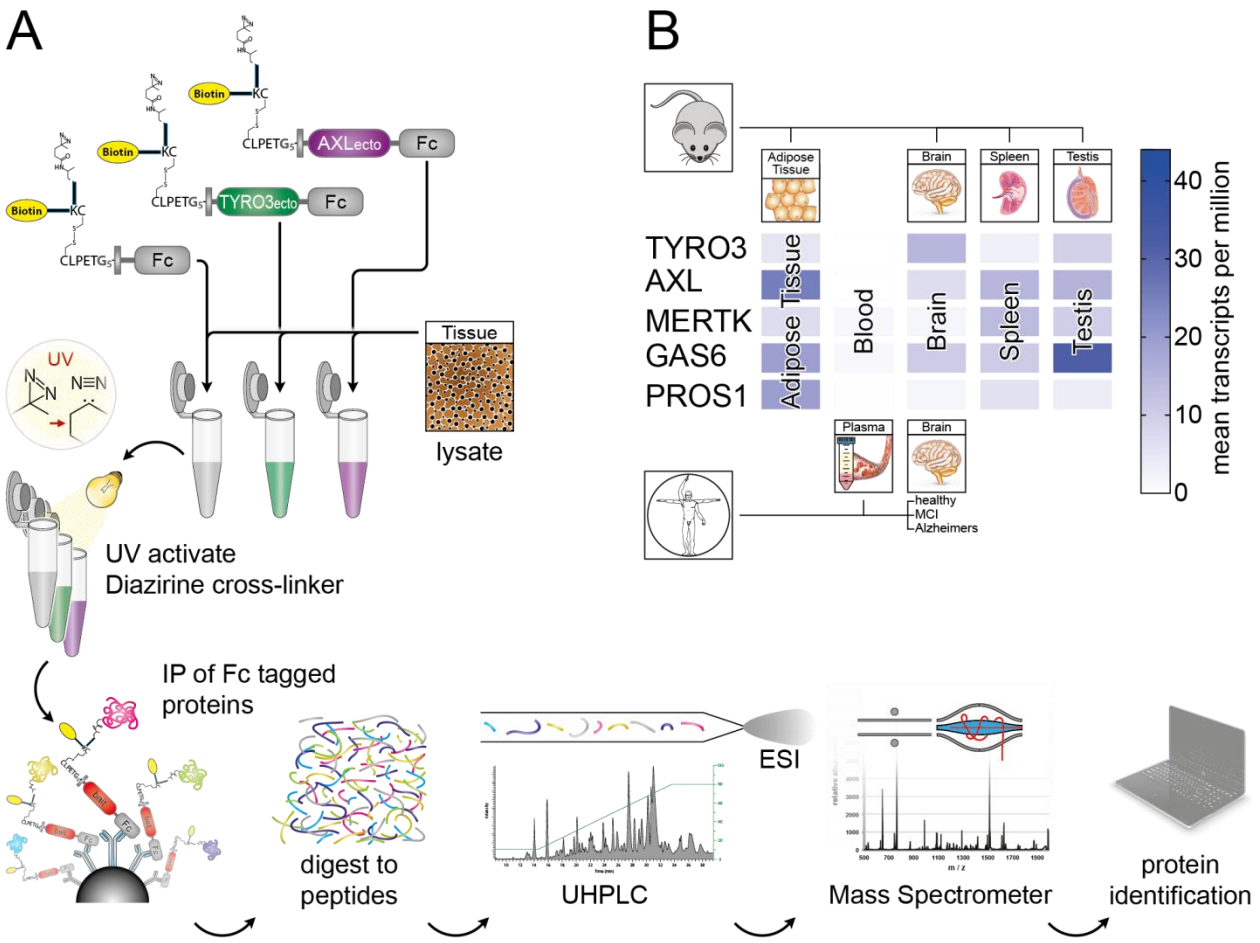

Figure 17. Screening method and tissue selection.
The method used to enrich TAM receptor binding proteins from various tissues begins with the addition of Diazirine tagged bait and control proteins to lysates of tissues. The photo-activatable cross-linker Diazirine is then irradiated with UV to cross-link any protein near to the bait and control proteins; preventing them to be removed by several wash steps during α-mouse IgG Dynabead based enrichment. The enriched proteins are then digested and separated by liquid chromatography and the mass to charge ratio (m/z) is measured my mass spectrometry. Finally peptides and thereby proteins are identified and label free quantified according to the m/z ratios detected (A). Tissue specific mRNA expression data provided by the online database BioGPS for TYRO3, AXL, MER, GAS6, and PROS1 are shown for the tissues screened for TAM receptor interacting proteins (B).

Figure 18. Comparison of enrichments by bait and control in screened tissues.
To describe and compare the enrichment characteristics of bait and control proteins to each other, and with regards to the method of enrichment used, samples were Spearman clustered (A, C, D) and principal component analysis was performed showing the data variance in terms of percentage at the y-axis (B, E, F).

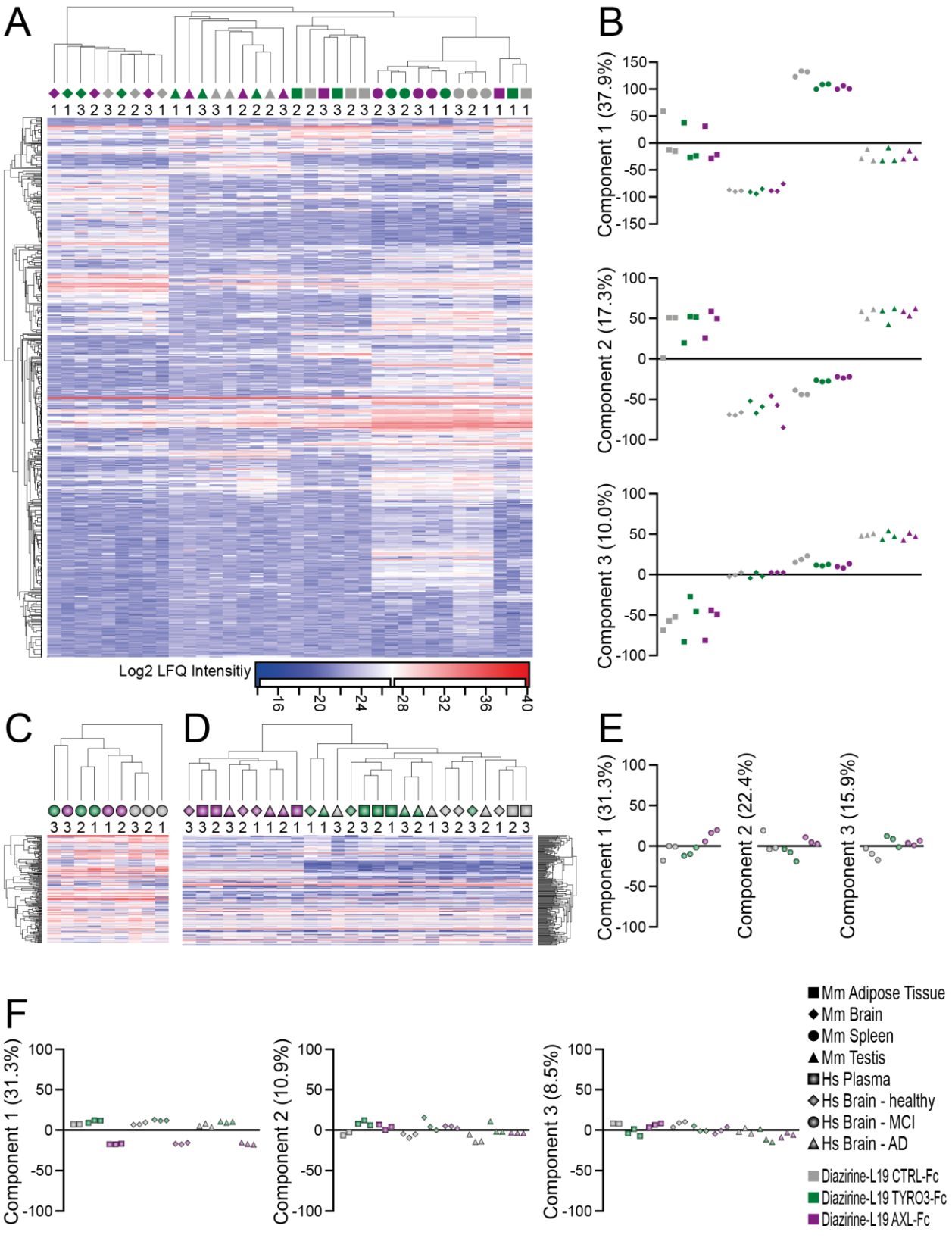

The proteins enriched by TYRO3-Fc and AXL-Fc were each tested for differential enrichment compared to control-Fc enriched proteins. T.Tests were performed and multiple testing was

corrected by applying a permutation based FDR of 5%. The comparisons illustrated per bait and per tissue in Figure 19 A-H show generally more proteins being significantly enriched by AXL-Fc compared to TYRO3-Fc according to the p value of the respective T.Tests. The correlation of mouse spleen samples according to bait indicates that the number of specifically bait or control enriched proteins is exceptionally high compared to the other tissues. The proteins enriched from spleen lysates were therefore subjected to a more stringent threshold of $q<0.01$ for the FDR correction as the other samples, where $q<0.05$ was considered a discovery. FDR approved discoveries are presented in Figure 20 and labeled with a golden star. The respective bait and tissue is marked with a circle ranging in color from white to back according to the q value. Further information included are white circles illustrating tests that were performed but did not result in significance of bait enrichment and white circles with black dots as tests that did reach significance but did not reach a $q<0.05$ in the FDR. As enrichments of weak and transient interacting proteins are expected to have a higher variance than proteins with a high affinity, such enrichments are expected to be less significantly different. Therefore proteins were taken into consideration as discoveries that were significantly enriched with T.Test's p values below 0.05 in at least three tests and therefore in at least 2 different tissues (marked with a blue star). 44 proteins fulfilled these requirements. Assuming random data normally distributed for these 44 proteins, the probability of at least the individual number of significant events was calculated considering the total number of tests of the respective protein. With the example of PRDX5, which was enriched 5 times significantly and tested for a total of 7 times, the probability of having an event happening with a probability of 0.025 five, six, or seven times within a total number of seven events is $0.025^5 * 0.975^2 * 21 + 0.025^6 * 0.975 * 7 + 0.025^7 = 0.0000002$. To maintain the chance of false accepting a protein as significant TAM interactor at 5% within 44 tests, the individual significance level (alpha) needs to be at $p<0.00117$. From these 44 proteins, the proteins RPL28 ($p=0.00164$), RPS14 ($p=0.00222$), RPS23 ($p=0.00222$), GNB2L1 ($p=0.00222$), PRDX1 ($p=0.00462$), SYNGAP1 ($p=0.00462$), and IGHG1 ($p=0.00685$) do not remain under the individual significance level. The probability of at least one false positive result within 44 tests is 26.098% when the individual significance level is p=00685 as obtained for IGHG1.

For proteins identified as discovery by FDR corrected T-Tests, including proteins significantly enriched at least three times by uncorrected T-Tests, as well as MER, GAS6, and Protein S, the online database STRING10 (11.04.2018) was used to identify published connections between these proteins (Figure 21). Sources searched for interactions were Text mining, Experiments, Databases, Co-expression, Neighborhood, Gene Fusion, and co-occurrence. The confidence of network connections is displayed by the thickness of connections. The network was clustered to

a "MCL inflation parameter" of 3 separating clusters by color and conections in between clusters as dashed line.

AHSG was the only protein that clustered together with the TAM receptors and the ligands GAS6 and Protein S being connected to Protein S, GAS6, and ACTN4. Protein S and AHSG were both identified to bind bions, mineralo-organic complexes formed from e.g. proteins, peptides, amino acids, lipids, or carbohydrates, that were identified in various body Fluids (*131*). Wu et al. identified AHSG as most, and Protein S as 8th most bion binding protein when preparing bions from DMEM with 5%FBS and a varriety of precipitating cations. Rawat et al. associated AHSG and GAS6 together with other proteins as inhibiting peptidase function or expression when characterizing differentially expressed proteins in a pregnancy biomarker screen in cows (*132*). Further AHSG and GAS6 were co-mentioned in articles investigating vascular mineralization and associated diseases (*133-137*). AHSG, ACTN4, GAS6, and Protein S were all listed as components in the currated patway: Exocytosis of platelet alpha granule contents. The indicated link between TYRO3 and RAN is based on a published screen for SYK interacting proteins, considering SYK a TYRO3 homologue. The screen based on co-IP enrichment and mass spectrometry identification of bound proteins identified RAN, as well as RanBP5 and XPO5 also called RAN binding protein 21 as SYK binding proteins (*138*). Further connections indicated are co-expression of homologs in *Drosophila melanogaster* and the yeast *Schizosaccharomyces pombe*, as well as co-mentioning in publications, which needs to be corrected as none of the indicated publications actually mentioned both indicated proteins together. ENO1 is linked experimentally as well as by co-mentioning in publications to the TYRO3 homologs SRC and FYN, as Enolase is used as an src-family kinase substrate (*139-142*). Further publications indicated by String10 linking ENO1 to TYRO3 were text-mining artifacts. TYRO3 and AXL were linked to GAPDH due to co-expression of the TAM receptor homologs TSSK3 and TSSK6, which only posses a kinase domain without sharing the extracellular domains of TAM receptors. Further connections based on text mining between GAPDH and both TAM receptors, as well as between GAPDH and Protein S, were artifacts due to the frequent use of GAPDH as loading control and house keeping gene.

Figure 19. Enrichment by TYRO3 and AXL for each tissue screened.
For each tissue, the proteins enriched by either TYRO3-Fc or AXL-Fc were compared to Control-Fc enriched proteins. Differential enrichment is represented by the difference in log2 LFQ intensities and the respective T-Test's log2 p-value graphed as volcano plots. Proteins identified as discoveries by permutation based FDR correction of the respective T-Test are indicated by darker coloration. Generally $q<0.05$ is considered a discovery, except for the spleen samples where the cut-off was $q<0.01$.

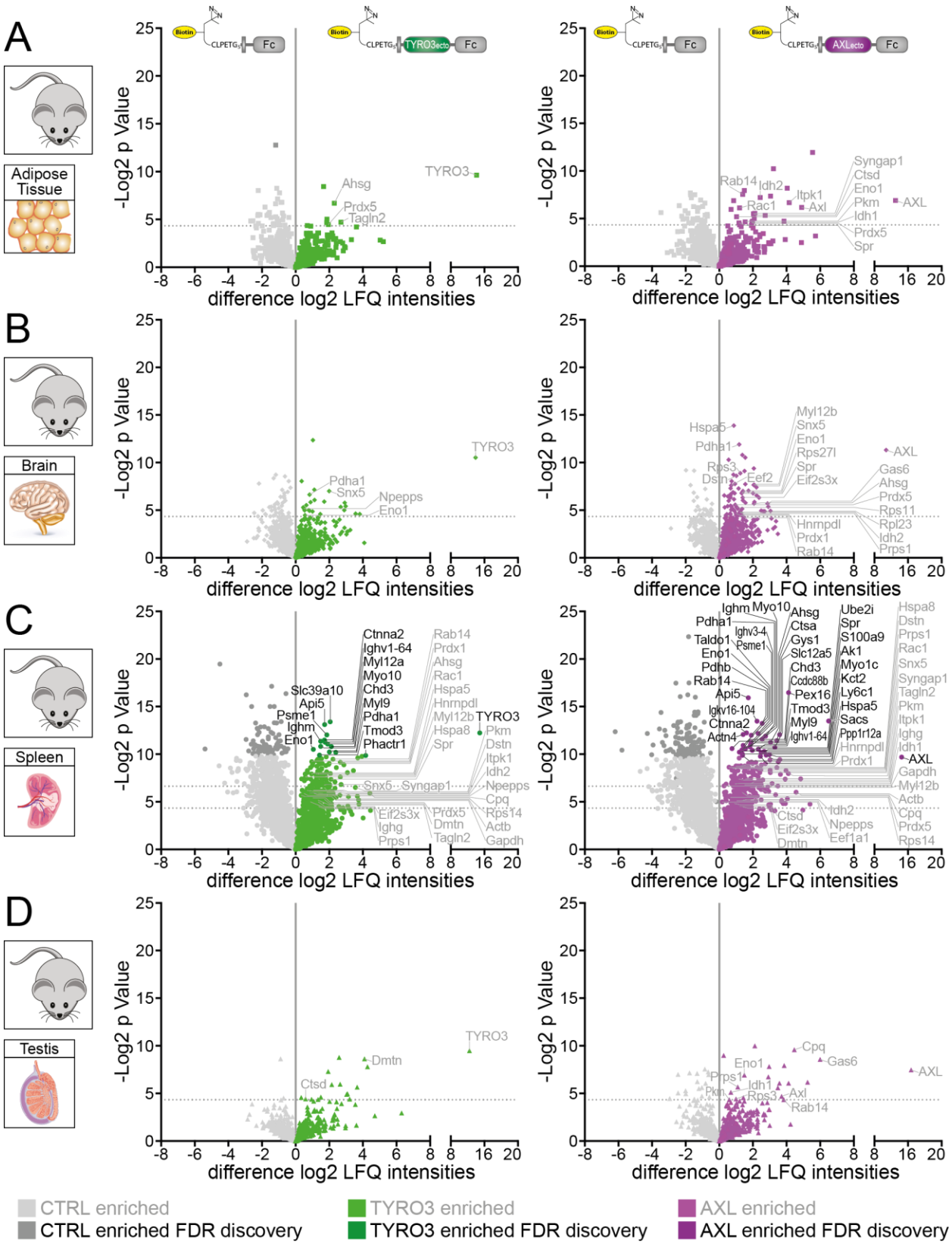
A
Adipose Tissue
B
Brain
C
Spleen
D
Testis
Biotin
CLPETG
Fc
TYRO3ecto
AXLecto
-Log2 p Value
difference log2 LFQ intensities
TYRO3
Ahsg
Prdx5
Tagln2
Syngap1
Ctsd
Eno1
Pkm
Idh1
AXL
Rab14
Idh2
Itpk1
Rac1
Axl
Spr
Pdha1
Snx5
Npepps
Hspa5
Myl12b
Rps27l
Eif2s3x
Gas6
Rps11
Rpl23
Prps1
Hnrnpdl
Prdx1
Ctnna2
Ighv1-64
Myl12a
Myo10
Chd3
Myl9
Tmod3
Phactr1
Slc39a10
Api5
Psme1
Ighm
Eno1
Hspa8
Pkm
Dstn
Cpq
Rps14
Actb
Gapdh
Eif2s3x
Ighg
Dmtn
Tagln2
Ighv3-4
Taldo1
Pdhb
Ighv16-104
Actn4
Ube2i
S100a9
Ak1
Myo1c
Kct2
Ly6c1
Sacs
Ppp1r12a
Ccdc88b
Pex16
Tmod3
Ighv1-64
Ctsd
Idh2
Npepps
Eef1a1
Cpq
Gas6
CTRL enriched
CTRL enriched FDR discovery
TYRO3 enriched
TYRO3 enriched FDR discovery
AXL enriched
AXL enriched FDR discovery

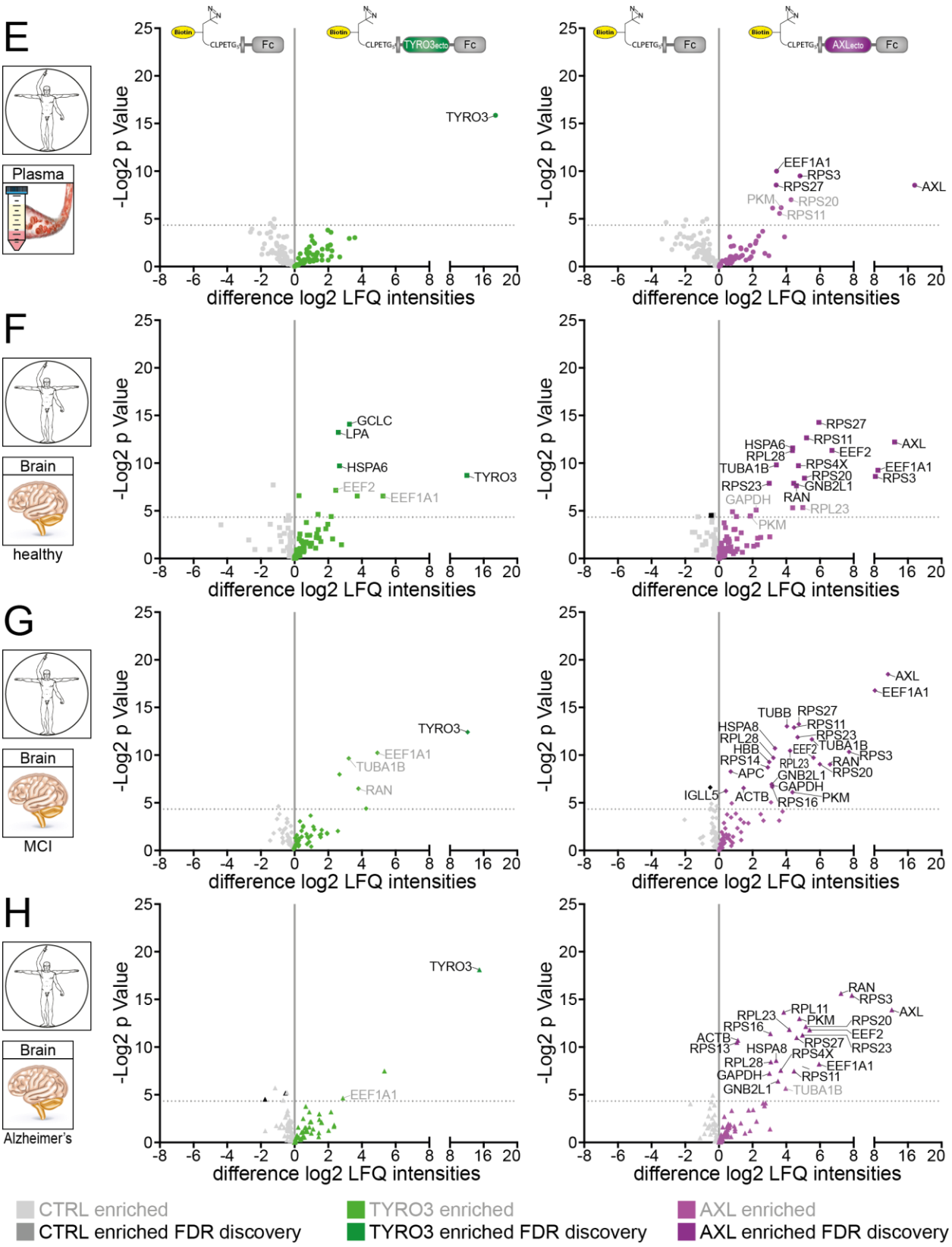
E
Plasma
F
Brain
healthy
G
Brain
MCI
H
Brain
Alzheimer's
Biotin
CLPETG
Fc
TYRO3ecto
AXLecto
-Log2 p Value
difference log2 LFQ intensities
TYRO3
GCLC
LPA
HSPA6
EEF2
EEF1A1
TUBA1B
RAN
AXL
RPS27
RPS11
HSPA6
RPL28
EEF2
TUBA1B
RPS4X
RPS20
GNB2L1
RPS23
GAPDH
RAN
RPL23
PKM
RPS3
TUBB
HSPA8
HBB
RPS14
APC
IGLL5
ACTB
RPS16
RPS13
CTRL enriched
CTRL enriched FDR discovery
TYRO3 enriched
TYRO3 enriched FDR discovery
AXL enriched
AXL enriched FDR discovery

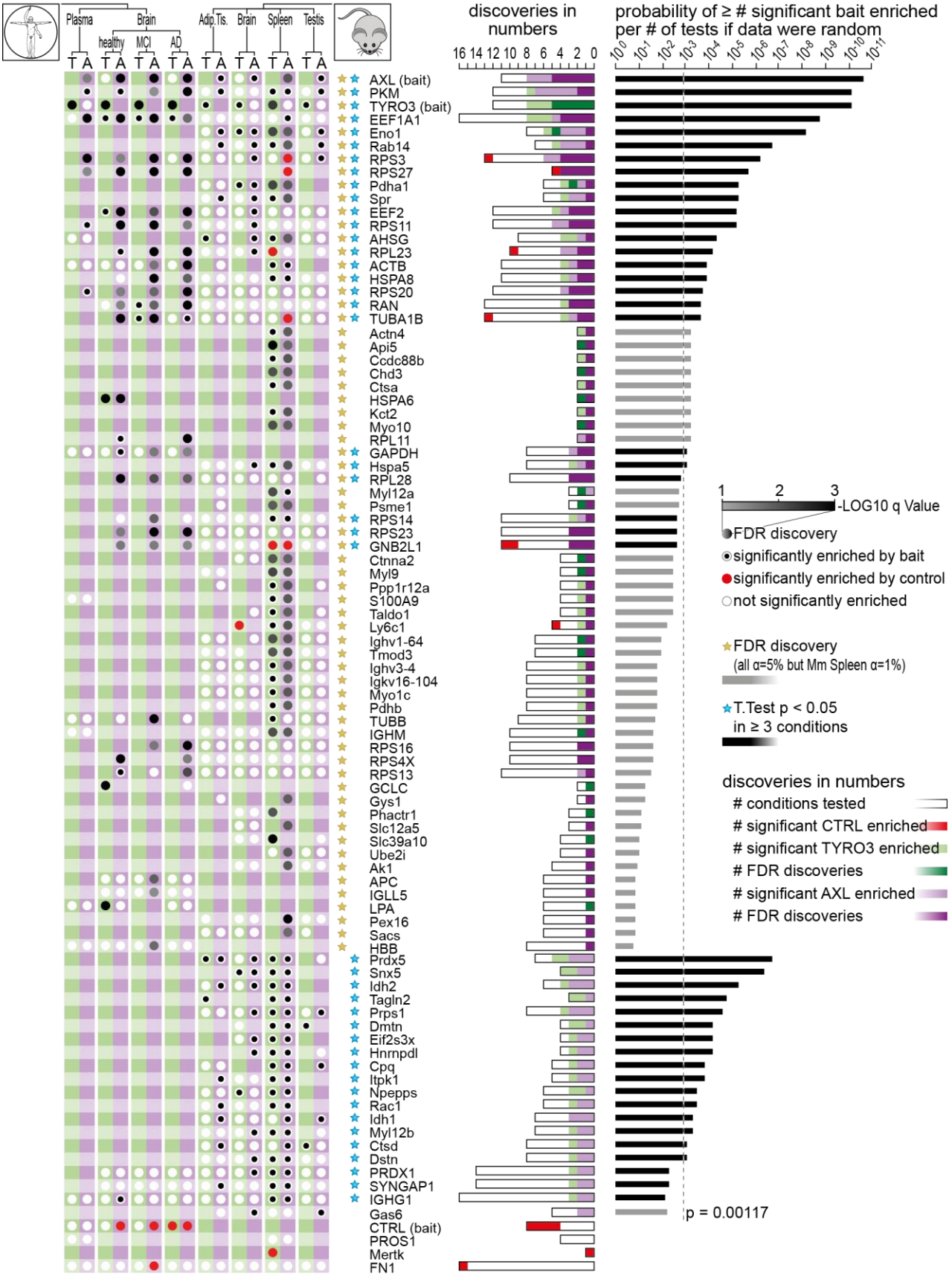
Plasma
Brain
healthy
MCI
AD
Adip.Tis.
Brain
Spleen
Testis
T A
discoveries in numbers
16 14 12 10 8 6 4 2 0
probability of ≥ # significant bait enriched per # of tests if data were random
AXL (bait)
PKM
TYRO3 (bait)
EEF1A1
Eno1
Rab14
RPS3
RPS27
Pdha1
Spr
EEF2
RPS11
AHSG
RPL23
ACTB
HSPA8
RPS20
RAN
TUBA1B
Actn4
Api5
Ccdc88b
Chd3
Ctsa
HSPA6
Kct2
Myo10
RPL11
GAPDH
Hspa5
RPL28
Myl12a
Psme1
RPS14
RPS23
GNB2L1
Ctnna2
Myl9
Ppp1r12a
S100A9
Taldo1
Ly6c1
Ighv1-64
Tmod3
Ighv3-4
Igkv16-104
Myo1c
Pdhb
TUBB
IGHM
RPS16
RPS4X
RPS13
GCLC
Gys1
Phactr1
Slc12a5
Slc39a10
Ube2i
Ak1
APC
IGLL5
LPA
Pex16
Sacs
HBB
Prdx5
Snx5
Idh2
Tagln2
Prps1
Dmtn
Eif2s3x
Hnrnpdl
Cpq
Itpk1
Npepps
Rac1
Idh1
Myl12b
Ctsd
Dstn
PRDX1
SYNGAP1
IGHG1
Gas6
CTRL (bait)
PROS1
Mertk
FN1
1 2 3
-LOG10 q Value
FDR discovery
significantly enriched by bait
significantly enriched by control
not significantly enriched
FDR discovery
(all α=5% but Mm Spleen α=1%)
T.Test p < 0.05
in ≥ 3 conditions
discoveries in numbers
# conditions tested
# significant CTRL enriched
# significant TYRO3 enriched
# FDR discoveries
# significant AXL enriched
# FDR discoveries
p = 0.00117

Figure 20. TAM receptor interacting proteins identified in multiple tissues.
Summarizing the Vulcano Plots of Figure 19, protein enrichments compared between bait and control samples via T-Test are shown for the respective baits compared to control for the respective tissues on the right. Proteins with $p>0.05$ comparing either TYRO3 or AXL to control via T-Test are labeled with an empty white circle for the respective tissue and bait. Proteins significantly enriched with $p<0.05$ are labeled with a black spot centered in a white circle for the respective tissue and bait. Proteins with a $q<0.05$, or in case of spleen samples with a $q<0.01$, correcting the T-Test via permutation based FDR, are labeled with circles who's intensity within a gray-scale from 50% gray (1) to black (3) represents the –LOG10 q value. Proteins that were identified as a discovery after FDR correction are labeled with a golden star. Proteins significantly bait enriched according to the T-Tests in at least three conditions are labeled with a blue star.
Summarizing the test results, a bar graph shows the total number of tested conditions by a black frame for each protein. Significant enrichments with $p<0.05$ for the respective T-Tests are shown in light green for TYRO3 and light violet for AXL. FDR discoveries are shown in darker green or violet respectively. The number of conditions where proteins were significantly control enriched are shown in red.
The log10 probability of the respective number of T-Test significant bait enrichments within the respective number of total tests is presented on the left. For those proteins significantly enriched in at least three conditions according to the T-Test (blue star) the bars are presented in black. For the number of these proteins the individual probability of $p<0.00117$ was calculated to maintain a probability of 5% of one or more false positives within the 44 proteins in case the data were random.

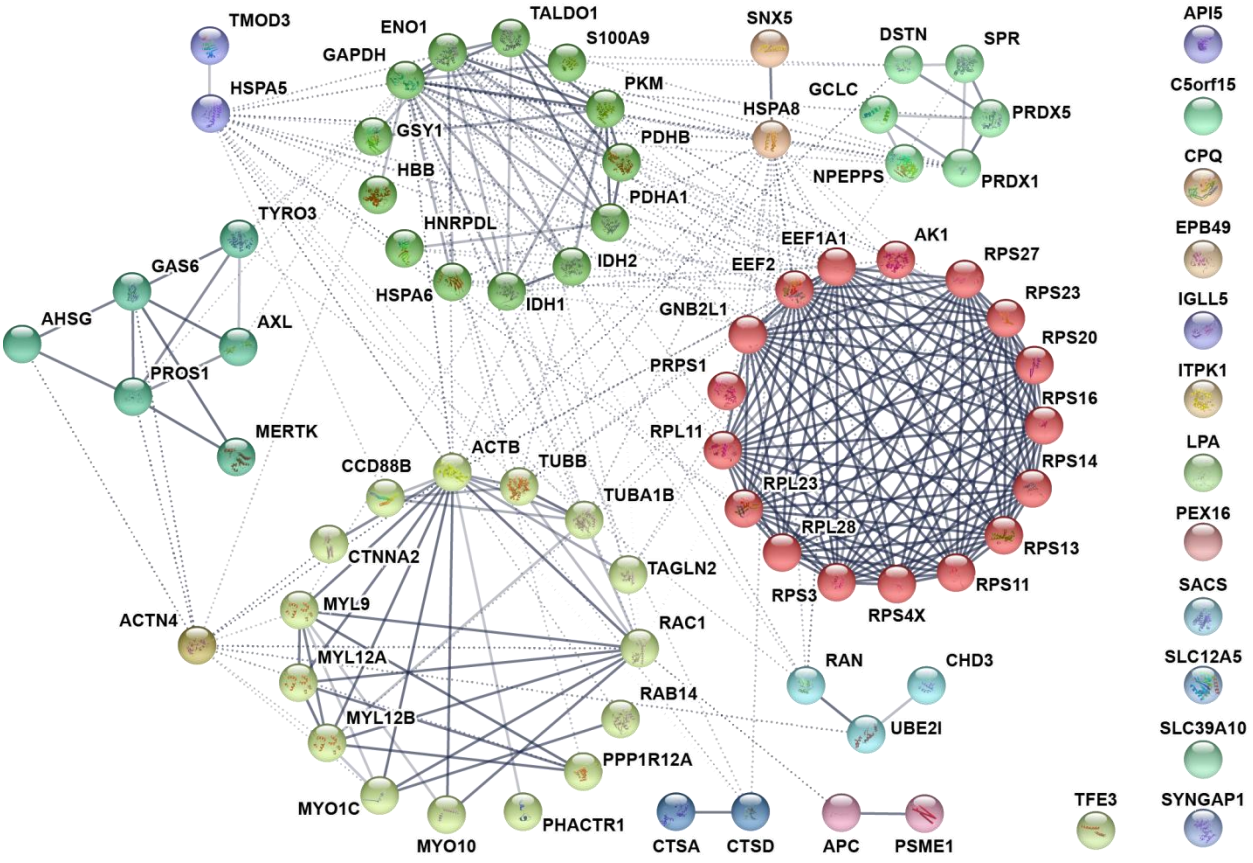

Figure 21. Protein-Protein interaction network.
To uncover connections in between proteins based on published data and information available online, the database STRING10 was used to cluster proteins identified as 'TYRO3 and AXL interacting' in Figure 20 by MCL clustering using an inflation parameter of 3. Interactions based on text mining, experiments, databases, co-expression, neighborhood, gene fusion, and co-occurrence between proteins of the same cluster are indicated as solid lines and in between proteins of different clusters as dotted line for those proteins recognized by the online tool. A higher confidence in the interaction is indicated by a darker coloration of the connection and vice versa.

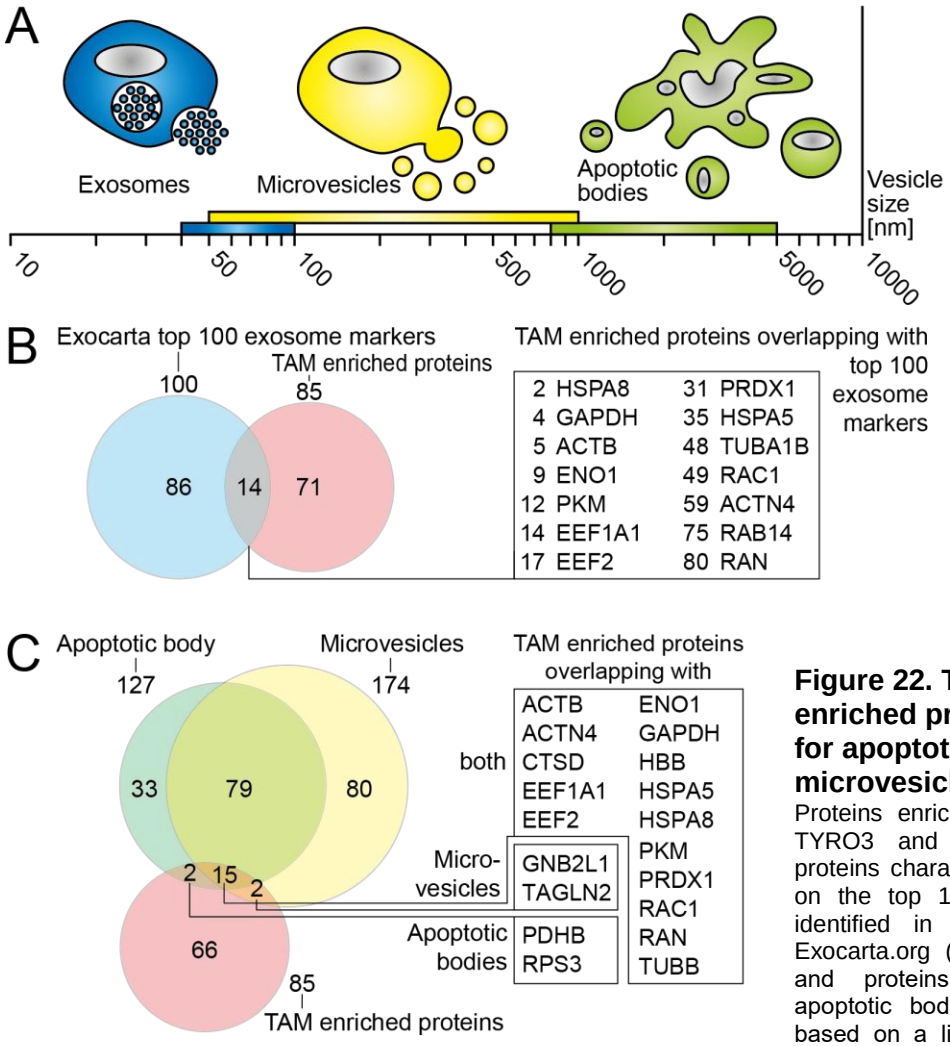

Figure 22. TAM receptor enriched proteins characteristic for apoptotic bodies, microvesicles, and exosomes.
Proteins enriched by the TAM receptors TYRO3 and AXL were compared to proteins characteristic to exosomes based on the top 100 proteins that are often identified in exosomes (B) based on Exocarta.org (*143*) (Appendix, Table 17), and proteins characteristic to either apoptotic bodies, microvesicles, or both based on a list of proteins published by Turiák et al. 2011 (*144*) (C).

The screen for novel TAM interacting proteins has identified 83 proteins of which 3 proteins, AHSG, RAN, and ENO1, have been indirectly linked to TAM receptors or their ligands GAS6 and Protein S. A majority of these proteins share one or more cellular compartment associations with TYRO3, AXL, MER, GAS6, or Protein S. However, after the successful identification of proteins interacting with TAM receptors based on mass spectrometry, the functional relevance of these interactions remain to be investigated.

Evaluation of putative TAM receptor interacting proteins

After the successful identification of proteins interacting with TYRO3 and AXL, these interactions remained to be further characterized. With the experiments described in the following chapter, it was tested whether the TAM receptors directly interact with candidates of the screen. For this

purpose, titrations of recombinant proteins of interest were immobilized in reaction vessels and incubated with TAM receptor ectodomain containing Bait-Fc proteins and Control-Fc protein. To minimize the potential effect of n-terminal tags on the interactions tested, Bait-Fc and Control-Fc proteins were used in their 2 amino acid linker version without the n-terminal hexa-His-LPET tag. Each protein of interest titration was compared to AXL-Fc interaction with 50 nM recombinant human GAS6 to control for the correct opperation of the test and to enable the comparison inbetween tests.

Recombinant human proteins tested in this assay were AHSG, ENO1, GNB2L1, IGHG1, PKM2, PRDX5, RAB14, RAN, RPS3, and SPR previously identified interacting with TAM receptors. These proteins were expressed in *E. coli* except for AHSG and the IGHG1 Fc domain (Figure 23). From these proteins only the Fc domain of IGHG1 showed significantly higher binding by TAM receptor bait proteins compared to control protein. The signal of MER-Fc binding 625 nM IGHG1 reached 3% of the signal AXL-Fc reaches when binding 50 nM GAS6, however the signal at 625 nM IGHG1 was rising in log phase indicating higher signals may be reached with higher concentrations. Further AHSG and ENO1 showed weak binding to the Bait-Fc, but not differing significantly to Control-Fc. Further the signals of bait and control proteins bound to 625 nM AHSG and ENO1 compared to approximately 2% of the signal measured with AXL-Fc binding 50 nM GAS6.

Additional to those proteins identified to interact with TAM receptors in Figure 20, further proteins considered potentially interacting with TAM receptors were tested (Figure 24). From the proteins tested, bovine ALB and human C6, CNDP2, and S100A6 do not show any interaction with neither TAM receptor bait-Fc proteins, nor the control-Fc protein. Human and mouse MPO show binding of both, the bait-Fc and the control-Fc proteins without significant differences in the respective binding curves. The scavenger receptor B1 did show significant differences in it's affinity to the three TAM receptor bait proteins, and most importantly, the affinity to Control-Fc was weakest. At 625 nM SR-B1 the binding curves of all proteins tested reach their maximum. MER-Fc reaches more than 13% of the signal detected by AXL-Fc bound to 50 nM GAS6. The second highest signal is reached by TYRO3-Fc with approximately 9.6% followed by AXL-Fc with 7% slightly higher than Control-Fc with 6%. When comparing the individual concentrations, AXL-Fc binding does not significantly differ from Control-Fc, unlike TYRO3-Fc and MER-Fc which significantly differ at 125 nM and 625 nM SR-B1-Fc. As the recombinant protein of SR-B1 used was a chimeric protein fused c-terminally to the Fc domain of IGHG1, the TAM receptor ectodomains possibly interacted with the Fc domain instead of SR-B1. As the Fc domain fused to SR-B1 is from IGHG1 who's TAM interaction curves are shown in Figure 24 H, a comparison of SR-B1-Fc to IGHG1 disects the binding to Fc from the binding to SR-B1. MER-Fc reaches a

relative signal of approximately 13% interacting with SR-B1-Fc while with IGHG1 Fc domain alone only 3% is reached. At 625 nM, the signal of MER-Fc and AXL-Fc is approximately 4.5 times higher binding SR-B1-Fc compared to IGHG1 and even more than 11 times higher for TYRO3.

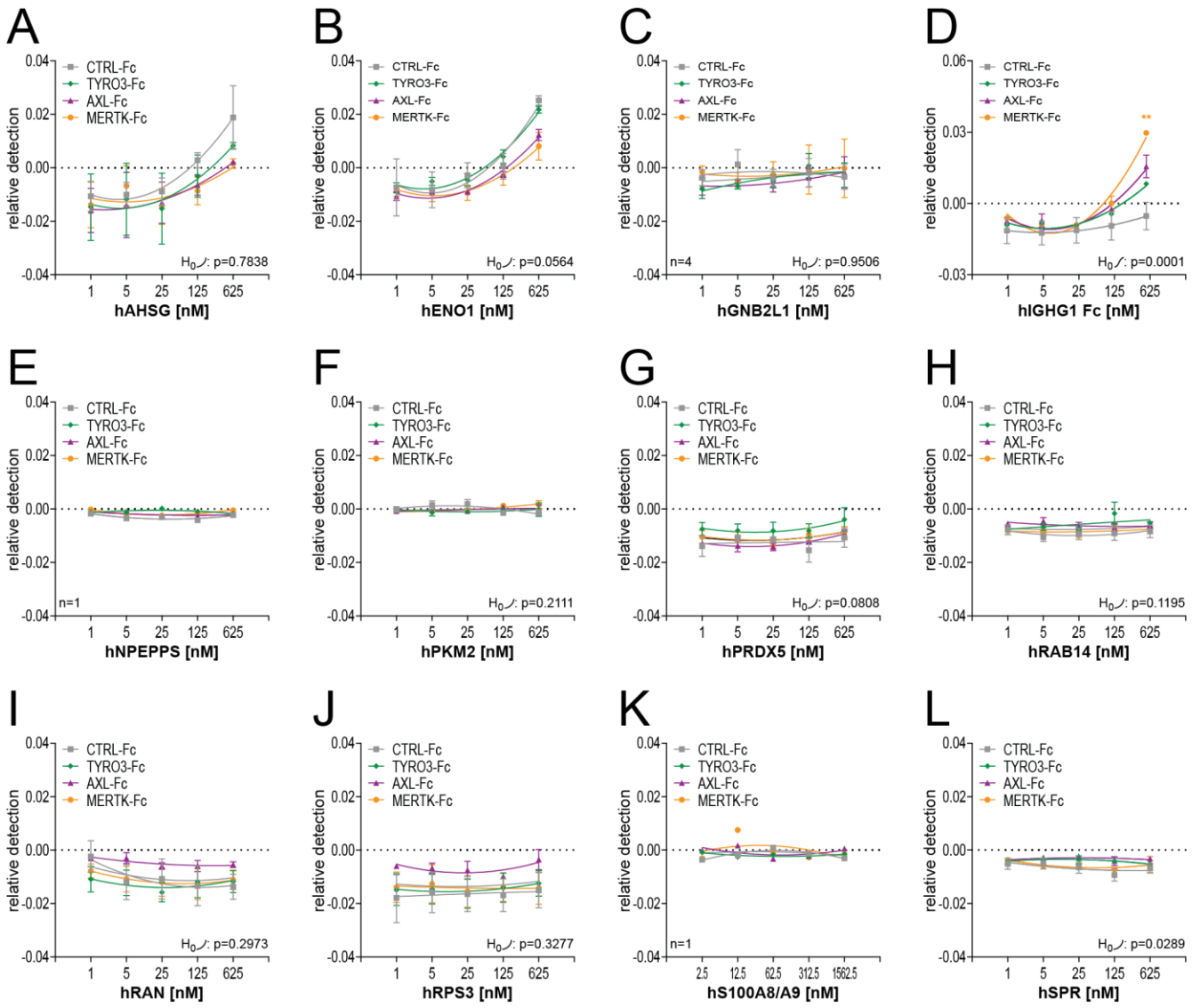

Figure 23. Binding of screening identified proteins to TAM receptor bait proteins.

The interaction of bait and control Fc proteins was measured by ELISA. Titrations of proteins identified as putative TAM interactors were bound to reaction vessels, blocked and incubated with 250 nM 2L versions of TYRO3-Fc, AXL-Fc, MER-Fc and Control-Fc. Bound bait or control protein was quantified by anti-mIgG2a-HRP dependent substrate conversion. Signals are relative to 2L AXL-Fc binding 50 nM GAS6.

MEAN and SEM of 3 technical repeats performed with technical duplicates are shown if not indicated otherwise. Probabilities of one curve fitting adequately all data sets were calculated by regression analysis for sigmoidal or exponential curves. In case of $p<0.05$, data sets of bait proteins were compared to the control within the individual conditions with two-stage step-up method of Benjamini, Krieger and Yekutieli FDR corrected multiple t-tests reporting bait enrichments significantly different to control as follows: * $q<0.05$ and ** $q<0.01$, *** $q<0.001$

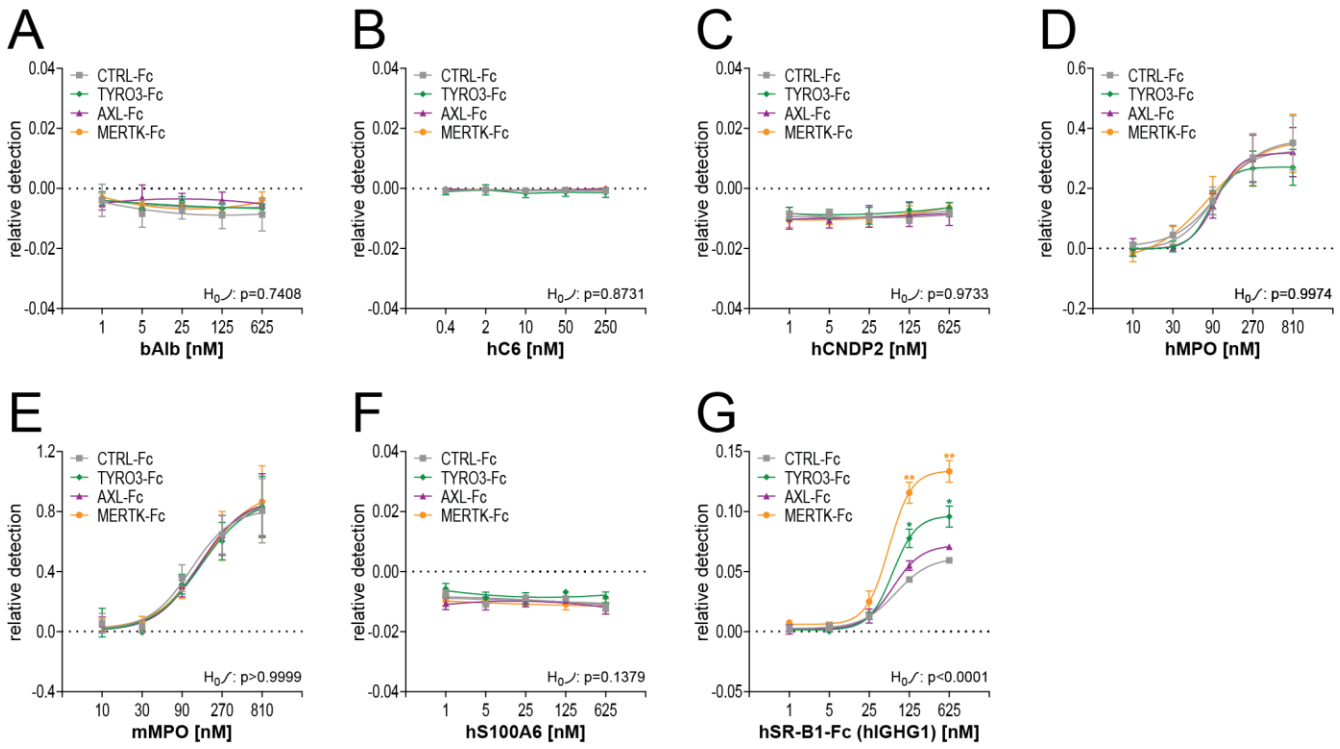

Figure 24. Binding of proteins of interest to TAM receptor bait proteins.
The interaction of bait and control Fc proteins was measured by ELISA. Titrations of proteins of interest were bound to reaction vessels, blocked and incubated with 250 nM 2L versions of TYRO3-Fc, AXL-Fc, MER-Fc and Control-Fc. Bound bait or control protein was quantified by anti-mIgG2a-HRP dependent substrate conversion. Signals are relative to 2L AXL-Fc binding 50 nM GAS6.
MEAN and SEM of 3 technical repeats performed with technical duplicates are shown if not indicated otherwise. Probabilities of one curve fitting adequately all data sets were calculated by regression analysis for sigmoidal or exponential curves. In case of $p<0.05$, data sets of bait proteins were compared to the control within the individual conditions with two-stage step-up method of Benjamini, Krieger and Yekutieli FDR corrected multiple t-tests reporting bait enrichments significantly different to control as follows: * $q<0.05$ and ** $q<0.01$, *** $q<0.001$

Testing several proteins of interest biochemically for direct interaction with TAM receptors sucessflly identified Scavenger receptor B1 and IGHG1 interaction with the TAM receptors TYRO3 and MER but not AXL, and MER but not TYRO3 and AXL respectively. As for the current test of protens identified as potential TAM receptor interacting mostly recombinant proteins expressed in bacteria were used lacking human post-translational modifications, little can be concluded from negative data. In order to draw a meaningful conclusion, also from negative data, the proteins of interest should be expressed in human cells and tested for their effect on TAM receptor function. With SR-B1 and IGHG1 confirmed to interact with TAM receptors and further promissing proteins to be investigated, future experiments will shed light on TAM receptor function and regulation.

4. Discussion

Benefits and improvements of the specialized screening method

Since the discovery of TYRO3, AXL, and MER and their classification as distinct receptor tyrosine kinase family in 1991 by Lemke and colleagues (*124*), few efforts were made to systematically screen for ligands and interacting proteins. Four years after the discovery of TAM receptors, Protein S and GAS6 were identified as ligands. First conditioned media were screened for their ability to cause TAM receptor phosphorylation, followed by receptor based affinity chromatography of TYRO3-Fc with fetal bovine serum and Axl-Fc with concentrated ABAE conditioned medium (*29*). Tubby and Tulp1 were characterized to be TAM receptor ligands inducing phagocytosis in retina and brain. Tubby binds Mer, while Tulp1 binds to Tyro3, Axl, and Mer (*38*, *39*). The initial discovery of Tubby and Tulp1, which act as 'eat me' signals for phagocytosis in the year 2010 was based on a phage display assay. In this assays, phages presenting proteins of a murine eye cDNA library were enriched by 4 rounds of phagocytosis by retinal pigment epithelial cells (*145*). The same group amended its phage display phagocytosis protocol by two additional Mer affinity purification steps and identified Galectin-3 as a Mer specific phagocytosis ligand (*41*). Galectin-3 was shown to opsonize desialylated cells for microglia (*40*) and might potentially be involved in other phagocytic processes with desialylation as 'eat me' signal as for example in platelets (*146*). The hypothesis that semian virus 40 mimics host ligands lead to the discovery that the major capsid protein VP1 binds to AXL and to a lesser extent to TYRO3 and MER. The homology of VP1 to GAS6 was uncovered by bioinformatic screening for VP1 homologous and receptor associated proteins (*104*).

Besides the binding of these ligands or ligand mimicking proteins, TAM receptors were shown to co-operate with other receptors to engage in various signaling pathways. Wu and colleagues characterized the co-operation of MER and αvβ5 integrin recognizing PtdSer by GAS6 or Protein S and by MFG-E3 respectively, after investigating both receptors signaling cascades. Only when MER recruits αvβ5 by FAK, a synergistic increase of phagocytic activity is reached (*71*). Like Wu and colleagues, Todt *et al.* found MER binding and co-operating with Scavenger Receptor A to synergize for phagocytosis as both receptors are involved in the same process (*147*). Carla Rothlin and colleagues discovered that simultaneous activation of AXL and IFNAR leads to the induction of SOCS1 and SOCS3 expression. They could demonstrate, that AXL usurps IFNAR signaling after direct binding. Together these findings explain the initial observation of dendritic cell's hyper activation in TAM receptor triple knock out mice. After establishing that GAS6

stimulation of TAM receptors induces SOCS1/3 expression in dependency of IFNAR, direct interaction of AXL and IFNAR1 was discovered via co-IP (*22*).

Focusing on the methods used for the identification of TAM receptor ligands, only bovine serum, conditioned ABAE media, and murine eye proteins were screened for ligands, representing a limited spectrum of TAM receptor expressing tissues (*29*, *145*). The affinity purification leading to the discovery of GAS6 and Protein S was majorly limited by the low sensitivity of staining differentially purified proteins in SDS-PAGE gels (*29*). The phage display assay successfully enriched Tubby and TULP1 by 4 rounds of phagocytosis and phage selection. However the assay was biased towards phagocytosis representing only one of three major TAM receptor functions. Another bias was the limitation of the screened protein library towards proteins expressed in murine eye (*145*). Retinal pigment epithelial cells are specialized to phagocytize the outer segments of photoreceptors (*148*). Subsequent studies were able to show a relevance of Tubby and Galectin 3 for Mer dependent phagocytosis by microglia, with Galectin 3 suggested to opsonize apoptotic cells presenting desialylated sugar chains (*39*, *40*). Beside desialylated sugar chains being indicated as a second ‘eat me’ signal additional to PtdSer for Mer dependent phagocytosis, the identification of Tubby and Galectin 3 did not reveal novel TAM receptor functions.

Using a method similar to the affinity purification used by Stitt et al., I was able to enrich Fibronectin bound to TYRO3-Fc from human plasma (Figure 6, A) and confirm its interaction to TAM receptors in a reverse ELISA assay (Figure 6, B). Fibronectin is a major component of the extracellular matrix and involved in wound healing (*149*), cell adhesion (*150*) and migration. It participates in biological processes like proliferation, survival, and differentiation (*151*). Interestingly, the effect of Fibronectin on proliferation, survival, and differentiation is dependent on FAK pp125 phosphorylation (*151*). FAK is phosphorylated by SRC upon MER activation and binds to the β5 subunit of integrin αvβ5, which then co-operates with MER to phagocytize the outer segments of photoreceptors (*70*, *152*). Finally McCutcheon and colleagues described the beneficial effect of Fibronectin addition on the phagocytosis of apoptotic neutrophils by macrophages, which is independent of β1 integrin (*153*). Together these findings suggest that Fibronectin is recognized by multiple receptors, and that Fibronectin supports of phagocytic events, which may involve TAM receptor activation.

Motivated by the TAM receptor specific enrichment of Fibronectin using simple affinity purification, I established a method to attach a photo-activatable cross-linker to TAM receptor baits to capture weak and transient interacting proteins and compared three methods of protein enrichments (Figures 7 to 16). After the successful establishment of bait protein modification, and after deciding for an optimal enrichment method, murine adipose tissue, brain, spleen and testis, as well as human plasma and brain samples from patients diagnosed with mild cognitive

impairment (MCI), Alzheimer's patients and control patients were chosen to be screened for novel TAM ligands. TAM receptor function is dependent on the ligand and co-receptor environment, which varies within tissues and within health and disease states. To decrease the bias introduced by selecting certain environments to be screened, the tissues were selected to represent the major TAM receptor functions including phagocytosis, immune inhibition, and proliferation and survival. In detail, human plasma was screened, as TAM functions were initially discovered in the hematopoietic system (*22*, *24*, *87*). Brain tissue was chosen, since microglia were described to express TYRO3, AXL, and MER and, additional to GAS6 and Protein S, bind ligands like Tubby, TULP1, and Galectin 3 (*40*, *82*, *154*, *155*). The utilization of alternative ligands indicates brain samples as valuable sources of further TAM receptor ligands. Like in testis (*25*), TAM receptors are reported to be involved in phagocytic processes in the spleen (*24*). In addition to phagocytosis TAM receptors are reported to essential for NK cell differentiation in spleen (*156*). Besides plasma, brain, testis and spleen representing tissues with described TAM receptor functions, adipose tissue was selected for screening. Although none of the three major TAM receptor function has been described in adipose tissue yet, mRNA expression data show that AXL is relatively high expressed compared to the other tissues described (Figure 17, B). GAS6 and AXL are indicated to have an effect in obesity, as increased GAS6 and soluble AXL levels were detected in overweight individuals (*157*). Like the diversity of TAM receptor functions, the tissues selected for the novel TAM interactor screening were chosen to represent diverse TAM receptor and ligand expression patterns (Figure17, B).
The screening method used for this study differs from the methods used before by the reduction of tissue bias, as multiple tissues of mouse and human origin, as well as in case of human brain healthy and diseased tissues were screened. Instead of enriching strong interacting proteins, the method used enables the capture of weak and transient interacting proteins. Finally, mass spectrometry was used to identify and quantify novel TAM interacting proteins with the highest sensitivity of all methods used for protein identification (Figure 17, A).

The screening for TAM interacting proteins identifies 83 novel candidates

Screening for TAM interacting proteins in lysates of the tissues defined above resulted in the enrichment of 83 proteins following no directly obvious pattern, except for an overrepresentation of ribosomal proteins (Figure 20). To reveal associations between the enriched proteins and TAM receptors as well as their ligands GAS6 and Protein S, the online database STRING10 was used. STRING10 is a protein interaction database based on published high throughput and co-expression experiments, automated text mining, genomic context predictions, and data provided

by other databases. Therefore, STRIN10 is a powerful tool to identify connections between proteins of interest. Provided with the list of 83 TAM enriched proteins completed with MER, GAS6, and Protein S, this meta-analysis revealed AHSG and ACTN4 to be associated with GAS6 and Protein S. RAN and ENO1 were found to be associated with TYRO3 (Figure 21). Using the Cytoscape applications ClueGO and CluePedia, gene ontology enrichment analysis for 'Biological Process' of the 83 TAM ligand candidates highlighted IGHG1, IGHM, and IGLL5 as proteins involved in phagocytosis. Further ribosomal proteins were enriched for several biological processes not directly associated with TAM receptors (Figure App 7). 'Cellular Component' GO terms associated with the TAM enriched proteins were grouped to commonly associated terms and beside the cellular localizations, a general pattern of vesicular association of 55 proteins was found (Figure App8). Differentiating the general vesicle patterns even further revealed 21 TAM enriched proteins described to be characteristic for exosomes, microvesicles and apoptotic bodies (Figure 22). In the following sections the identified patterns and associated proteins will be discussed regarding their potential role to engage in TAM receptor functions.

AHSG or Fetuin A may bridge mineral complexes and mineralized vesicles to TAM receptors for phagocytosis

To identify previously reported interactions, the online database STRING10 was used (Figure 21). STRING10 linked the acute-phase protein AHSG, or Fetuin A, to the TAM receptor ligands GAS6 and Protein S due to their binding of mineralo-organic complexes and cardiovascular calcification (*131*, *133*). Vascular calcification can be prevented by Vitamin K, but GAS6 was shown to not aggravate calcification (*133*). AHSG was found to have a cytoprotective effect on neurons after challenges of oxidative stress *in vitro* (*158*), as do GAS6 and Protein S. Loss of AHSG leads to increased inflammatory gene expression in spleen indicating an anti-inflammatory role (*159*). On the contrary, AHSG was shown to function as an adaptor for free-fatty acids (FFA) to induce TLR4 dependent inflammation in adipose tissues (*160*). AHSG clusters calcium and phosphate into larger aggregates preventing soft-tissue mineralization (*161*). These calciprotein particles are cleared by liver Kupffer cells and marginal zone macrophages in spleen involving scavenger receptor A (SR-A) (*162*). Elevated calcium and phosphate levels synergistically induce calcification of vascular smooth muscle cells (VSMC) in the absence of serum (*163*). AHSG found at high concentrations in human plasma with 0.3 mg/ml (*164*) was shown to inhibit apoptosis (*165*) and thereby prevent vascular calcification (*166*). Another serum protein inhibiting apoptosis induced by elevated inorganic phosphate is GAS6 by engaging AXL and the PI3K/AKT survival pathway (*167*). Under conditions of high

calcium and phosphate concentrations, VSMC release apoptotic bodies and matrix vesicles containing high concentrations of calcium and phosphate together with AHSG (*163*). The accumulation of matrix vesicles and apoptotic bodies due to impaired phagocytosis increases vascular calcification (*166*). Acetylated LDL (acLDL) was shown to compete with apoptotic bodies for binding to phagocytes (*168*) and by competing with apoptotic bodies for SR-A dependent phagocytosis. Thereby, acLDL increases vascular calcification (*169*). Another nucleating factor, which contributes to the formation of calcium phosphate complexes, is Phosphatidylserine (PtdSer) presented on the inner plasma membrane of matrix vesicles and on the outer leaflet of apoptotic body membranes (*170*).

The characterization of AHSG interaction with TAM receptors as implicated by multiple significant enrichments in various tissues including spleen (Figure 20) may shed light on TAM receptor and ligand function in atherosclerosis beyond promoting VSMC survival.

A novel function of TAM receptors in the recognition of extracellular vesicles

The two proteins ENO1 and RAN identified in my screen were related to TYRO3 by STRING10 (Figure 21). ENO1's indicated relationship is based on TYRO3's homology to the non-receptor tyrosine kinase FYN, where ENO1 is used as a phosphorylation substrate (*171*). RAN's indicated relationship is based on TYRO3's homology to the non-receptor tyrosine kinase SYK, where RAN was enriched in a SYK co-immunoprecipitation (*138*). Comparing the kinase domains of the proteins, TYRO3 (ref: Q06418, aa518-790) was found to share 34.3% pairwise identity with FYN (ref: XP_016866139.1, aa271-524) and a 32.1% pairwise identity with SYK (ref: P43405, aa371-631). Indeed TYRO3 is described to bind and use FYN for signaling to induce Schwann cell myelination (*172*), while SYK binds to activated AXL in B-cells from chronic lymphatic leukemia patients (*173*). Therefore, TYRO3 adaptor proteins potentially may have indirectly enriched ENO1 and RAN. However, adaptors like SYK and Fyn are not able to interact with the kinase domains of TYRO3 and AXL in case of this screen, as they are not included in the bait proteins used.

ENO1 and RAN, as well as 9 other proteins including PKM, EEF2, ACTB, HSPA8, ACTN4, GAPDH, HSPA5, RAC1, and PRDX1 are proteins characteristically identified in apoptotic bodies, microvesicles, and exosomes (*144*). Further EEF1A1, RAB14, RPS3, TUBA1B, GNB2L1, TUBB, TAGLN2, and CTSD are associated with one or two of the extracellular vesicle types, but not all three of them indicating an interaction with multiple types of vesicles (Figure 22). Literature research revealed an association of TAM receptors with the clearance of apoptotic cells is abundantly available. In contrast, only few publications describe a direct

connection of extracellular vesicles to TAM receptors. However these few publications indicate potential delivery signals to activate TAM receptors by apoptotic bodies, microvesicles, ectosomes, and exosomes. For example, Eken and colleagues could show that ectosomes released by activated neutrophils have a regulatory effect on TLR activation of macrophage lasting for 24h, which is MER dependent (*174*, *175*). Additionally, exosomes were shown to induce STAT1 phosphorylation in dependence of GAS6 or Protein S on TAM/IFNγR1 reporter cells (*176*), indicating that exosomes participate in the induction of anti-inflammatory cell programs by binding to TAM receptors. Another example for TAM activation by vesicles are plasma membrane-derived microparticles (PMPs) released by Platelets upon activation (*177*). Endothelial cells phagocytize these PMPs in dependence of AXL and GAS6. Further the clearance of PMPs was not reduced in GAS6 knock out mice, leading to the hypothesis, that the GAS6/AXL interaction is targeted and local but that this mechanism is not the main mechanism to clear the vast majority of PMPs from the circulation (*177*). Microvesicles from chronic lymphatic leukemia patients were found to activate PI3K/AKT signaling in bone marrow stromal cells. The authors concluded, that the microvesicles induced the intracellular signaling cascades either by the activation of AXL, or by the delivery of active AXL via microvesicles. The authors further postulate the hypothesis, that activated AXL is delivered by microvesicles to recipient cells even in the absence of GAS6 expression in those recipient cells (*178*).

The herein described screening for novel TAM ligands (Figure 22) enriched multiple proteins associated to apoptotic bodies, but also microvesicles and exosomes. The high number of vesicle-associated proteins might indicate an enrichment of total vesicles complexes, rather than TAM receptor interactions with single vesicle components. Comparing bait and tissue combinations where GAS6 was significantly enriched to those where the vesicle-associated proteins were significantly enriched, no co-enrichment of GAS6 with vesicle markers was found. To verify proteins like PKM, ENO1, RAB14, RPS3, GNB2L1, and RAN, which were identified as novel potential TAM ligands, ELISA assays were performed to test their affinity to TAM receptors. Yet the screening identified these proteins as TAM interacting proteins, the ELISA assay did not reveal direct interaction (Figure 23, B, C, F, H, I, and J). However, the recombinant proteins used for these assays were mostly *E. coli* derived and after TAM receptor binding, several washing steps ensured stringency but impaired the detection of weak and transient interaction.

In summary, deeper investigation of TAM receptor activation is needed to clarify how TAM receptors are able to elicit differential responses to at first glace similar signals like GAS6 and Protein S bound to PtdSer presented by apoptotic (*24-26*) or living cells (*55*) or to vesicles. The illumination of vesicular signal transmission via TAM receptor activation will deepen our

understanding of immune regulation by TAM receptors and offer ways to target cells and direct their responses via vesicles carrying therapeutics.

Apoptotic cell associated molecular patters

Additional to the proteins identified by screening multiple tissue lysates, further proteins were tested for TAM receptor interaction via ELISA assays (Figure 24). C6 and MPO, as representatives of proteins reported to label membranes for immune cells (*179*, *180*), were tested. Neither protein demonstrated affinities to any TAM receptor bait protein exceeding the affinity to the control Fc protein (Figure 24, B, D, E). Another candidate based on literature research was the scavenger receptor B (SR-B), as it's family member SR-A was described to synergize with MER for efficient phagocytosis in murine macrophages (*147*). SR-B was shown to directly bind PtdSer on apoptotic cells and induces phagocytosis (*181*) highlighting the receptor as a potential TAM cooperation partner. Titration of recombinant SR-B1 protein in an ELISA assay showed direct binding of MER and TYRO3 (Figure 24, G), an interaction yet unpublished. Further characterization is needed to investigate the interaction of TAM receptors and Scavenger receptor B with respect to phagocytosis, potentially in absence of TAM receptor ligands GAS6 and Protein S.

Beside Phosphatidylserine presentation on the outer plasma membrane recognized by TAM receptors, Scavenger receptors, and integrins (*71*, *147*), apoptotic bodies present a unique range of proteins (*144*) discriminating them from living cells. In 1994, the Rosens described blebs of RNA surrounded by ribonucleoprotein Ro, fragmented endoplasmic reticulum and ribosomes, and DNA blebs surrounded by ribonucleoproteins Ro, La, and small nuclear ribonucleoproteins and considered them to be targets of auto-antibodies in systemic lupus erythematosus (SLE) (*182*). Nishida and colleagues further characterized the degradation of ribosomal proteins, structural change of ribosomes and the surface presentation of ribosomal proteins during apoptosis (*183*). Mice expressing a kinase deficient MER variant develop systemic lupus including autoantibodies against chromatin, DNA, and IgG due to impaired clearance of apoptotic cells (*63*). Moreover mice lacking TAM receptors express autoantibodies against a range of ribonucleoproteins, but especially against heterogeneous nuclear ribonucleoprotein P2 (*184*). The presentation of ribosomes and ribosomal proteins on apoptotic cell surfaces, together with the TAM receptor specific enrichment of 40S ribosomal proteins RPS3, RPS4X, RPS11, RPS13, RPS14, RPS16, RPS20, RPS23, RPS27, and 60S ribosomal proteins RPL11, RPL23, and RPL28 (Figure 20) indicate an interaction of TAM receptors with ribosomes presented on the surface of apoptotic cells. Yet the arguments for a direct interaction

of ribosomes with TAM receptors are strong, recombinant RPS3 was negatively tested for direct interaction with TAM receptors using ELISA (Figure 23, J). The bait proteins used in the ELISA assay did not capture weak and transient interacting proteins via cross-linking and therefore the interaction may be too weak to be detected. In conclusion, the interactions of TAM receptors with ribosomal proteins need to be confirmed with more sensitive methods to characterize the interaction and potential discrimination of living and dead cells presenting PtdSer.

TAM receptor enriched proteins and cancer

Searching for TAM receptor enriched proteins associated with cancer by PubMed revealed 15 proteins with more than 100 publications, which were therefore considered as cancer associated (Appendix, Table 18). Of these 15 cancer associated proteins, PKM, ENO1, ACTB, HSPA8 & HSPA5, RAN, and GAPDH were enriched in multiple tissues with at least one FDR discovery in the TAM receptor ligand screen (Figure 20). Most interestingly, ENO1 was described to regulate pancreatic cancer adhesion, invasion, and metastasis by αvβ3 integrin. Small hairpin RNA knockdown of ENO1 resulted in an impaired ability to adhere to Collagen I and IV and Fibronectin (*185*). ENO1 is expressed on the cell surface, where it binds and activates plasminogen (*186*) leading to extracellular matrix break down (*187*). HSPA8 is another surface protein associated with influencing the metastatic potential of cancer cells, promoting proliferation and cell survival (*188*). Extracellular GAPDH interacts with the cell adhesion molecule L1 (*189*), which shows parallels to TAM receptors due to the domain structure containing Ig-like domains and Fibronectin-type III-like domains (*189*) as do TAM receptors. Further parallels of L1 to TAM receptors are shedding by ADAM10 and ADAM17, cytosolic tail release by γ-secretase, and ERK signaling (*190*, *191*). L1 is cancer associated, as L1's expression correlated with tumor proliferation (*192*), and it's identification as survival factor in colon cancer cells (*193*). A link to TAM receptor ligands is the expressional regulation of GAS6 and L1 by TWIST1 (*45*). Another twist to the involvement of TAM receptors might be the communication between cancer cells and their environment via vesicles. B-cells from chronic lymphatic leukemia patients were demonstrated to release microvesicles activating TAM receptors bone marrow stromal cells (*178*). Although this particular interaction might just be due to the transfer of active AXL by vesicles, further indications for TAM receptor involvement in vesicle mediated cancer cross talk can be found. Examples are the involvement of MER binding Fibronectin in target cell interaction (*194*), the MER interacting αvβ5 integrin on lung-tropic 4175-LuT exosomes increasing liver metastasis (*195*), and gastric cancer exosomes activating

PI3K/AKT and MAPK/ERK pathways (*196*). PI3K/AKT, as well as MAPK/ERK are pathways engaged by TAM receptors to induce proliferation and survival.

In summary, the recognition of extracellular vesicles by TAM receptors might not only contribute to the regulation of immune responses, but also support proliferation and survival in case of vesicles released by cancer cells. Characterizations of the indicated connections might improve our understanding of how extracellular vesicles of immunologic or malignant cells elicit differential TAM receptor function in recipient cells.

Conclusion

TAM receptor function in cell proliferation and survival, phagocytosis, and inhibition of inflammatory responses are well established with respect to the ligands GAS6 and Protein S. The only alternative ligands discovered and characterized are TUBBY, TULP1, and Galectin 3. Early studies reported TAM receptor activation by GAS6 or Protein S bound to Phosphatidylserine (PtdSer) to induce phagocytosis and immune inhibition when studying apoptotic cells. Recently, living cells were found to present PtdSer, which is bound by GAS6 and Protein S and thereby inducing TAM receptor dependent immune inhibition but not phagocytosis. As PtdSer is described to induce differential effector functions via TAM receptor activation when presented either by living or dead cells, additional yet unknown factors must enable the differentiation of messages.

To discover novel TAM receptor interacting proteins, a novel method of screening was required. The method used for this study was tailored for the capture of weak and transient interacting proteins. A sortase A based transpeptidation method was successfully established for the site specific application of cross-linker molecules to the n-terminus of bait proteins. By employing these baits in multiple tissues, 83 proteins, not previously associated with the TAM receptor family, were enriched. AHSG (Fetuin A) was identified indicating TAM receptor dependent phagocytosis of mineralo-organic complexes and mineralized apoptotic cells, as present in atherosclerotic lesions. Ribosomal proteins were highly represented amongst the identified novel interacting proteins. Together with the reported development of anti-ribosomal protein autoantibodies in the absence of MER, this may indicate the recognition of apoptotic bodies by TAM receptors via ribosomal proteins in addition to PtdSer. Another pattern that emerged from the proteins enriched were vesicle markers. Several publications indicate the utilization of vesicles by immune cells to regulate responses of neighboring cells via TAM receptors, a concept further employed by malignant cells. Finally, it is shown in the here presented study,

that Scavenger receptor B binds directly to TYRO3 and MER. This highlights once more the variability of TAM receptor co-operation with other receptors.

This study reveals 83 points of reference for a more extensive dissection of phagocytic and anti-inflammatory TAM receptor stimuli beyond Phosphatidylserine to maintain tissue homeostasis, regulate inflammatory responses, and cell proliferation and survival. Such insights would especially improve the design of extracellular vesicle therapeutics towards an additional mode of anti-inflammatory action and targeted phagocytosis.

References

1. K. Zhang, M. W. Hornef, A. Dupont, The intestinal epithelium as guardian of gut barrier integrity. *Cell. Microbiol.* **17**, 1561–1569 (2015).
2. S. H. Lee, S. K. Jeong, S. K. Ahn, An update of the defensive barrier function of skin. *Yonsei Med. J.* **47**, 293–306 (2006).
3. K. Brune, J. Frank, A. Schwingshackl, J. Finigan, V. K. Sidhaye, Pulmonary epithelial barrier function: some new players and mechanisms. *Am. J. Physiol. Lung Cell Mol. Physiol.* **308**, L731–45 (2015).
4. D. Ribatti, The development of human mast cells. An historical reappraisal. *Exp. Cell Res.* **342**, 210–215 (2016).
5. M. G. Manz, D. Traver, T. Miyamoto, I. L. Weissman, K. Akashi, Dendritic cell potentials of early lymphoid and myeloid progenitors. *Blood*. **97**, 3333–3341 (2001).
6. Y. Mori *et al.*, Identification of the human eosinophil lineage-committed progenitor: revision of phenotypic definition of the human common myeloid progenitor. *J. Exp. Med.* **206**, 183–193 (2009).
7. D. Kurotaki, H. Sasaki, T. Tamura, Transcriptional control of monocyte and macrophage development. *Int. Immunol.* **29**, 97–107 (2017).
8. S. Carta *et al.*, Cell stress increases ATP release in NLRP3 inflammasome-mediated autoinflammatory diseases, resulting in cytokine imbalance. *Proc. Natl. Acad. Sci. U.S.A.* **112**, 2835–2840 (2015).
9. K. Miyake, Innate immune sensing of pathogens and danger signals by cell surface Toll-like receptors. *Semin. Immunol.* **19**, 3–10 (2007).
10. A. M. Kerrigan, G. D. Brown, C-type lectins and phagocytosis. *Immunobiology*. **214**, 562–575 (2009).
11. E. Latz, T. S. Xiao, A. Stutz, Activation and regulation of the inflammasomes. *Nat. Rev. Immunol.* **13**, 397–411 (2013).
12. Y. K. Chan, M. U. Gack, RIG-I-like receptor regulation in virus infection and immunity. *Curr Opin Virol*. **12**, 7–14 (2015).
13. J. Giang *et al.*, Complement Activation in Inflammatory Skin Diseases. *Front Immunol*. **9**, 639 (2018).
14. E. Market, F. N. Papavasiliou, V(D)J recombination and the evolution of the adaptive immune system. *PLoS Biol.* **1**, E16 (2003).
15. M. Diaz, P. Casali, Somatic immunoglobulin hypermutation. *Curr. Opin. Immunol.* **14**, 235–240 (2002).
16. A. J. Feeney, K. D. Victor, K. Vu, B. Nadel, R. U. Chukwuocha, Influence of the V(D)J recombination mechanism on the formation of the primary T and B cell repertoires. *Semin. Immunol.* **6**, 155–163 (1994).
17. Q. Qi *et al.*, Diversity and clonal selection in the human T-cell repertoire. *Proceedings of the National Academy of Sciences*. **111**, 13139–13144 (2014).
18. A. G. Rolink, C. Schaniel, M. Busslinger, S. L. Nutt, F. Melchers, Fidelity and infidelity in commitment to B-lymphocyte lineage development. *Immunol. Rev.* **175**, 104–111 (2000).
19. J. Stavnezer, C. T. Amemiya, Evolution of isotype switching. *Semin. Immunol.* **16**, 257–275 (2004).
20. C. D. Castro, A. M. Luoma, E. J. Adams, Coevolution of T-cell receptors with MHC and non-MHC ligands. *Immunol. Rev.* **267**, 30–55 (2015).
21. V. Golubovskaya, L. Wu, Different Subsets of T Cells, Memory, Effector Functions, and CAR-T Immunotherapy. *Cancers (Basel)*. **8**, 36 (2016).
22. C. V. Rothlin, S. Ghosh, E. I. Zuniga, M. B. A. Oldstone, G. Lemke, TAM receptors are pleiotropic inhibitors of the innate immune response. *Cell*. **131**, 1124–1136 (2007).
23. T. D. Camenisch, B. H. Koller, H. S. Earp, G. K. Matsushima, A novel receptor tyrosine kinase, Mer, inhibits TNF-alpha production and lipopolysaccharide-induced endotoxic shock. *The Journal of Immunology*. **162**, 3498–3503 (1999).

24. R. S. Scott *et al.*, Phagocytosis and clearance of apoptotic cells is mediated by MER. *Nature*. **411**, 207–211 (2001).

25. W. Xiong *et al.*, Gas6 and the Tyro 3 receptor tyrosine kinase subfamily regulate the phagocytic function of Sertoli cells. *Reproduction*. **135**, 77–87 (2008).

26. Q. Lu *et al.*, Tyro-3 family receptors are essential regulators of mammalian spermatogenesis. *Nature*. **398**, 723–728 (1999).

27. T. Burstyn-Cohen, M. J. Heeb, G. Lemke, Lack of protein S in mice causes embryonic lethal coagulopathy and vascular dysgenesis. *J. Clin. Invest.* **119**, 2942–2953 (2009).

28. T. Nakano, K. Kawamoto, K. Higashino, H. Arita, Prevention of growth arrest-induced cell death of vascular smooth muscle cells by a product of growth arrest-specific gene, gas6. *FEBS Lett.* **387**, 78–80 (1996).

29. T. N. Stitt *et al.*, The anticoagulation factor protein S and its relative, Gas6, are ligands for the Tyro 3/Axl family of receptor tyrosine kinases. *Cell*. **80**, 661–670 (1995).

30. J. Chen, K. Carey, P. J. Godowski, Identification of Gas6 as a ligand for Mer, a neural cell adhesion molecule related receptor tyrosine kinase implicated in cellular transformation. *Oncogene*. **14**, 2033–2039 (1997).

31. F. J. Walker, Regulation of bovine activated protein C by protein S: the role of the cofactor protein in species specificity. *Thromb. Res.* **22**, 321–327 (1981).

32. K. Nagata *et al.*, Identification of the product of growth arrest-specific gene 6 as a common ligand for Axl, Sky, and Mer receptor tyrosine kinases. *J. Biol. Chem.* **271**, 30022–30027 (1996).

33. D. Prasad *et al.*, TAM receptor function in the retinal pigment epithelium. *Mol. Cell. Neurosci.* **33**, 96–108 (2006).

34. C. Lai, M. Gore, G. Lemke, Structure, expression, and activity of Tyro 3, a neural adhesion-related receptor tyrosine kinase. *Oncogene*. **9**, 2567–2578 (1994).

35. K. S. Gajiwala *et al.*, The Axl kinase domain in complex with a macrocyclic inhibitor offers first structural insights into an active TAM receptor kinase. *J. Biol. Chem.* **292**, 15705–15716 (2017).

36. L. Ling, D. Templeton, H. J. Kung, Identification of the major autophosphorylation sites of Nyk/Mer, an NCAM-related receptor tyrosine kinase. *J. Biol. Chem.* **271**, 18355–18362 (1996).

37. T. Sasaki *et al.*, Structural basis for Gas6-Axl signalling. *EMBO J.* **25**, 80–87 (2006).

38. N. B. Caberoy, Y. Zhou, W. Li, Tubby and tubby-like protein 1 are new MerTK ligands for phagocytosis. *EMBO J.* **29**, 3898–3910 (2010).

39. N. B. Caberoy, G. Alvarado, W. Li, Tubby regulates microglial phagocytosis through MerTK. *Journal of Neuroimmunology*. **252**, 40–48 (2012).

40. K. Nomura, A. Vilalta, D. H. Allendorf, T. C. Hornik, G. C. Brown, Activated Microglia Desialylate and Phagocytose Cells via Neuraminidase, Galectin-3, and Mer Tyrosine Kinase. *J. Immunol.* **198**, 4792–4801 (2017).

41. N. B. Caberoy, G. Alvarado, J.-L. Bigcas, W. Li, Galectin-3 is a new MerTK-specific eat-me signal. *J. Cell. Physiol.* **227**, 401–407 (2012).

42. K. N. Couper, D. G. Blount, E. M. Riley, IL-10: the master regulator of immunity to infection. *The Journal of Immunology*. **180**, 5771–5777 (2008).

43. S. Scutera *et al.*, Survival and migration of human dendritic cells are regulated by an IFN-alpha-inducible Axl/Gas6 pathway. *J. Immunol.* **183**, 3004–3013 (2009).

44. M. N. Sharif *et al.*, Twist mediates suppression of inflammation by type I IFNs and Axl. *J. Exp. Med.* **203**, 1891–1901 (2006).

45. C. M. Roberts *et al.*, TWIST1 drives cisplatin resistance and cell survival in an ovarian cancer model, via upregulation of GAS6, L1CAM, and Akt signalling. *Sci Rep*. **6**, 37652 (2016).

46. S. Wormald, D. J. Hilton, Inhibitors of cytokine signal transduction. *J. Biol. Chem.* **279**, 821–824 (2004).

47. A. Yoshimura, H. Nishinakamura, Y. Matsumura, T. Hanada, Negative regulation of cytokine signaling and immune responses by SOCS proteins. *Arthritis Res. Ther.* **7**, 100–110 (2005).

48. A. Mansell *et al.*, Suppressor of cytokine signaling 1 negatively regulates Toll-like receptor signaling by mediating Mal degradation. *Nat. Immunol.* **7**, 148–155 (2006).

49. H. Frobøse *et al.*, Suppressor of cytokine Signaling-3 inhibits interleukin-1 signaling by targeting the TRAF-6/TAK1 complex. *Mol. Endocrinol.* **20**, 1587–1596 (2006).

50. A. Ryo *et al.*, Regulation of NF-kappaB signaling by Pin1-dependent prolyl isomerization and ubiquitin-mediated proteolysis of p65/RelA. *Mol. Cell*. **12**, 1413–1426 (2003).

51. J. I. Elliott *et al.*, Membrane phosphatidylserine distribution as a non-apoptotic signalling mechanism in lymphocytes. *Nat. Cell Biol.* **7**, 808–816 (2005).

52. K. Fischer *et al.*, Antigen recognition induces phosphatidylserine exposure on the cell surface of human CD8+ T cells. *Blood*. **108**, 4094–4101 (2006).

53. E. A. Carrera Silva *et al.*, T cell-derived protein S engages TAM receptor signaling in dendritic cells to control the magnitude of the immune response. *Immunity*. **39**, 160–170 (2013).

54. S. R. Dillon, A. Constantinescu, M. S. Schlissel, Annexin V binds to positively selected B cells. *The Journal of Immunology*. **166**, 58–71 (2001).

55. C. V. Rothlin, E. A. Carrera Silva, L. Bosurgi, S. Ghosh, TAM receptor signaling in immune homeostasis. *Annu. Rev. Immunol.* **33**, 355–391 (2015).

56. P. García de Frutos, R. I. Alim, Y. Härdig, B. Zöller, B. Dahlbäck, Differential regulation of alpha and beta chains of C4b-binding protein during acute-phase response resulting in stable plasma levels of free anticoagulant protein S. *Blood*. **84**, 815–822 (1994).

57. C. Ekman, J. Stenhoff, B. Dahlbäck, Gas6 is complexed to the soluble tyrosine kinase receptor Axl in human blood. *J. Thromb. Haemost.* **8**, 838–844 (2010).

58. J. P. O'Bryan, Y. W. Fridell, R. Koski, B. Varnum, E. T. Liu, The transforming receptor tyrosine kinase, Axl, is post-translationally regulated by proteolytic cleavage. *J. Biol. Chem.* **270**, 551–557 (1995).

59. E. Thorp *et al.*, Shedding of the Mer tyrosine kinase receptor is mediated by ADAM17 protein through a pathway involving reactive oxygen species, protein kinase Cδ, and p38 mitogen-activated protein kinase (MAPK). *J. Biol. Chem.* **286**, 33335–33344 (2011).

60. L. D. Hughes, L. Bosurgi, S. Ghosh, C. V. Rothlin, Chronicles of Cell Death Foretold: Specificities in the Mechanism of Disposal. *Front Immunol*. **8**, 1743 (2017).

61. M. Herrmann *et al.*, Impaired phagocytosis of apoptotic cell material by monocyte-derived macrophages from patients with systemic lupus erythematosus. *Arthritis Rheum.* **41**, 1241–1250 (1998).

62. H. M. Seitz, T. D. Camenisch, G. Lemke, H. S. Earp, G. K. Matsushima, Macrophages and dendritic cells use different Axl/Mertk/Tyro3 receptors in clearance of apoptotic cells. *The Journal of Immunology*. **178**, 5635–5642 (2007).

63. P. L. Cohen *et al.*, Delayed apoptotic cell clearance and lupus-like autoimmunity in mice lacking the c-mer membrane tyrosine kinase. *J. Exp. Med.* **196**, 135–140 (2002).

64. S.-H. Lee, X. W. Meng, K. S. Flatten, D. A. Loegering, S. H. Kaufmann, Phosphatidylserine exposure during apoptosis reflects bidirectional trafficking between plasma membrane and cytoplasm. *Cell Death Differ.* **20**, 64–76 (2013).

65. T. Nakano *et al.*, Requirement of gamma-carboxyglutamic acid residues for the biological activity of Gas6: contribution of endogenous Gas6 to the proliferation of vascular smooth muscle cells. *Biochem. J.* **323 (Pt 2)**, 387–392 (1997).

66. I. Hasanbasic, I. Rajotte, M. Blostein, The role of gamma-carboxylation in the anti-apoptotic function of gas6. *J. Thromb. Haemost.* **3**, 2790–2797 (2005).

67. O. Benzakour, C. Kanthou, The anticoagulant factor, protein S, is produced by cultured human vascular smooth muscle cells and its expression is up-regulated by thrombin. *Blood*. **95**, 2008–2014 (2000).

68. H. A. Anderson *et al.*, Serum-derived protein S binds to phosphatidylserine and stimulates the phagocytosis of apoptotic cells. *Nat. Immunol.* **4**, 87–91 (2003).

69. C. Nishi, S. Toda, K. Segawa, S. Nagata, Tim4- and MerTK-mediated engulfment of apoptotic cells by mouse resident peritoneal macrophages. *Mol. Cell. Biol.* **34**, 1512–1520 (2014).

70. S. C. Finnemann, E. F. Nandrot, MerTK activation during RPE phagocytosis in vivo requires alphaVbeta5 integrin. *Adv. Exp. Med. Biol.* **572**, 499–503 (2006).

71. Y. Wu, S. Singh, M.-M. Georgescu, R. B. Birge, A role for Mer tyrosine kinase in alphavbeta5

integrin-mediated phagocytosis of apoptotic cells. *J. Cell. Sci.* **118**, 539–553 (2005).

72. A. Angelillo-Scherrer *et al.*, Deficiency or inhibition of Gas6 causes platelet dysfunction and protects mice against thrombosis. *Nat. Med.* **7**, 215–221 (2001).
73. A. Angelillo-Scherrer *et al.*, Role of Gas6 receptors in platelet signaling during thrombus stabilization and implications for antithrombotic therapy. *J. Clin. Invest.* **115**, 237–246 (2005).
74. Y. S. Kim *et al.*, Gas6 stimulates angiogenesis of human retinal endothelial cells and of zebrafish embryos via ERK1/2 signaling. *PLOS ONE*. **9**, e83901 (2014).
75. G. P. Gasic, C. P. Arenas, T. B. Gasic, G. J. Gasic, Coagulation factors X, Xa, and protein S as potent mitogens of cultured aortic smooth muscle cells. *Proc. Natl. Acad. Sci. U.S.A.* **89**, 2317–2320 (1992).
76. Q. Lu, G. Lemke, Homeostatic regulation of the immune system by receptor tyrosine kinases of the Tyro 3 family. *Science*. **293**, 306–311 (2001).
77. Z. S. M. Rahman, W.-H. Shao, T. N. Khan, Y. Zhen, P. L. Cohen, Impaired apoptotic cell clearance in the germinal center by Mer-deficient tingible body macrophages leads to enhanced antibody-forming cell and germinal center responses. *J. Immunol.* **185**, 5859–5868 (2010).
78. U. S. Gaipl *et al.*, Clearance of apoptotic cells in human SLE. *Curr. Dir. Autoimmun.* **9**, 173–187 (2006).
79. P. Zezos *et al.*, Thrombophilic abnormalities of natural anticoagulants in patients with ulcerative colitis. *Hepatogastroenterology*. **54**, 1417–1421 (2007).
80. B. Cakal *et al.*, Natural anticoagulant protein levels in Turkish patients with inflammatory bowel disease. *Blood Coagul. Fibrinolysis*. **21**, 118–121 (2010).
81. I. E. Koutroubakis *et al.*, Resistance to activated protein C and low levels of free protein S in Greek patients with inflammatory bowel disease. *Am. J. Gastroenterol.* **95**, 190–194 (2000).
82. H. J. Hoehn *et al.*, Axl-/- mice have delayed recovery and prolonged axonal damage following cuprizone toxicity. *Brain Res.* **1240**, 1–11 (2008).
83. M. D. Binder *et al.*, Gas6 increases myelination by oligodendrocytes and its deficiency delays recovery following cuprizone-induced demyelination. *PLOS ONE*. **6**, e17727 (2011).
84. V. Tsiperson, X. Li, G. J. Schwartz, C. S. Raine, B. Shafit-Zagardo, GAS6 enhances repair following cuprizone-induced demyelination. *PLOS ONE*. **5**, e15748 (2010).
85. G. Z. M. Ma *et al.*, Polymorphisms in the receptor tyrosine kinase MERTK gene are associated with multiple sclerosis susceptibility. *PLOS ONE*. **6**, e16964 (2011).
86. A. K. Keating *et al.*, Lymphoblastic leukemia/lymphoma in mice overexpressing the Mer (MerTK) receptor tyrosine kinase. *Oncogene*. **25**, 6092–6100 (2006).
87. J. P. O'Bryan *et al.*, axl, a transforming gene isolated from primary human myeloid leukemia cells, encodes a novel receptor tyrosine kinase. *Mol. Cell. Biol.* **11**, 5016–5031 (1991).
88. J. W. Janssen *et al.*, A novel putative tyrosine kinase receptor with oncogenic potential. *Oncogene*. **6**, 2113–2120 (1991).
89. G. Wu *et al.*, Targeting Gas6/TAM in cancer cells and tumor microenvironment. *Mol. Cancer*. **17**, 20 (2018).
90. A. B. Lee-Sherick *et al.*, Aberrant Mer receptor tyrosine kinase expression contributes to leukemogenesis in acute myeloid leukemia. *Oncogene*. **35**, 6270–6270 (2016).
91. S. P. Whitman *et al.*, GAS6 expression identifies high-risk adult AML patients: potential implications for therapy. *Leukemia*. **28**, 1252–1258 (2014).
92. R. S. Cook *et al.*, MerTK inhibition in tumor leukocytes decreases tumor growth and metastasis. *J. Clin. Invest.* **123**, 3231–3242 (2013).
93. L. Bosurgi *et al.*, Paradoxical role of the proto-oncogene Axl and Mer receptor tyrosine kinases in colon cancer. *Proc. Natl. Acad. Sci. U.S.A.* **110**, 13091–13096 (2013).
94. R. Akitake-Kawano *et al.*, Inhibitory role of Gas6 in intestinal tumorigenesis. *Carcinogenesis*. **34**, 1567–1574 (2013).
95. Y. Lu *et al.*, Regulated intramembrane proteolysis of the AXL receptor kinase generates an intracellular domain that localizes in the nucleus of cancer cells. *FASEB J.* **31**, 1382–1397 (2017).

96. M. Shimojima *et al.*, Tyro3 family-mediated cell entry of Ebola and Marburg viruses. *J. Virol.* **80**, 10109–10116 (2006).

97. M. Shimojima, Y. Ikeda, Y. Kawaoka, The mechanism of Axl-mediated Ebola virus infection. *J. Infect. Dis.* **196 Suppl 2**, S259–63 (2007).

98. K. Morizono *et al.*, The soluble serum protein Gas6 bridges virion envelope phosphatidylserine to the TAM receptor tyrosine kinase Axl to mediate viral entry. *Cell Host Microbe*. **9**, 286–298 (2011).

99. M. Shimojima, U. Ströher, H. Ebihara, H. Feldmann, Y. Kawaoka, Identification of cell surface molecules involved in dystroglycan-independent Lassa virus cell entry. *J. Virol.* **86**, 2067–2078 (2012).

100. L. Meertens *et al.*, The TIM and TAM families of phosphatidylserine receptors mediate dengue virus entry. *Cell Host Microbe*. **12**, 544–557 (2012).

101. S. Bhattacharyya *et al.*, Enveloped viruses disable innate immune responses in dendritic cells by direct activation of TAM receptors. *Cell Host Microbe*. **14**, 136–147 (2013).

102. R. Hamel *et al.*, Biology of Zika Virus Infection in Human Skin Cells. *J. Virol.* **89**, 8880–8896 (2015).

103. D. Gatherer, A. Kohl, Zika virus: a previously slow pandemic spreads rapidly through the Americas. *J. Gen. Virol.* **97**, 269–273 (2016).

104. N. Drayman *et al.*, Pathogens use structural mimicry of native host ligands as a mechanism for host receptor engagement. *Cell Host Microbe*. **14**, 63–73 (2013).

105. H. Ton-That, G. Liu, S. K. Mazmanian, K. F. Faull, O. Schneewind, Purification and characterization of sortase, the transpeptidase that cleaves surface proteins of Staphylococcus aureus at the LPXTG motif. *Proc. Natl. Acad. Sci. U.S.A.* **96**, 12424–12429 (1999).

106. S. K. Mazmanian, G. Liu, H. Ton-That, O. Schneewind, Staphylococcus aureus sortase, an enzyme that anchors surface proteins to the cell wall. *Science*. **285**, 760–763 (1999).

107. D. Ní Eidhin *et al.*, Clumping factor B (ClfB), a new surface-located fibrinogen-binding adhesin of Staphylococcus aureus. *Mol. Microbiol.* **30**, 245–257 (1998).

108. Y. A. Que *et al.*, Reassessing the role of Staphylococcus aureus clumping factor and fibronectin-binding protein by expression in Lactococcus lactis. *Infect. Immun.* **69**, 6296–6302 (2001).

109. B. Sinha *et al.*, Heterologously expressed Staphylococcus aureus fibronectin-binding proteins are sufficient for invasion of host cells. *Infect. Immun.* **68**, 6871–6878 (2000).

110. P. K. Peterson, J. Verhoef, L. D. Sabath, P. G. Quie, Effect of protein A on staphylococcal opsonization. *Infect. Immun.* **15**, 760–764 (1977).

111. C. Giai *et al.*, Shedding of tumor necrosis factor receptor 1 induced by protein A decreases tumor necrosis factor alpha availability and inflammation during systemic Staphylococcus aureus infection. *Infect. Immun.* **81**, 4200–4207 (2013).

112. W. J. Weiss *et al.*, Effect of srtA and srtB gene expression on the virulence of Staphylococcus aureus in animal models of infection. *J. Antimicrob. Chemother.* **53**, 480–486 (2004).

113. J. Kwiecinski, T. Jin, E. Josefsson, Surface proteins of Staphylococcus aureus play an important role in experimental skin infection. *APMIS*. **122**, 1240–1250 (2014).

114. H. Mao, S. A. Hart, A. Schink, B. A. Pollok, Sortase-mediated protein ligation: a new method for protein engineering. *Journal of the American Chemical Society*. **126**, 2670–2671 (2004).

115. I. Chen, B. M. Dorr, D. R. Liu, A general strategy for the evolution of bond-forming enzymes using yeast display. *Proc. Natl. Acad. Sci. U.S.A.* **108**, 11399–11404 (2011).

116. L. Chen *et al.*, Improved variants of SrtA for site-specific conjugation on antibodies and proteins with high efficiency. *Sci Rep*. **6**, 31899 (2016).

117. T. Heck, P.-H. Pham, A. Yerlikaya, L. Thöny-Meyer, M. Richter, Sortase A catalyzed reaction pathways: a comparative study with six SrtA variants. *Catal. Sci. Technol.* **4**, 2946–2956 (2014).

118. H. Hirakawa, S. Ishikawa, T. Nagamune, Design of Ca2+-independent Staphylococcus aureus sortase A mutants. *Biotechnol. Bioeng.* **109**, 2955–2961 (2012).

119. B. M. Dorr, H. O. Ham, C. An, E. L. Chaikof, D. R. Liu, Reprogramming the specificity of sortase enzymes. *Proc. Natl. Acad. Sci. U.S.A.* **111**, 13343–13348 (2014).

120. S. Massa *et al.*, Sortase A-mediated site-specific labeling of camelid single-domain antibody-fragments: a versatile strategy for multiple molecular imaging modalities. *Contrast Media Mol Imaging*. **11**, 328–339 (2016).

121. T. Yamamoto, T. Nagamune, Expansion of the sortase-mediated labeling method for site-specific N-terminal labeling of cell surface proteins on living cells. *Chem. Commun. (Camb.)*. **16**, 1022–1024 (2009).

122. M.-È. Lebel *et al.*, Nanoparticle adjuvant sensing by TLR7 enhances CD8+ T cell-mediated protection from Listeria monocytogenes infection. *J. Immunol.* **192**, 1071–1078 (2014).

123. A. Thérien *et al.*, A versatile papaya mosaic virus (PapMV) vaccine platform based on sortase-mediated antigen coupling. *J Nanobiotechnology*. **15**, 54 (2017).

124. C. Lai, G. Lemke, An extended family of protein-tyrosine kinase genes differentially expressed in the vertebrate nervous system. *Neuron*. **6**, 691–704 (1991).

125. N. B. Caberoy, W. Li, Unraveling the molecular mystery of retinal pigment epithelium phagocytosis. *Adv. Exp. Med. Biol.* **723**, 693–699 (2012).

126. P. J. Godowski *et al.*, Reevaluation of the roles of protein S and Gas6 as ligands for the receptor tyrosine kinase Rse/Tyro 3. *Cell*. **82**, 355–358 (1995).

127. G. Moody *et al.*, Antibody-mediated neutralization of autocrine Gas6 inhibits the growth of pancreatic ductal adenocarcinoma tumors in vivo. *Int. J. Cancer*. **139**, 1340–1349 (2016).

128. X. Wang, L. Huang, Identifying Dynamic Interactors of Protein Complexes by Quantitative Mass Spectrometry. *Molecular & Cellular Proteomics*. **7**, 46–57 (2008).

129. L. M. Sternicki, K. L. Wegener, J. B. Bruning, G. W. Booker, S. W. Polyak, Mechanisms Governing Precise Protein Biotinylation. *Trends Biochem. Sci.* **42**, 383–394 (2017).

130. L. Liu, Pharmacokinetics of monoclonal antibodies and Fc-fusion proteins. *Protein Cell*. **9**, 15–32 (2018).

131. C.-Y. Wu, L. Young, D. Young, J. Martel, J. D. Young, Bions: a family of biomimetic mineralo-organic complexes derived from biological fluids. *PLOS ONE*. **8**, e75501 (2013).

132. P. Rawat *et al.*, Identification of potential protein biomarkers for early detection of pregnancy in cow urine using 2D DIGE and label free quantitation. *Clin Proteomics*. **13**, 15 (2016).

133. N. Kaesler *et al.*, Gas6 protein: its role in cardiovascular calcification. *BMC Nephrol*. **17**, 52 (2016).

134. M. J. Hosen, P. J. Coucke, O. Le Saux, A. De Paepe, O. M. Vanakker, Perturbation of specific pro-mineralizing signalling pathways in human and murine pseudoxanthoma elasticum. *Orphanet J Rare Dis*. **9**, 66 (2014).

135. M. Shuvy *et al.*, Raloxifene attenuates Gas6 and apoptosis in experimental aortic valve disease in renal failure. *Am. J. Physiol. Heart Circ. Physiol.* **300**, H1829–40 (2011).

136. A. Idelevich, Y. Rais, E. Monsonego-Ornan, Bone Gla protein increases HIF-1alpha-dependent glucose metabolism and induces cartilage and vascular calcification. *Arterioscler. Thromb. Vasc. Biol.* **31**, e55–71 (2011).

137. N. Leclerc *et al.*, Gene expression profiling of glucocorticoid-inhibited osteoblasts. *J. Mol. Endocrinol.* **33**, 175–193 (2004).

138. J. A. Galan *et al.*, Proteomic studies of Syk-interacting proteins using a novel amine-specific isotope tag and GFP nanotrap. *J. Am. Soc. Mass Spectrom.* **22**, 319–328 (2011).

139. T. Tezuka, H. Umemori, T. Akiyama, S. Nakanishi, T. Yamamoto, PSD-95 promotes Fyn-mediated tyrosine phosphorylation of the N-methyl-D-aspartate receptor subunit NR2A. *Proc. Natl. Acad. Sci. U.S.A.* **96**, 435–440 (1999).

140. M. Ojaniemi, S. S. Martin, F. Dolfi, J. M. Olefsky, K. Vuori, The proto-oncogene product p120(cbl) links c-Src and phosphatidylinositol 3'-kinase to the integrin signaling pathway. *J. Biol. Chem.* **272**, 3780–3787 (1997).

141. J. Li, X.-L. Niu, N. R. Madamanchi, Leukocyte antigen-related protein tyrosine phosphatase negatively regulates hydrogen peroxide-induced vascular smooth muscle cell apoptosis. *J. Biol. Chem.* **283**, 34260–34272 (2008).

142. T. Miyazaki *et al.*, Src kinase activity is essential for osteoclast function. *J. Biol. Chem.* **279**, 17660–17666 (2004).

143. S. Keerthikumar *et al.*, ExoCarta: A Web-Based Compendium of Exosomal Cargo. *J. Mol. Biol.* **428**, 688–692 (2016).

144. L. Turiák *et al.*, Proteomic characterization of thymocyte-derived microvesicles and apoptotic bodies in BALB/c mice. *J Proteomics*. **74**, 2025–2033 (2011).

145. N. B. Caberoy, D. Maiguel, Y. Kim, W. Li, Identification of tubby and tubby-like protein 1 as eat-me signals by phage display. *Exp. Cell Res.* **316**, 245–257 (2010).

146. J. Li *et al.*, Desialylation is a mechanism of Fc-independent platelet clearance and a therapeutic target in immune thrombocytopenia. *Nat Commun*. **6**, 7737 (2015).

147. J. C. Todt, B. Hu, J. L. Curtis, The scavenger receptor SR-A I/II (CD204) signals via the receptor tyrosine kinase Mertk during apoptotic cell uptake by murine macrophages. *Journal of Leukocyte Biology*. **84**, 510–518 (2008).

148. P. M. D'Cruz *et al.*, Mutation of the receptor tyrosine kinase gene Mertk in the retinal dystrophic RCS rat. *Hum. Mol. Genet.* **9**, 645–651 (2000).

149. A. F. Muro *et al.*, Regulated splicing of the fibronectin EDA exon is essential for proper skin wound healing and normal lifespan. *J. Cell Biol.* **162**, 149–160 (2003).

150. M. Hashimoto-Uoshima, Y. Z. Yan, G. Schneider, I. Aukhil, The alternatively spliced domains EIIIB and EIIIA of human fibronectin affect cell adhesion and spreading. *J. Cell. Sci.* **110 (Pt 18)**, 2271–2280 (1997).

151. J. L. Sechler, J. E. Schwarzbauer, Control of cell cycle progression by fibronectin matrix architecture. *J. Biol. Chem.* **273**, 25533–25536 (1998).

152. B. P. Eliceiri *et al.*, Src-mediated coupling of focal adhesion kinase to integrin αv β5 in vascular endothelial growth factor signaling. *J. Cell Biol.* **157**, 149–160 (2002).

153. J. C. McCutcheon *et al.*, Regulation of macrophage phagocytosis of apoptotic neutrophils by adhesion to fibronectin. *Journal of Leukocyte Biology*. **64**, 600–607 (1998).

154. H. Sadahiro *et al.*, Activation of the receptor tyrosine kinase AXL regulates the immune microenvironment in glioblastoma. *Cancer Res.*, canres.2433.2017 (2018).

155. G. Wu, D. W. McBride, J. H. Zhang, Axl activation attenuates neuroinflammation by inhibiting the TLR/TRAF/NF-κB pathway after MCAO in rats. *Neurobiology of Disease*. **110**, 59–67 (2018).

156. A. Caraux *et al.*, Natural killer cell differentiation driven by Tyro3 receptor tyrosine kinases. *Nat. Immunol.* **7**, 747–754 (2006).

157. F.-C. Hsiao *et al.*, Circulating growth arrest-specific 6 protein is associated with adiposity, systemic inflammation, and insulin resistance among overweight and obese adolescents. *J. Clin. Endocrinol. Metab.* **98**, E267–74 (2013).

158. T. Kanno, K. Yasutake, K. Tanaka, S. Hadano, J.-E. Ikeda, A novel function of N-linked glycoproteins, alpha-2-HS-glycoprotein and hemopexin: Implications for small molecule compound-mediated neuroprotection. *PLOS ONE*. **12**, e0186227 (2017).

159. V. K. Harris *et al.*, Fetuin-A deficiency protects mice from Experimental Autoimmune Encephalomyelitis (EAE) and correlates with altered innate immune response. *PLOS ONE*. **12**, e0175575 (2017).

160. D. Pal *et al.*, Fetuin-A acts as an endogenous ligand of TLR4 to promote lipid-induced insulin resistance. *Nat. Med.* **18**, 1279–1285 (2012).

161. W. Jahnen-Dechent, A. Heiss, C. Schäfer, M. Ketteler, Fetuin-A regulation of calcified matrix metabolism. *Circ Res*. **108**, 1494–1509 (2011).

162. M. Herrmann *et al.*, Clearance of fetuin-A--containing calciprotein particles is mediated by scavenger receptor-A. *Circ Res*. **111**, 575–584 (2012).

163. J. L. Reynolds *et al.*, Human vascular smooth muscle cells undergo vesicle-mediated calcification in response to changes in extracellular calcium and phosphate concentrations: a potential mechanism for accelerated vascular calcification in ESRD. *J. Am. Soc. Nephrol.* **15**, 2857–2867 (2004).

164. A. Y.-M. Wang *et al.*, Associations of serum fetuin-A with malnutrition, inflammation, atherosclerosis and valvular calcification syndrome and outcome in peritoneal dialysis patients. *Nephrol. Dial. Transplant.* **20**, 1676–1685 (2005).

165. J. L. Reynolds *et al.*, Multifunctional roles for serum protein fetuin-a in inhibition of human

vascular smooth muscle cell calcification. *J. Am. Soc. Nephrol.* **16**, 2920–2930 (2005).

166. D. Proudfoot *et al.*, Apoptosis regulates human vascular calcification in vitro: evidence for initiation of vascular calcification by apoptotic bodies. *Circ Res*. **87**, 1055–1062 (2000).

167. B.-K. Son *et al.*, Gas6/Axl-PI3K/Akt pathway plays a central role in the effect of statins on inorganic phosphate-induced calcification of vascular smooth muscle cells. *Eur. J. Pharmacol.* **556**, 1–8 (2007).

168. D. A. Bird *et al.*, Receptors for oxidized low-density lipoprotein on elicited mouse peritoneal macrophages can recognize both the modified lipid moieties and the modified protein moieties: implications with respect to macrophage recognition of apoptotic cells. *Proceedings of the National Academy of Sciences*. **96**, 6347–6352 (1999).

169. D. Proudfoot, Acetylated Low-Density Lipoprotein Stimulates Human Vascular Smooth Muscle Cell Calcification by Promoting Osteoblastic Differentiation and Inhibiting Phagocytosis. *Circulation*. **106**, 3044–3050 (2002).

170. L. N. Y. Wu, B. R. Genge, R. E. Wuthier, Analysis and molecular modeling of the formation, structure, and activity of the phosphatidylserine-calcium-phosphate complex associated with biomineralization. *J. Biol. Chem.* **283**, 3827–3838 (2008).

171. J. Li, X.-L. Niu, N. R. Madamanchi, Leukocyte antigen-related protein tyrosine phosphatase negatively regulates hydrogen peroxide-induced vascular smooth muscle cell apoptosis. *J. Biol. Chem.* **283**, 34260–34272 (2008).

172. Y. Miyamoto *et al.*, Involvement of the Tyro3 receptor and its intracellular partner Fyn signaling in Schwann cell myelination. *Mol. Biol. Cell*. **26**, 3489–3503 (2015).

173. A. K. Ghosh *et al.*, The novel receptor tyrosine kinase Axl is constitutively active in B-cell chronic lymphocytic leukemia and acts as a docking site of nonreceptor kinases: implications for therapy. *Blood*. **117**, 1928–1937 (2011).

174. C. Eken, S. Sadallah, P. J. Martin, S. Treves, J. A. Schifferli, Ectosomes of polymorphonuclear neutrophils activate multiple signaling pathways in macrophages. *Immunobiology*. **218**, 382–392 (2013).

175. C. Eken *et al.*, Ectosomes released by polymorphonuclear neutrophils induce a MerTK-dependent anti-inflammatory pathway in macrophages. *J. Biol. Chem.* **285**, 39914–39921 (2010).

176. K. Geng *et al.*, Requirement of Gamma-Carboxyglutamic Acid Modification and Phosphatidylserine Binding for the Activation of Tyro3, Axl, and Mertk Receptors by Growth Arrest-Specific 6. *Front Immunol*. **8**, 1521 (2017).

177. K. E. Happonen *et al.*, The Gas6-Axl Protein Interaction Mediates Endothelial Uptake of Platelet Microparticles. *J. Biol. Chem.* **291**, 10586–10601 (2016).

178. A. K. Ghosh *et al.*, Circulating microvesicles in B-cell chronic lymphocytic leukemia can stimulate marrow stromal cells: implications for disease progression. *Blood*. **115**, 1755–1764 (2010).

179. A. Klinke *et al.*, Myeloperoxidase attracts neutrophils by physical forces. *Blood*. **117**, 1350–1358 (2011).

180. D. Ricklin, G. Hajishengallis, K. Yang, J. D. Lambris, Complement: a key system for immune surveillance and homeostasis. *Nat. Immunol.* **11**, 785–797 (2010).

181. A. Rigotti, S. L. Acton, M. Krieger, The class B scavenger receptors SR-BI and CD36 are receptors for anionic phospholipids. *J. Biol. Chem.* **270**, 16221–16224 (1995).

182. L. A. Casciola-Rosen, Autoantigens targeted in systemic lupus erythematosus are clustered in two populations of surface structures on apoptotic keratinocytes. *J. Exp. Med.* **179**, 1317–1330 (1994).

183. J. Nishida, A. Shiratsuchi, D. Nadano, T.-A. Sato, Y. Nakanishi, Structural change of ribosomes during apoptosis: degradation and externalization of ribosomal proteins in doxorubicin-treated Jurkat cells. *J. Biochem.* **131**, 485–493 (2002).

184. M. Z. Radic *et al.*, Heterogeneous nuclear ribonucleoprotein P2 is an autoantibody target in mice deficient for Mer, Axl, and Tyro3 receptor tyrosine kinases. *The Journal of Immunology*. **176**, 68–74 (2006).

185. M. Principe *et al.*, Alpha-enolase (ENO1) controls alpha v/beta 3 integrin expression and regulates pancreatic cancer adhesion, invasion, and metastasis. *J Hematol Oncol*. **10**, 16 (2017).

186. L. A. Miles *et al.*, Role of cell-surface lysines in plasminogen binding to cells: identification of .alpha.-enolase as a candidate plasminogen receptor. *Biochemistry*. **30**, 1682–1691 (1991).

187. K. Danø *et al.*, Plasminogen activation and cancer: Basic mechanisms and perspectives. *European Journal of Cancer Supplements*. **4**, 5 (2006).

188. Y. Zhang, N. Shan, W. Zhou, S. Zhang, Identification of HSPA8 as a candidate biomarker for endometrial carcinoma by using iTRAQ-based proteomic analysis. *OncoTargets and Therapy*. **9**, 2169–2179 (2016).

189. T. Makhina *et al.*, Extracellular GAPDH binds to L1 and enhances neurite outgrowth. *Mol. Cell. Neurosci.* **41**, 206–218 (2009).

190. U. Cavallaro, E. Dejana, Adhesion molecule signalling: not always a sticky business. *Nat. Rev. Mol. Cell Biol.* **12**, 189–197 (2011).

191. S. Raveh, N. Gavert, A. Ben-Ze'ev, L1 cell adhesion molecule (L1CAM) in invasive tumors. *Cancer Letters*. **282**, 137–145 (2009).

192. Y. Allory *et al.*, The L1 cell adhesion molecule is induced in renal cancer cells and correlates with metastasis in clear cell carcinomas. *Clin. Cancer Res.* **11**, 1190–1197 (2005).

193. M. S. Gelman *et al.*, Identification of cell surface and secreted proteins essential for tumor cell survival using a genetic suppressor element screen. *Oncogene*. **23**, 8158–8170 (2004).

194. A. Purushothaman *et al.*, Fibronectin on the Surface of Myeloma Cell-derived Exosomes Mediates Exosome-Cell Interactions. *J. Biol. Chem.* **291**, 1652–1663 (2016).

195. A. Hoshino *et al.*, Tumour exosome integrins determine organotropic metastasis. *Nature*. **527**, 329–335 (2015).

196. J. L. Qu *et al.*, Gastric cancer exosomes promote tumour cell proliferation through PI3K/Akt and MAPK/ERK activation. *Digestive and Liver Disease*. **41**, 875–880 (2009).

Appendix

List of Abbreviations

Abbreviation	Complete form
aa	Amino acids
ABC	Ammonium bicarbonate
AD	Alzheimer's Disease
APC	Antigen presenting cell
ATP	Adenosine triphosphate
BCA	Bicinchoninic acid assay
CDS	Coding sequence
CmR	Chloramphenicol resistance protein
DAMP	Danger associated molecular pattern
DMEM	Dulbecco's Modified Eagle's Medium
DMSO	Dimethylsulfoxide
DNA	Deoxyribonucleic acid
dsDNA	Double stranded DNA
DTT	Dithiothreitol
E. coli	*Escherichia coli*
ELISA	Enzyme Linked Immunosorbent Assay
FBS	Fetal Bovine Serum
FCS	Fluorescence Correlation Spectroscopy
FLCS	Fluorescence Lifetime Correlation Spectroscopy
FLIM	Fluorescence Lifetime Imaging
ESI	Electrospray ionization
h	Hour / hours
Hg	Mercury
His / H	Histidine
IAA	Iodoacetamide
Ig	Immunoglobulin
IP	Immunoprecipitation
p	probability
PBS	Phosphate buffered saline
PCA	Principle Component Analysis
PEI	Polyethylenimine
PMSF	Phenylmethylsulfonyl fluoride
PtdSer	Phosphatidylserine
q	corrected probability
L2	2 amino acid Linker
L9	9 amino acid Linker
L19	19 amino acid Linker
LC	Liquid chromatography
LysC	Lysyl endopeptidase
MCI	Mild Cognitive Impairment
min	Minute / minutes
MS	Mass spectrometry
ms	Milliseconds
n.a.	Not applicable
OD	Optical density
OD600	Optical density at 600 nm
PAMP	Pathogen associated molecular pattern
REF number	Reference number
ref. seq.	Reference sequence
rpm	Rounds per minute
RT	Room temperature
s	Second / seconds
S. aureus	*Staphylococcus aureus*
S. pyogenes	*Streptococcus pyogenes*
SLE	Systemic lupus erythematosus
SMD	Single Molecule Detection
TBS	Tris buffered saline
TCS	True Confocal Scanner
TFA	Trifluoroacetic acid
UHPLC	Ultra-high pressure liquid chromatography
v/v	Volume by volume
WB	Western Blot
w/v	Weight by volume
Xe	Xenon
α	Alpha or anti (context dependent)
°C	Degree Celsius
‘	Minutes
“	Seconds

Table 16. List of abbreviations.

List of Figures

Figure 1. TAM receptors and the regulation of inflammation, phagocytosis and survival. 5
Figure 2. Transpeptidation reaction by sortase A. 8
Figure 3. Schematic setup for magnetic separation of microbeads. 26
Figure 4. Schematic setup of the Hg/Xe Arc Lamp. 31
Figure 5. Affinity of TAM receptor bait proteins to hGAS6 and hProtein S. 43
Figure 6. Co-IP enriching FN1 as TAM receptor interacting protein in human plasma. 44
Figure 7. SrtA titration for the first tagging step. 46
Figure 8. Titration of TAMRA-LPET*GG in srtA reactions. 47
Figure 9. SrtA titration for second tagging step. 48
Figure 10. Time course for second srtA tagging reaction. 49
Figure 11. Comparison of control and bait proteins linker variants. 50
Figure 12. Inhibition of srtA by chelation of Calcium ions. 51
Figure 13. Effect of n-terminal modification of bait and control proteins on GAS6 binding. 53
Figure 14. Photo-activation of Diazirine via a UV box and an Arc lamp. 55
Figure 15. Specificity of label transferred by Diazirine-L19 AXL-Fc compared to Diazirine-L19 Control-Fc. 58
Figure 16. Comparison of enrichment methods. 59
Figure 17. Screening method and tissue selection. 63
Figure 18. Comparison of enrichments by bait and control in screened tissues. 63
Figure 19. Enrichment by TYRO3 and AXL for each tissue screened. 66
Figure 20. TAM receptor interacting proteins identified in multiple tissues. 70
Figure 21. Protein-Protein interaction network. 70
Figure 22. TAM receptor enriched proteins characteristic for apoptotic bodies, microvesicles, and exosomes. 71
Figure 23. Binding of screening identified proteins to TAM receptor bait proteins. 73
Figure 24. Binding of proteins of interest to TAM receptor bait proteins. 74

List of Tables

Table 1. List of instruments. 12
Table 2. List of software. 12
Table 3. List of general chemicals and reagents. 13
Table 4. List of buffers, solutions, media, and cell lines for tissue culture. 14
Table 5. List of buffers, tissues and mice for preparation of lysis samples. 15
Table 6. List of buffers, reagents, and bacterial strains for plasmid cloning. 18
Table 7. List and description of plasmids. 21
Table 8. List of buffers, reagents, bacterial strains, and equipment for protein expression and purification. 24
Table 9. List of reagents and material for immunoprecipitation of proteins. 27
Table 10. List of buffers and reagents for the detection of protein-protein interaction. 29
Table 11. List of buffers and reagents used for sortase tagging. 30
Table 12. List of buffers, reagents, and kits for immunoblots. 35
Table 13. List of Buffers and Solutions for Co-IP of cross-linked bait and control proteins. 36
Table 14. List of equipment and software for LC & MS analysis. 38
Table 15. List of buffers and reagents for LC & MS analysis 39
Table 16. List of abbreviations. i
Table 17. Exocarta list of top 100 proteins that are often identified in exosomes. xi
Table 18. Number of PubMed search results of TAM enriched proteins plus 'cancer'. xi

Supplemental data

Comparing purification strategies used for n-terminal sortase A transpeptidation.

The two-step process of n-terminal sortase A tagging contains necessary purifications of the intermediate and end product. Purification after the first tagging step is necessary to separate the protein with the exposed n-terminal glycine from the removed LPET containing peptide to prevent a re-ligation of LPET containing peptides to the free n-terminal glycine, and from the triglycine, which would interfere with the second step. Following the second tagging step, where a LPETG motif-containing payload is tagged to the free n-terminal glycine, another purification is performed to separate the tagged product from the srtA enzyme and from the unused payload.

Three purification methods were tested for srtA transpeptidation efficiency, protein recovery, and reliability. Protein A elution buffers, based on low pH and high salt concentrations were tested for elution of proteins from Protein A Dynabeads. The best elution of approximately 75% compared to the LDS eluted control was achieved with the Pierce IgG Elution Buffer (Figure App 3). Protein A microbeads were tested as an alternative to Dynabeads as microbeads, due to their size of 50 nm, they are described to distribute equally in liquids, and not to sediment over time. Further each particle binds less protein leading to a homogenous distribution of particle bound bait and control protein in a sample. During the use of microbeads in srtA reaction buffer the beads aggregated. Variations of the reaction buffer could not fully prevent the aggregation, especially following magnetic attraction and washing in the HOKImag (data not shown). The efficiency and reliability of the three methods was further compared performing both tagging steps exemplary with hexa-His-L2 AXL-Fc (Figure App 1).

The first srtA tagging step was performed equally for all three conditions without purification by beads or column. The L2 AXL-Fc proteins were then purified either by dyna-, or microbeads or by using a FPLC column. In case of the FPLC purification, proteins were eluted, the buffer was exchanged to srtA reaction buffer and the proteins were quantified before further steps. In case of the bead purifications, L2 AXL-Fc proteins were bound by the respective and washed with srtA reaction buffer before the second tagging step without elution and quantification. The second tagging step was performed with L2 AXL-Fc protein being either bound to Dynabeads, or microbeads, or in solution after FPLC purification and TAMRA-LPETGG. The reaction was stopped by denaturing proteins in DTT containing LDS buffer at 95°C and separation in SDS-PAGE (Figure App 5).

As the first steps for each purification method was performed under equal conditions, removing the hexa-His-LPET peptide resulted in equally high efficiencies. Following the purification and second tagging step, only low amounts of L2 AXL-Fc protein was detected for dynabead and microbead based methods (Figure App 1, B, C). Losses during FPLC purification, buffer exchange and quantification were compensated for the second tagging step, which resulted in TAMRA being detected on the L2 AXL-Fc protein comparable to the positive control (Figure App 1, D).

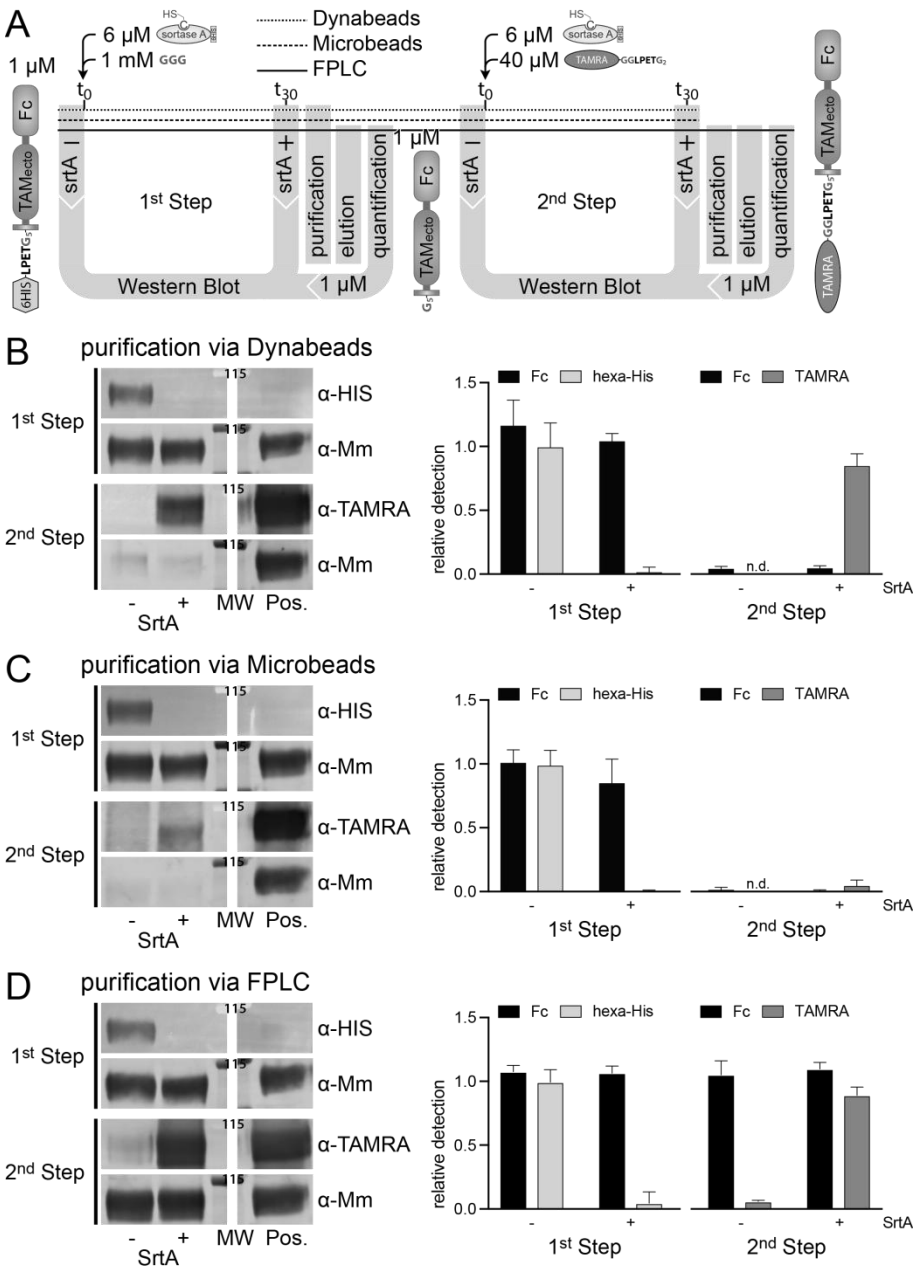

Figure App 1. Purification methods used for n-terminal srtA transpeptidation. A schematic workflow shows the different purification methods that were compared to purify tagged Fc protein after srtA transpeptidation (A). The first srtA tagging step was performed with 1 µM hexa-His-L2-AXL-Fc, 6 µM 5M srtA, 1 mM triglycine in srtA reaction buffer at 37°C for 30 minutes. The reaction was stopped with 20 µM EDTA and samples for western blot were taken. The AXL-Fc proteins were then purified with either Dynabeads, Microbeads or via FPLC columns. The second srtA step was performed with either the AXL-Fc protein bound to the respective beads or 1 µM of FPLC purified AXL-Fc together with 6 µM 5M srtA and 40 µM TAMRA-LPET*GG at 37°C for 30 minutes. After completion of the second tagging step, the reaction was stopped with 20 µM EDTA and samples for western blot were taken. As a positive control (Pos.), 1 µM of either hexa-His-L2 AXL-Fc, or L2 AXL-Fc, or TAMRA-L2 AXL-Fc previously prepared by FPLC were added. (B, C, D) N-terminal srtA tagging was performed on hexa-His-L2 AXL-Fc bait protein either using Protein A Dynabeads (B), Microbeads (C), or FPLC columns (D) for the purification steps. The presence of hexa-His tag and Fc-tag before and after the first srtA tagging step, as well as the presence of TAMRA and Fc-tag before and after the second srtA tagging step were detected via SDS-PAGE and western blotting. Relative hexa-His detection was determined by dividing the detected hexa-His signal by the Fc signal relative to the mean of hexa-His/Fc of the – srtA samples of the first srtA tagging step. The relative detection of Fc or TAMRA of the second srtA tagging step was determined by dividing the detected Fc or TAMRA signal of a sample by the detected Fc or TAMRA signal of the positive control. The MEAN and SD of three technical replicates is shown.

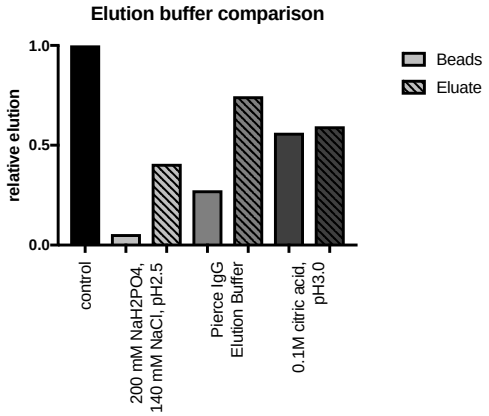

Figure App 2. Comparison of Ig elution buffers.

Comparison of buffers to elute protein from Protein A Dynabeads. Hexa-His-L2 control protein was loaded on Protein A Dynabeads and eluted the described buffers. Proteins remaining on the beads and beads without previous elution were eluted with DTT containing LDS buffer at 95°C. Proteins were detected via Western Blot after SDS-PAGE gel electrophoresis and quantified.

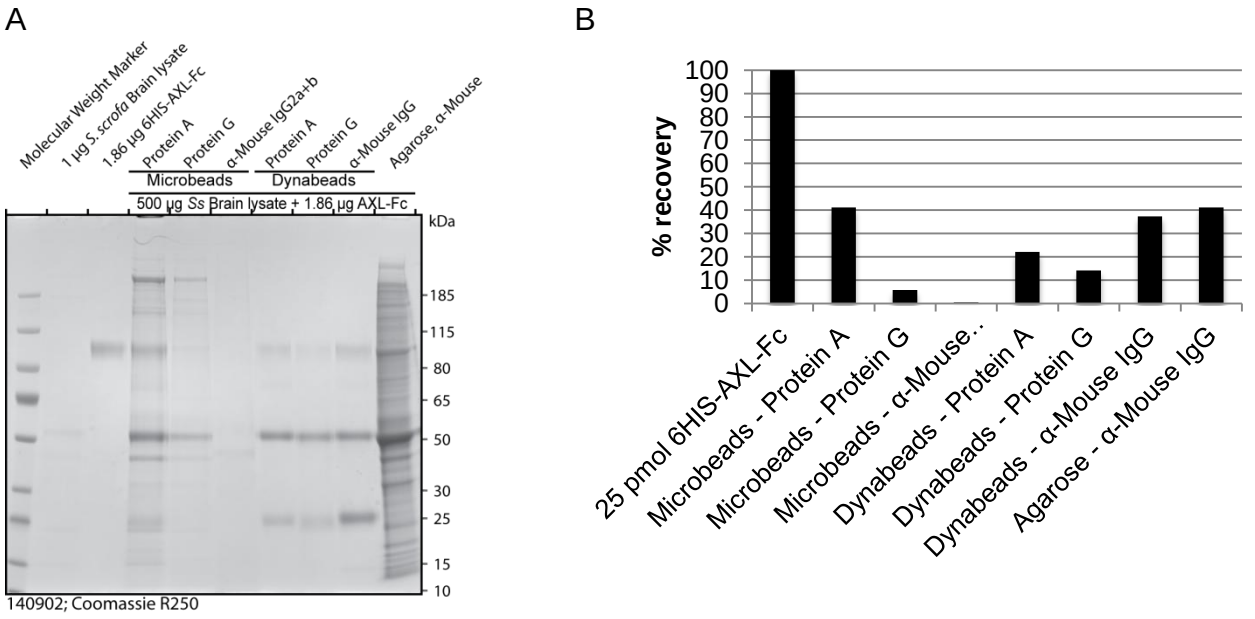

Figure App 3. Comparison of beads for separation of bait proteins from complex matrices.

A defined amount of AXL-Fc was spiked into brain lysate samples. Recovery by various beads was compared according to efficiency and purity. Recovery was determined by quantifying bands in Coomassie stained SDS-PAGE gels. n=1

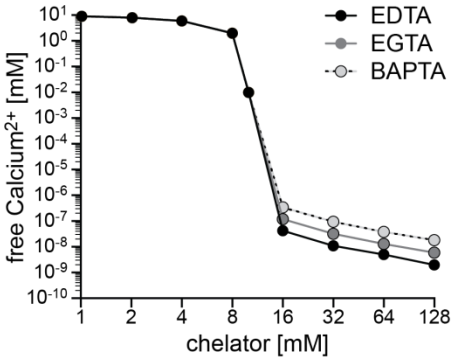

Figure App 4. Prediction of free Ca2+ in titrations of EDTA, EGTA, and BAPTA.

The concentration of free Calcium ions in dependence on the concentration of the chelators EDTA, EGTA, and BAPTA for a total concentration of 10 mM Calcium were predicted by the online tool MAXCHELATOR.

Concentrations were predicted for the following conditions: pH7.4, 20°C, and an ionic strength of 0.16 (http://maxchelator.stanford.edu/webmaxc/webmaxcS.htm, 09.02.2018).

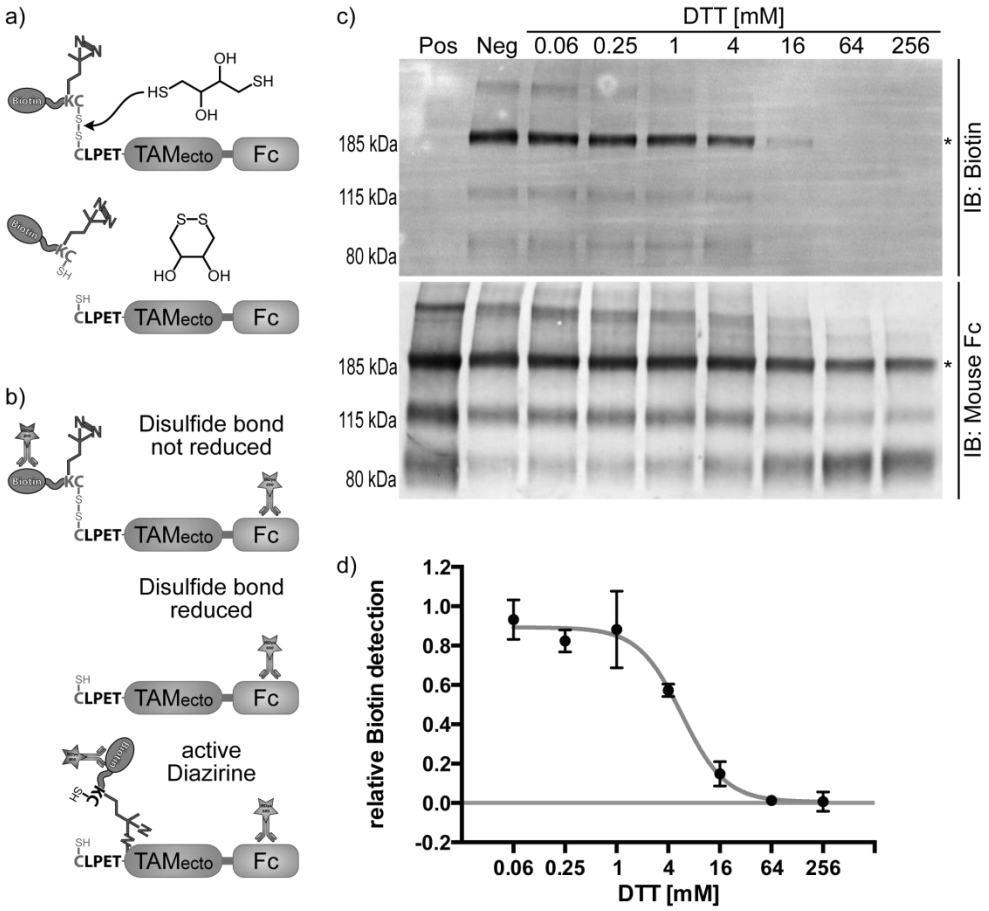

Figure App 5. Titration of DTT to release Diazirine/Biotin part of cross-linker molecule.
Titration of Dithiothreitol (DTT) to determine efficient concentration for reduction of disulfide bond connecting the Diazirine cross-linker and the biotin label to the bait protein. Bait protein not tagged with the Diazirine cross-linker was used as the positive control (Pos), while Diazirine cross-linker tagged bait protein not treated with DTT was used as negative control (Neg). The bait protein and the biotin were detected via western blot. The * marked bands were quantified. The ratio of biotin to bait protein was calculated, subtracted by Pos and divided by the Neg. MEAN and SD of technical triplicates

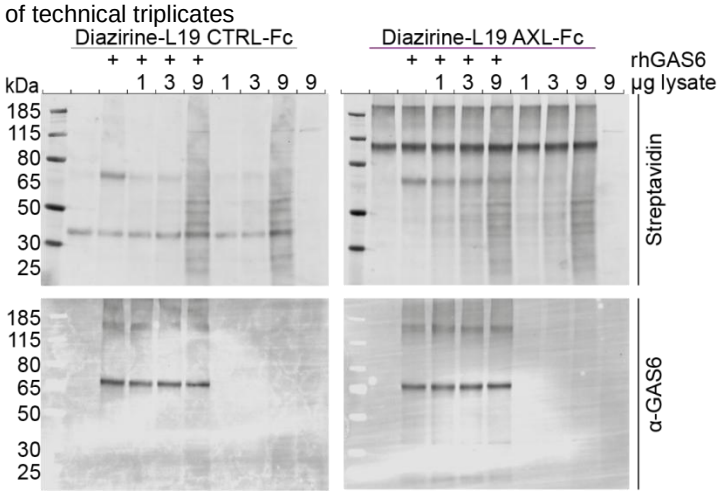

Figure App 6. Label transfer from Diazirine tagged AXL-Fc or CTRL-Fc to GAS6.
Supplemental illustration of less cropped representative Western Blots for label transfer from either Diazirine-L19 AXL-Fc or Diazirine-L19 Control-Fc to GAS6 in matrices of increasing complexities.

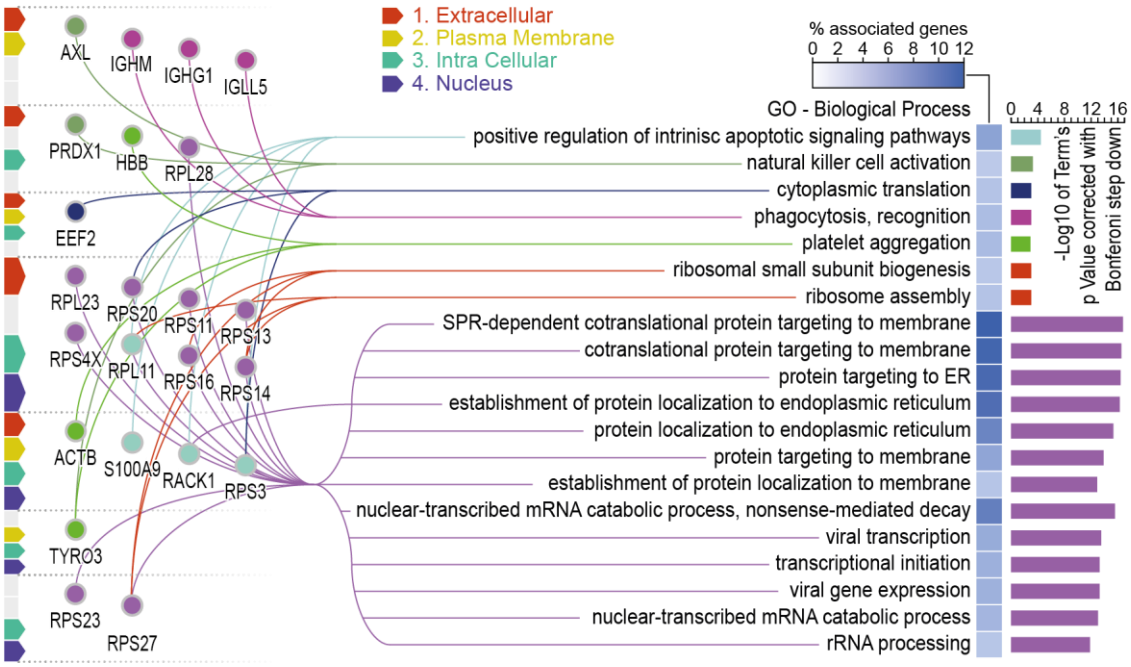

Figure App 7. Gene Ontology enrichment for Biological Processes and protein localization.

Cytoscape and the application ClueGO+CluePedia were used to perform an enrichment analysis of the GO term 'Biological Process' with the proteins listed in Figure 20 as significantly TAM receptor enriched. Proteins included are linked to the respective biological processes are sorted for their cellular localization.

Figure App 8. Cellular Components and associated proteins identified in screen.

The online database GeneALaCart (https://genealacart.genecards.org/) was used to identify 'Cellular Component' GO terms associated with the proteins identified as significantly TAM receptor enriched in Figure 20. Identified terms were regrouped into commonly associated terms thereafter named according to the common term and 'associated'. Proteins including terms not associated with any common term were grouped to 'Cellular Component associated'. TYRO3, AXL, MER, GAS6, and Protein S are specially marked.

A

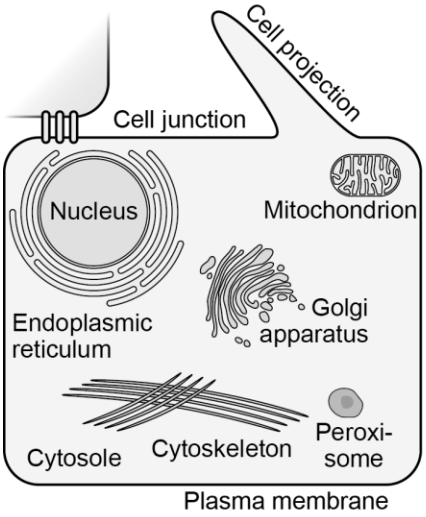

endoplasmic reticulum associated

AHSG	CCDC88B	CPQ	CTSA	**GAS6**
HSPA5	PEX16	RAB14	RAC1	RPS3
RPS23	**TYRO3**			

golgi apparatus associated

AHSG	CCDC88B	CPQ	**GAS6**	RAB14
RAC1				

mitochondrion associated

GNB2L1	HSPA5	IDH1	IDH2	PDHA1
PDHB	PKM	PRDX1	PRDX5	RPS3
RPS14	SACS			

nucleus associated

ACTB	ACTN4	APC	API5	CHD3
CTNNA2	CTSA	EEF1A1	EEF2	ENO1
GAPDH	GNB2L1	HNRNPDL	HSPA5	HSPA8
MYO1C	MYO10	NPEPPS	PDHA1	PDHB
PHACTR1	PKM	PPP1R12A		PRDX1
PRDX5	PSME1	RAB14	RAN	RPL11
RPL23	RPS3	RPS4X	RPS11	RPS13
RPS14	RPS16	RPS20	RPS23	RPS27
S100A9	SACS	SPR	TALDO1	TUBB
TYRO3	UBE2I			

peroxisome associated

IDH1	IDH2	PEX16	PRDX5

cell projection associated

ACTN4	AK1	APC	CTNNA2	DMTN	EEF1A1
GNB2L1	MYL12B	MYO1C	MYO10	PKM	RAB14
RAC1	RAN	RPL28	RPS3	SACS	SLC12A5
SNX5	SYNGAP1				

cell junction associated

ACTB	ACTN4	APC	CTNNA2	HSPA5	HSPA8
PHACTR1	PPP1R12A	RAC1	RPL23	RPS3	RPS4X
RPS11	RPS13	RPS14	RPS16	S100A9	TMOD3

cytoplasm associated

ACTB	ACTN4	AK1	APC	API5	CCDC88B
CHD3	CPQ	CTNNA2	DMTN	DSTN	EEF1A1
EEF2	Eif2s3x	ENO1	GAPDH	**GAS6**	GCLC
GNB2L1	GYS1	HBB	HNRNPDL	HSPA5	HSPA6
HSPA8	IDH1	IDH2	ITPK1	MYL9	MYL12A
MYL12B	MYO1C	MYO10	NPEPPS	PDHA1	PDHB
PHACTR1	PKM	PPP1R12A	PRDX1	PRDX5	PRPS1
PSME1	RAB14	RAC1	RAN	RPL11	RPL23
RPS3	RPS4X	RPS11	RPS13	RPS14	RPS16
RPS20	RPS23	RPS27	RPL28	S100A9	SACS
SNX5	SPR	SYNGAP1	TAGLN2	TALDO1	TMOD3
TUBA1B	TUBB	UBE2I			

cytoskeleton associated

ACTB	ACTN4	AK1	APC	CCDC88B	CHD3
CTNNA2	DMTN	DSTN	EEF1A1	GAPDH	HSPA6
MYL9	MYL12A	MYL12B	MYO1C	MYO10	PPP1R12A
RAC1	RAN	RPS3	S100A9	TUBA1B	TUBB
TMOD3					

extracellular region associated

ACTB	ACTN4	AHSG	**AXL**	CPQ	CTSA
CTSD	EEF1A1	EEF2	ENO1	GAPDH	**GAS6**
HBB	HSPA5	HSPA6	HSPA8	IDH1	IGHG1
IGHM	IGLL5	LPA	PKM	PRDX1	PRDX5
RAC1	RAN	RPS3	RPS4X	RPS11	RPS13
RPS14	RPS16	RPS20	RPL11	RPL23	S100A9
TAGLN2	TUBB				

intracellular associated associated

ACTN4	**AXL**	CPQ	CTSA	DMTN	DSTN	EEF2
GAPDH	**GAS6**	GYS1	HSPA8	ITPK1	PDHA1	
PRDX5	RAB14	RAC1	RAN	RPL11	RPL28	RPS3
RPS4X	RPS11	RPS13	RPS20	RPS23	RPS27	SNX5
SYNGAP1	TALDO1					

plasma membrane associated

ACTB	AK1	APC	**AXL**	CTNNA2	DMTN	
EEF1A1	EEF2	ENO1	GAPDH	GNB2L1	HSPA5	HSPA8
IGHG1	IGHM	IGLL5	ITPK1	Ly-6c1	MYO1C	
MYO10	RAB14	RAC1	RPS3	S100A9	SLC12A5	
SLC39A10	SNX5	SYNGAP1	**TYRO3**			

membrane associated

ACTB	APC	API5	**AXL**	CCDC88B	CTNNA2	CTSA
CTSD	DMTN	EEF1A1	EEF2	ENO1	GAPDH	GCLC
GNB2L1	GYS1	HSPA5	HSPA8	IGHG1	IGHM	KCT2
Ly-6c1	MYO1C	MYO10	PEX16	RAB14	RAC1	RAN
RPL11	RPL23	RPL28	RPS3	RPS4X	RPS11	RPS13
RPS14	RPS16	RPS20	RPS23	S100A9	SLC12A5	
SLC39A10	SNX5	SYNGAP1	TUBA1B	TUBB	**TYRO3**	

B

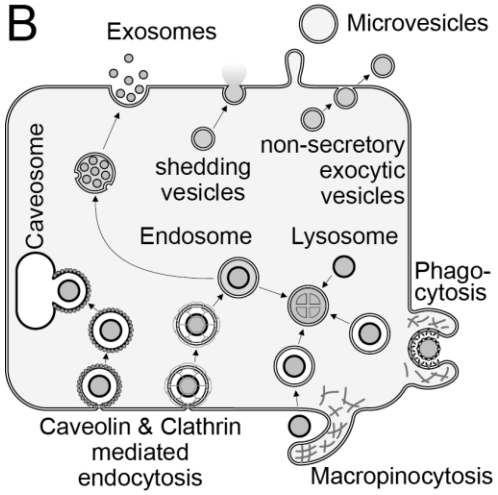

extracellular exosome

ACTB	ACTN4	AHSG	AK1	**AXL**	CPQ
CTSA	CTSD	DSTN	EEF1A1	EEF2	ENO1
GAPDH	**GAS6**	GNB2L1	HBB	HNRNPDL	HSPA5
HSPA6	HSPA8	IDH1	IDH2	IGHG1	IGHM
IGLL5	MYL12A	MYL12B	MYO1C	NPEPPS	PDHB
PKM	PRDX1	PRDX5	PSME1	RAB14	RAC1
RAN	RPL11	RPL23	RPL28	RPS3	RPS4X
RPS11	RPS13	RPS14	RPS16	RPS20	S100A9
SPR	TAGLN2	TALDO1	TUBA1B	TUBB	

endosome associated

HSPA8 RAB14 RAN SNX5

lysosome associated

CPQ CTSA CTSD EEF1A1 HSPA8 RAB14
TUBB

phagosome associated

GNB2L1 MYO1C RAB14 SNX5

macropinocytic cup

SNX5

clathrin-sculpted gamma-aminobutyric acid transport vesicle membr.

HSPA8

intracellular vesicle associated

CTSD	DMTN	HBB	HSPA5	HSPA8
MYO1C	PRDX1	PRDX5	RAB14	RAC1
RAN	SNX5			

secretory granule associated

ACTN4	AHSG	CTSD	EEF1A1	EEF2	**GAS6**
HBB	HSPA6	HSPA8	IDH1	PKM	RAB14
RAC1	S100A9				

extracellular vesicle - PKM

vesicle - ACTB GAPDH PKM TAGLN2

C

contractile fiber associated

ACTN4	ENO1	MYL9	MYL12A
MYL12B	PPP1R12A		TMOD3

endomembrane system - DMTN

proteasome complex associated - PSME1

COP9 signalosome - HSPA5 & HSPA6

cellular component associated

ACTB ACTN4 APC AXL EEF1A1 GAPDH GNB2L1 HBB HSPA5 HSPA8 MYL12B
MYO10 PDHA1 PKM PPP1R12A PRDX1 RAN RPL11 RPL23 RPL28 SLC12A5 TUBA1B TUBB
UBE2I

ribonucleoprotein complex associated

ACTB	ACTN4	EEF2	GAPDH	GNB2L1	HNRNPDL
HSPA8	RAC1	RPL11	RPL23	RPL28	RPS3
RPS4X	RPS11	RPS13	RPS14	RPS16	RPS20
RPS23	RPS27	TUBB			

synapse associated

CTNNA2 DMTN HSPA8 PHACTR1 SYNGAP1 UBE2I

viral nucleocapsid - HNRNPDL

	Gene Symbol	# of times identified		Gene Symbol	# of times identified		Gene Symbol	# of times identified		Gene Symbol	# of times identified
1	CD9	98	26	VCP	62	51	HSPA1A	53	76	HIST2H4A	47
2	PDCD6IP	96	27	TPI1	62	52	GNAI2	53	77	GNB1	47
3	**HSPA8**	96	28	PPIA	62	53	ANXA1	53	78	THBS1	46
4	**GAPDH**	95	29	MSN	62	54	RHOA	52	79	**RAN**	46
5	**ACTB**	93	30	CFL1	62	55	MFGE8	52	80	RAB5A	46
6	ANXA2	83	31	**PRDX1**	61	56	PRDX2	51	81	PTGFRN	46
7	CD63	82	32	PFN1	61	57	GDI2	51	82	CCT5	46
8	SDCBP	78	33	RAP1B	60	58	EHD4	51	83	CCT3	46
9	**ENO1**	78	34	ITGB1	60	59	**ACTN4**	51	84	AHCY	46
10	HSP90AA1	77	35	**HSPA5**	58	60	YWHAB	50	85	UBA1	45
11	TSG101	75	36	SLC3A2	57	61	RAB7A	50	86	RAB5B	45
12	**PKM**	72	37	HIST1H4A	57	62	LDHB	50	87	RAB1A	45
13	LDHA	72	38	GNB2	57	63	GNAS	50	88	LAMP2	45
14	**EEF1A1**	71	39	ATP1A1	57	64	RAB5C	49	89	ITGA6	45
15	YWHAZ	69	40	YWHAQ	56	65	ARF1	49	90	HIST1H4B	45
16	PGK1	69	41	FLOT1	56	66	ANXA6	49	91	BSG	45
17	**EEF2**	69	42	FLNA	56	67	ANXA11	49	92	YWHAH	44
18	ALDOA	69	43	CLIC1	56	68	ACTG1	49	93	TUBA1A	44
19	HSP90AB1	67	44	CCT2	56	69	KPNB1	48	94	TKT	44
20	ANXA5	67	45	CDC42	55	70	EZR	48	95	TCP1	44

21	FASN	66	46	YWHAG	54	71	ANXA4	48	96	STOM	44
22	YWHAE	65	47	A2M	54	72	ACLY	48	97	SLC16A1	44
23	CLTC	64	48	**TUBA1B**	53	73	TUBA1C	47	98	RAB8A	44
24	CD81	64	49	**RAC1**	53	74	TFRC	47	99	MYH9	44
25	ALB	63	50	LGALS3BP	53	75	**RAB14**	47	100	MVP	44

Table 17. Exocarta list of top 100 proteins that are often identified in exosomes.
exocarta.org (2018.06.18)

Search name + cancer	PubMed hits	Search name + cancer	PubMed hits	Search name + cancer	PubMed hits
APC (plus Adenomatous polyposis coli protein)	2274	Psme1	39	LPA (plus Apolipoprotein)	10
Idh1 (plus Isocitrate)	1470	HBB (plus Hemoglobin)	38	Taldo1	10
GAPDH	1076	Api5	36	Gys1	9
RAN (RAN excluded from autor)	1076	Cpq	32	RPL23	9
AXL	670	Ppp1r12a	32	Phactr1	8
Idh2 (plus Isocitrate)	546	RPS27	30	RPS11	8
S100A9	364	Myl9	29	RPS4X	8
ACTB	210	Tagln2	28	Slc39a10	8
Ly6c1 (replaced with Ly6c)	184	Ak1	27	Myo1c	7
Eno1	176	HSPA6	27	TUBA1B	7
HSPA8	149	RPS3	26	RPL28	6
PRDX1	147	Rab14	25	Snx5	6
GCLC	139	Pdha1	24	IGLL5	5
Ctsd	129	Myo10	23	Slc12a5	5
TYRO3	128	Chd3	20	Tmod3	5
PKM	113	Prps1	20	Pex16	4
Hspa5	104	IGHG1	18	Spr	4
Rac1 (plus Ras-related protein)	98	GNB2L1	16	Myl12a	3
EEF1A1	91	Prdx5	16	SYNGAP1	3
Actn4	90	RPS20	16	Eif2s3x	2
EEF2	84	Dstn	15	Ccdc88b	1
Ighv3-4 (replaced with IGHV3)	79	IGHM	13	Dmtn	1
AHSG	70	Pdhb	13	Itpk1	1
RPL11	69	RPS23	13	Myl12b	1
Ighv1-64 (replaced with IGHV1)	68	Ube2i	13	Npepps	1
TUBB	48	Ctnna2	12	Sacs (plus Sacsin)	1
Ctsa	43	RPS13	12	Igkv16-104 (replaced with IGKV16)	0
Hnrnpdl	42	RPS16	11	Kct2	0
RPS14	41				

Table 18. Number of PubMed search results of TAM enriched proteins plus 'cancer'.
PubMed searches were performed using the TAM enriched proteins name if not stated otherwise together with 'cancer' to determine the number of cancer related publications (2018.06.19).

Image license information:

Image	Name	Source / License information
	Max Quant Software logo	http://www.biochem.mpg.de/5111795/maxquant _ 14.02.20147
	Different laptop desiang template vector Free vector 8.27MB	freedesignfile.com; License: Creative Commons (Attribution 3.0); part of image implemented into figure
	Simple Cartoon Mouse clip art Free vector	www.openclipart.org; License: Public domain license; image implemented into figures

Acknowledgements

First and foremost I want to thank my Doktorvater Professor Eicke Latz for his support and the opportunity to conduct the research and thesis in the Institute of Innate Immunity. Especially I want to thank him for his inspirational scientific guidance and the overwhelming opportunities to experiment, learn, and share experience. It was a great pleasure to work here.

I would like to thank Prof. Joachim Schultze for agreeing to supervise my thesis as the second official reviewer. Further thanks go to the third and fourth official reviewer of my thesis.

I would also like to especially thank Dr. Felix Meissner and Annika Frauenstein for their support and guidance during the preparation and analysis of the mass spectrometry screen, and of course for measuring the samples in the first place. I have learnt a great deal from this cooperation.

I would like to acknowledge the collaborators who supported my work by providing resources and experience. Prof. Hidde Ploegh I would like to thank for providing the various Sortases I extensively used. For providing the opportunity to screen human brain samples I would like to thank Prof. Michael Heneka. Further, I appreciated the provision of the ARPE-19 cell line by Dr. Wen Allen Tseng, and the support for setting up the HOKImag by Prof. Stefan Schütze, and Dr. Vladimir Tchikov.

I would like to thank all my colleagues with whom I had a great time at the Institute of Innate Immunity for all the advices, inspiration, and motivation, but especially for the friendship shared. It has been a great atmosphere to work in.

Finally, I would like to thank my friends and family, especially my wife and children and my parents, for their encouraging support and love.